MATERIAL MODELLING AND FINITE ELEMENT SIMULATION OF UNIAXIAL AND MULTIAXIAL LOW CYCLE FATIGUE AND RATCHETING FOR SA333 C-Mn STEEL

THESIS SUBMITTED FOR THE FULFILLMENT OF THE DEGREE OF

DOCTOR OF PHILOSOPHY (ENGINEERING)

BY

SNEHASISH BHATTACHARJEE

DEPARTMENT OF MECHANICAL ENGNEERING

FACULTY OF ENGINEERING AND TECHNOLOGY

JADAVPUR UNIVERSITY

KOLKATA, INDIA

MAY, 2018

MATERIAL MODELLING AND FINITE ELEMENT SIMULATION OF UNIAXIAL AND MULTIAXIAL LOW CYCLE FATIGUE AND RATCHETING FOR SA333 C-Mn STEEL

THESIS SUBMITTED FOR THE FULFILLMENT OF THE DEGREE OF
DOCTOR OF PHILOSOPHY (ENGINEERING)
BY

SNEHASISH BHATTACHARJEE

DEPARTMENT OF MECHANICAL ENGNEERING
FACULTY OF ENGINEERING AND TECHNOLOGY
JADAVPUR UNIVERSITY
KOLKATA, INDIA

MAY, 2018

Blank Page

JADAVPUR UNIVERSITY
KOLKATA – 700032

INDEX NUMBER: 244/13/E

1. **Title of the Thesis:** Material Modelling and Finite Element Simulation of Uniaxial and Multiaxial Low Cycle Fatigue and Ratcheting for SA333 C-Mn Steel.

2. **Name, Designation and Institution of Supervisor(s):**
   1. Prof. Sankar Dhar
      Former Professor,
      Department of Mechanical Engineering,
      Jadavpur University.
   2. Prof. Sanjib Kumar Acharyya
      Professor,
      Department of Mechanical Engineering,
      Jadavpur University.

3. **List of Publication:**
   1. J. De, **S. Bhattacharjee**, S. Dhar, S. K. Acharyya, S. K. Gupta and S. Tarafdar, "Finite Element Simulation of Multi-Axial Low Cycle Fatigue of Material SA333", Proceedia Engineering, 86 (2014), 158 – 165.
   2. **S. Bhattacharjee**, S. Dhar, and S. K. Acharyya, "Dislocation based controlling of kinematic hardening contribution to simulate primary and secondary stages of uniaxial ratcheting", IOP Conf. Series: Materials Science and Engineering, 219 (2017), 012012.
   3. **S. Bhattacharjee**, S. Dhar, S. K. Acharyya and S. K. Gupta, "Cyclic softening based on dislocation annihilation at sub-cell boundary for SA333 Grade-6 C-Mn steel", Modelling and Simulation in Material Science and Engineering, 26 (2018), 015001.

4. **List of Patents:** Nil

5. **List of Presentations in National/ International Conferences/ Workshops:**
   1. **S. Bhattacharjee**, S. Dhar, S. K. Acharyya and S. K. Gupta, "Modification of cyclic yield stress using 'MARQUIS' approach to simulate cyclic softening", Proceedings of the First International Conference on Mechanical Engineering (INCOM – 2018), ISBN: 978-93-83660-38-4, 118-121.

Blank Page

CERTIFICATE FROM THE SUPERVISORS

*This is to certify that the thesis entitled "**Material modelling and finite element simulation of uniaxial and multiaxial low cycle fatigue and ratcheting for SA333 C-Mn steel**" submitted by Shree **Snehasish Bhattacharjee**, who got his name registered on 13 November, 2013 for the award of **Ph. D. (Engineering) degree** from **Jadavpur University** is absolutely based upon his own work under our supervision and neither his thesis nor any part of the same has been submitted for any degree/diploma or any other academic award anywhere before.*

Supervisor: Prof. Sankar Dhar
Former Professor,
Dept. of Mechanical Engg.,
Jadavpur University,
Kolkata – 700032.

Supervisor: Prof. Sanjib Kumar Acharyya
Professor,
Dept. of Mechanical Engg.,
Jadavpur University,
Kolkata – 700032.

Blank Page

Dedicated to:

My Parents and Teachers

Blank Page

ACKNOWLEDGEMENT

There are many great personalities, I am afraid, I will not be able to recollect them all who silently gave what is required to bring this entire work in success. Words of thanks fall short to express my gratitude to them in proper dimensions. Without their generous and arduous efforts, the present work could have turned into one fruitless attempt or even less. I humbly acknowledge them all.

I owe a deep sense of gratitude to my respected guides Prof. Sankar Dhar and Prof. Sanjib Kumar Acharyya, for their valuable guidance and continuous encouragement throughout this work. Their patient and compassionate support and generous involvements helped me to get over the critical phases of this work.

I shall remain indebted to my parents forever, for their sheer blessings and unconditional grueling sacrifices when I remained absorbed in the work throughout the long period.

I would like to express my gratefulness to Pradip Sir and, all other laboratory personnel and all my fellow colleagues of the Fatigue Fracture and Damage Analysis Laboratory, Applied Mechanics Laboratory, Machine Elements Laboratory, Hydraulics Laboratory, Neptune Laboratory and other laboratories of this department, for their sympathetic encouragement and generous assistance during the entire period. Their intellectual assembly helps me conceive certain ideas and kept me motivated during the good and bad days of the work.

I thankfully acknowledge the support I received from the organizations namely, Bhabha Atomic Research Centre, Mumbai and National Metallurgical Laboratory, Jamshedpur in the form material, experimental data and relevant information and infrastructural support respectively. I oblige the financial support from Bhabha Atomic Research Centre, Mumbai through collaborative project and University Grants Commission through Basic Scientific Research Fellowship during the course of time.

I must acknowledge the unconditional supports from Prof. Surajit Kumar Paul of IIT, Patna; and Dr. S. Sivaprasad, Dr. Himadri Nandan Bar, Dr. Soumitra Tarafder and other officials of National Metallurgical Laboratory, Jamshedpur; Dr. Suneel Kumar Gupta of Bhabha Atomic Research Centre, Mumbai. Their keen knowledge and understanding substantially assisted me to complete this work and rightfully earned the appreciation.

I thank the authorities of Jadavpur University, for the cooperation and extending the facilities for this work. I am indebted to all my teachers in this department and many others who have encouraged me during this period. I would also like to thank all the staffs and officials of the Mechanical Engineering Department for their sympathetic cooperation.

In the end, I would like to conclude by sharing the credit to all for making the years of attempt an accomplishment. Thank you.

_____

SNEHASISH BHATTACHARJEE

Blank Page

CONTENT

SUBJECT **PAGE**

Chapter 4 – Asymmetric loading

Chapter 5 – Conclusion

Blank Page

SYNOPSYS

In the piping material, multiaxial state of stress and strain is a considerable fact and the variation in loading can be expected due to the changes in operating condition, structural aspect or environmental condition. Therefore, the study of multiaxial cyclic behaviour of the material is important. The material can undergo cyclic plastic deformation, when the load amplitude goes beyond its yield limit or sometimes local stress concentrators like - the geometrical discontinuities, surface roughness, persistent slip bands, grain interfaces, inclusions, defects etc., may cause local cyclic plastic deformation even for small amplitude of loadings. Cyclic plastic deformation comprises several stress-strain phenomena of practical interest in design because, these stress-strain responses indicate the symptoms of any secondary damage mechanism evolved and influencing the fatigue life.

SA333 Grade-6 C-Mn steel is used to make Primary Heat Transport (PHT) pipes in Indian Pressurized Heavy Water Reactors (PHWR). During start up and shut down or, due to fluctuations in operating conditions or, seismic activities can trigger cyclic plastic loading. The field of application make the material 'safety critical'. Hence, considering the structural integrity aspect, it is important to comprehend the cyclic plastic behaviour of the material.

The fatigue behaviour of metals is quite structure sensitive. It is sometimes meticulous and often impossible to conduct physical experiment for every component or the entire assembly. Therefore, numerical simulation is promoted. An accurate simulation requires a technically sound material model. The present work intends to model the material behaviour comprehending the minute details on the basis of observable micro-mechanics. In order to model the cyclic plastic behaviour of the material SA333, some mechanical tests are done under different complex cyclic loading conditions for simple geometries. It is realized, in the course of the work, that the dislocation interactions holds the key to explain the material responses observed in the experiment, and therefore, the metallurgical investigations are carried out and revealed a detailed inner view of the variety of cyclic plasticity phenomena shown by the material.

Experimentation: the low cycle fatigue behaviour of SA333 is evaluated for uniaxial and for both proportional and non-proportional multiaxial (biaxial tension-torsion) loading conditions. The material is also subjected to uniaxial and multiaxial asymmetric (ratcheting) loading conditions.

The predominant behaviour of the material includes cyclic softening, non-proportional hardening and ratcheting due to asymmetry in loading (figure 1). Modellings for the observed behaviours are attempted in this work and therefore, a sound understanding of the micro-mechanism is indispensable.

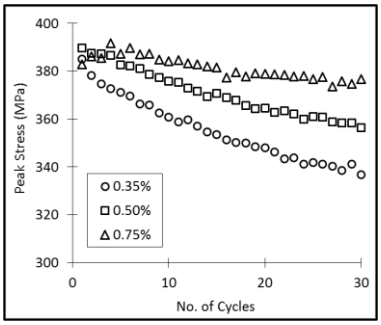

Figure 1a: *Cyclic softening.*

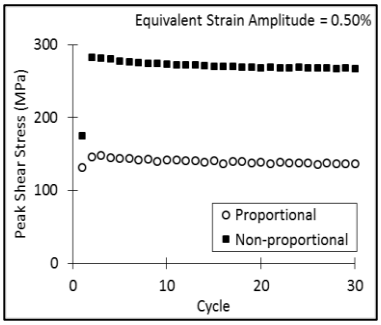

Figure 1b: *Non-proportional hardening.*

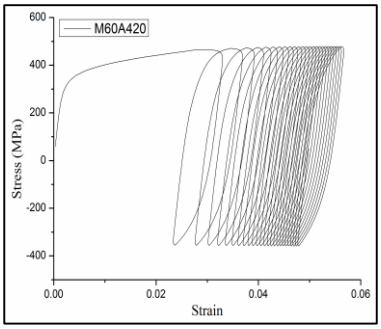

Figure 1c: *Ratcheting.*

In order to understand the physics behind the macroscopic phenomena, relevant metallurgical investigations are carried out and discussed later in the context of modelling. But before that, some of the pertinent theories and significant philosophies are reviewed and acquainted with.

Understanding of the micro-mechanics: It is the nature of the dislocations and their interactions, which distinguishes macroscopic material behaviours. The hardening functions, which are directly related to the dislocation interactions, can be used to mathematically describe the stress-strain responses in the plastic domain. Hardening response is developed due to the restriction to the free glide of mobile dislocations. These restrictions are evolved due to many reasons, among which, interaction of two dislocations shows versatile behaviour including softening. Interacting dislocations can have different kinetics and can lie in different slip systems. In the work of Kubin et. al. (2008), the possible interactions of dislocations are classified in six kinds, three of them are accounted for forest interactions between non-coplanar slip systems, resulting in the formation of junctions or locks, namely the Lomer–Cottrell lock, the Hirth lock and the glissile junction. There are two non-contact interactions for dislocations gliding in parallel slip planes with same or different Burger's vectors, known as the self-interaction and the coplanar interaction. And the last interaction is the collinear interaction, produces annihilations. In BCC and FCC crystals, there are twelve such slip systems exist, which can be activated easily.

Table 1: *BCC Slip Systems*

Slip Plane	Slip Direction	No. of Slip Systems
{110}	<111>	12
{112}	<111>	12
{123}	<111>	24

The total possible interactions between mobile dislocations in a BCC crystal can be captured by a matrix of 144 (12×12) interaction coefficients (Franciosi, 1985). This interaction matrix actually designates the generalised hardening character of the material. It is reported by Kubin and his co-workers (2008) that, there are only six independent coefficients, are associated with six different types of dislocation interactions, can represent the entire matrix considering symmetry assumptions.

During cyclic plastic deformation, continuous generation and annihilation of dislocations occur simultaneously and, the remaining dislocations at any instance, try to align themselves such as to reduce their individual contribution to the stored energy. The reorganisation of dislocations can resolve through entanglements quickly within a few cycles. The rearrangements of dislocations are resulting in from the dissimilar rotations of the neighbouring lattices (Read and Shockley, 1950). These reorientations of the dislocations continue to occur to a certain extent of plastic deformation, and by the time, the stable dislocation substructures are fully developed (Sedláček et. al., 2002). Ackermann et. al. (1984) suggested an evolution procedure which described the formation of dislocation substructures as a function of the cycles in cyclic loadings.

Doong et. al. (1990) explained that, In general, the dislocation substructure may be classified into five categories – planar dislocations, matrix veins, ladders or walls, cells, and labyrinths. Structures consisting of only planar dislocations occur in low stacking-fault energy materials. Matrix veins are tangles of edge dislocations along the major slip plane of the material. Between these tangles, channels free of dislocations are formed by the movement of screw dislocations. Ladders are bands of cleared channels and dense walls. It has been suggested that the ladder and wall structures are formed by small-scale secondary glide in the matrix vein when a critical dislocation density is reached. The formation of cell structures was found to be associated with multiple slip systems.

The cellular substructures are surrounded by walls consist of rough tangles of dislocations and the interiors of the cells have a correspondingly much lower dislocation density. The sub-cells often disoriented during initial stages of plastic deformation. The simplest case of ‘misorientation’ can be tilted sub-grains forming low angle tilt boundary (as sub-grains are tilted symmetry of one another – Bragg, 1940; Burger, 1940; Shockley and Read, 1949; Read and Shockley, 1950) with an array of edge dislocations and with misorientation angle less than 15°. The orientation of dislocations in their minimum energy positions leave traces may be manifested as the memory effect.

The interacting dislocations, for the sake of simplified model, can be broadly categorised into three families, namely forward, reverse and latent dislocations depending on their origins. The total instantaneous dislocation density can be additively decomposed into three families, $\rho = \rho_f + \rho_r + \rho_l$ respectively associated with the forward, reverse and latent interactions. For monotonic loading, the net dislocation density available at any instance can be regarded as the forward dislocation density (ρ_f). This mainly contributes to the hardening by forest pile-up according to the Taylor model (Taylor, 1934; Davoudi, 2014). The standard kinematic hardening rules of Armstrong-Frederick (1966) format include the changes of forward dislocation densities through its hardening (first) term.

In-process Change in strain-path, may activate new slip systems in the crystals lattice and the total or a part of the available dislocations (density ρ_f), stored in the previously activated slip

systems (before the strain-path change occur), are transferred into the newly activated slip systems. This transfer causes a sudden dislocation crowd most likely to entangle in the newly active slip systems. The resistance because of the pile-up thus produces a hardening effect in those slip systems.

Any dislocations with opposite Berger's vector originate the reverse dislocation family even during the monotonic forward loading. In addition, when the strain-path is reversed (180°), a part of the available (previously stored) dislocation density, sensitive to the polarity of the stress, fortifies the reverse family and disappears gradually (Rauch et. al., 2007) due to strong collinear interactions. The disappearance of the polarized fraction of the dislocation density (ρ_r) is manifested as the Bauschinger effect. The dynamic recovery terms of any standard kinematic hardening rules in Armstrong-Frederick format, is designed to reproduce the reverse dislocations interactions in mathematical material models and thereby simulate the Bauschinger effect.

The changes in direction of strain-path between 0° to 180° is classified as non-proportional loading. The part of the dislocation density to be transferred is related on the degree of non-proportionality and causes the latent hardening effect. The kinematic hardening rules do not incorporate the additional (latent) hardening due to non-proportional strain-path change. Just after the strain path changes, the sudden increase in the flow stress is observed in the respective (newly active) slip system due to the dislocation pile-up, which causes the cross hardening effect with non-proportional hardening. The effect of latent hardening should be manifested in the latent slip direction only. Therefore, in the material model, anisotropy is required to be incorporated, enabling the provision of adding the non-proportional hardening to the anisotropic flow stress in specific slip system as a function of latent dislocation density. The built-up dislocation structure in the first deformation path becomes unstable when a sudden and abrupt change in strain-path occurs (Barlat et. al., 2003; 2011), though, after considerable plastic deformation and ample time for the strain-path change events to familiarise, multi-slip structures begin to form (Doong et. al., 1990).

Micro-mechanics based mathematical modelling of the material behaviour: Beyond yield (represented by suitable criterion), the basic stress-strain hysteresis loops are modelled by incorporating a kinematic hardening rule in the model. The Armstrong-Frederick (1966) format of the kinematic hardening rule includes a dynamic recovery term which represents the contribution of reverse dislocation family and simulates the Bauschinger effect. The dynamic recovery of back stress introduces the non-linearity in the hysteresis curvature. The kinematic hardening rule is described as a function of plastic strain. Sometimes, for achieving better agreement with the hysteresis non-linearity, coefficients are evaluated segment-wise based on the plastic strain range. Inspired by Besseling (1958) type multi-segment formation and conforming non-linear Armstrong-Frederick (1966) phenomenology for each segments, Ohno and Wang (1993) developed a multi-segmented (generally 6) non-linear kinematic hardening rule. The first terms of each segment offers the hardening due to dislocation pile-up and the

seconds, gives the recovered energy due to annihilation of mobile dislocations at certain state of plastic deformation. The recovery activities of each segment can be controlled by a fitting parameter and are limited by the back stress thresholds.

The incorporation of non-linear and segmented kinematic hardening rule successfully simulate the saturated stress-strain hysteresis loops (figure 2), because the kinematic hardening parameters were extracted from the Masing saturated cycles.

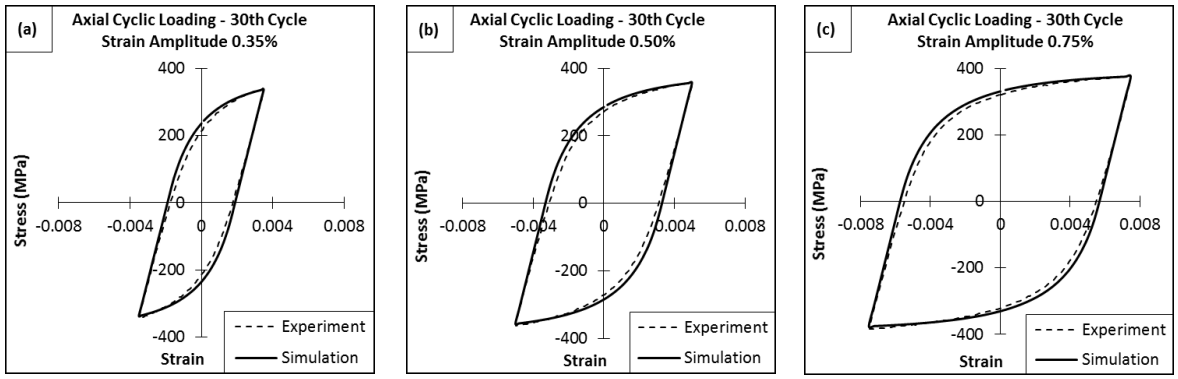

Figure 2: *Comparison of (uniaxial) experimental and simulated stress-strain hysteresis loops for strain amplitude* ***(a)*** *0.35%,* ***(b)*** *0.50% and* ***(c)*** *0.75% at saturated (30th) cycle.*

The experimental observation shows (figure 1a) that the material, under study, shows predominant cyclic softening in initial transition cycles for proportional and non-proportional loading conditions, but the kinematic hardening rule cannot simulate cyclic softening response although the effect of the annihilations of the mobile dislocations are already incorporated in the dynamic recovery. In search of the source of cyclic softening, further metallurgical investigation revealed that, sub-granular dislocation structure formed in-process (figure 3). The formations of adequate number of sub-structures depend on loading conditions and many other factors like, material microstructure, previous loading history, undergone heat treatment, etc.

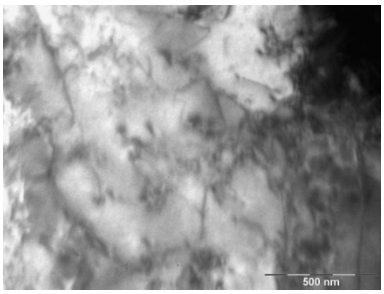

Figure 3a: *TEM micrograph at 'as received' condition.*

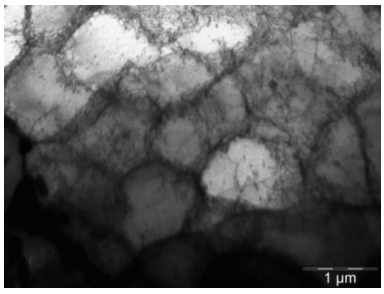

Figure 3b: *TEM micrograph after 10 cycles (1% Strain amplitude).*

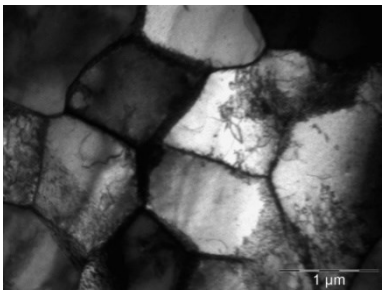

Figure 3c: *TEM micrograph after failure (1% strn ampl, 500 cycles).*

A moving dislocation, in the vicinity of sub-structure, takes part either by pilling-up at sub-grain walls reinforcing the wall entanglements or, by getting annihilated with its compatible pair, undermining the wall and relieving some stored energy, schematically shown in the fig.4.

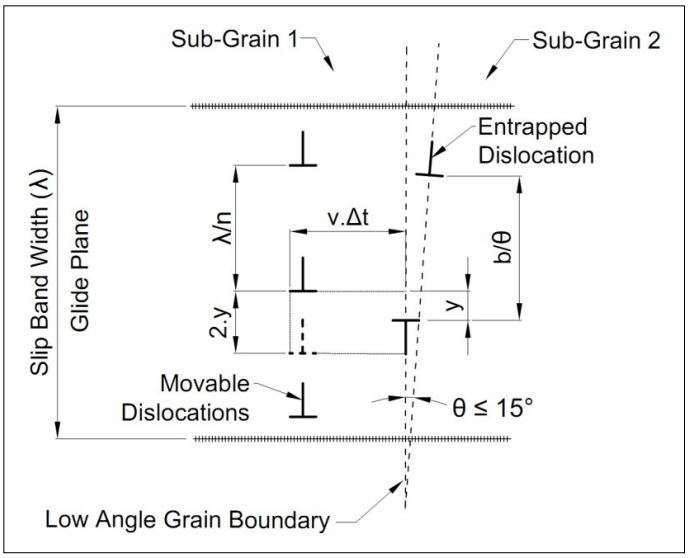

Figure 4: *schematic representation of annihilation of dislocations at low angle grain boundary.*

The released energy makes free passage for the remaining dislocations resulting the isotropic softening effect. Though the overall manifestation of the annihilation is softening, the dissimilar kinetics of the dislocations involved, have different impacts on the microstructure and the stress response of the material. The effect of annihilated mobile dislocations is generally included in the 'dynamic recovery' of the kinematic hardening (KH) rule (Mecking and Kocks, 1981; Kocks and Mecking, 2003) with the directional behaviour. Annihilation of the stationary dislocations entrapped in the sub-cell wall, can undermine the sub-granular structure (Sauzay et. al., 2005; Fournier et. al., 2011). The reductions of boundary dislocations primarily resolve the boundary misorientation and eventually cause the dissolution of the boundary as observed for large strain applications. Thus, the effect of annihilations of boundary dislocations can be a reasonable phenomenon to justify cyclic softening in low cycle fatigue (LCF) loadings.

Lattice reorientation facilitates accumulation of dislocations at favourable locations and gradually piled-up to form the boundary for misoriented sub-grains. Simultaneous annihilations of dislocations from the locality undermine the formation and eventually disband the boundary (grain growth). With increasing plastic deformation, the reorganisation of the crystal lattices gradually get optimized and the misorientation of the sub-grains reduces. The reduction of the misorientation is directly related to the saturation of cyclic softening.

The mechanism is incorporated in the model as isotropic stress, and the results obtained are in good agreement with the symmetric uniaxial low cycle fatigue experimental results (figure 5). Therefore, it can be said that the mechanism of annihilation of low angle grain boundary dislocation can be responsible for the cyclic softening.

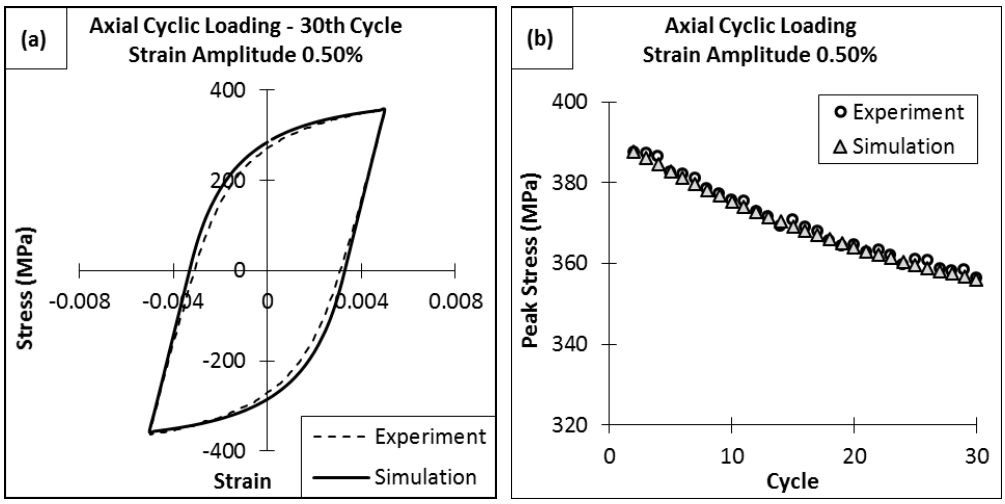

Figure 5: *Comparison of uniaxial experimental and simulated results for 0.50% strain amplitude,* ***(a)*** *stress-strain hysteresis loops at 30th cycle,* ***(b)*** *peak stress vs. number of cycles.*

The multiaxial proportional loading shows alike behaviour as uniaxial case for symmetric loading, as in both the cases no non-parallel strain-path changes occur. Therefore, the transferability of the softening model can be checked in symmetric proportional multiaxial tension-torsion loading. The matching between experimental and simulated peak stress softening curve assures the efficacy of the model for the said loading conditions also (figure 6 shows such comparison for one representative strain amplitude). The deformation induced non-proportionality, causes the mismatch observed in one axis, which is required to be investigated.

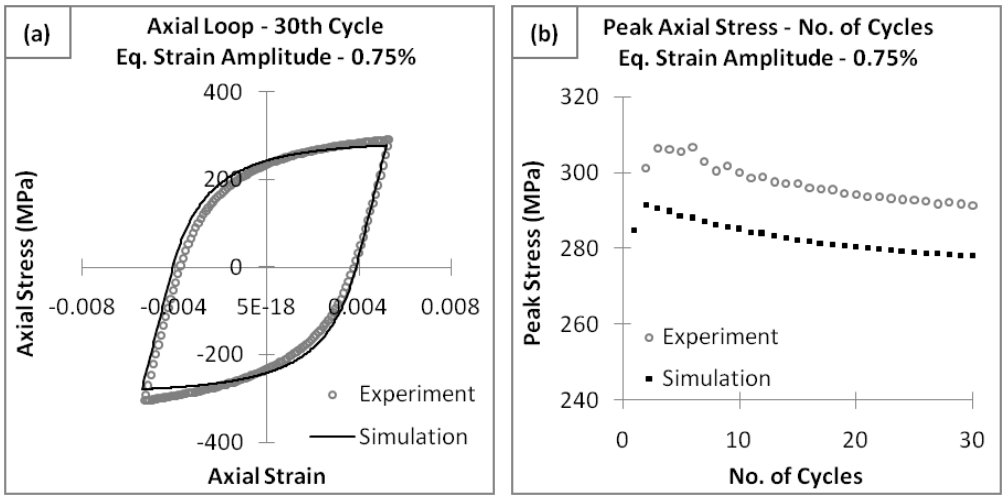

Figure 6: *Comparison of in-phase biaxial tension-torsion experimental and simulated results for 0.75% equivalent strain amplitude,* ***(a)*** *axial stress-strain hysteresis loops at 30th cycle,* ***(b)*** *Peak axial stress vs. cycles.*

The non-proportionality in loading condition gives rise to two types of additional hardening in the material, namely: non-proportional hardening and cross hardening effect (Benallal and Marquis, 1987). Further metallurgical study reveals that, these additional hardenings evolve due to the changes occur in the strain-path.

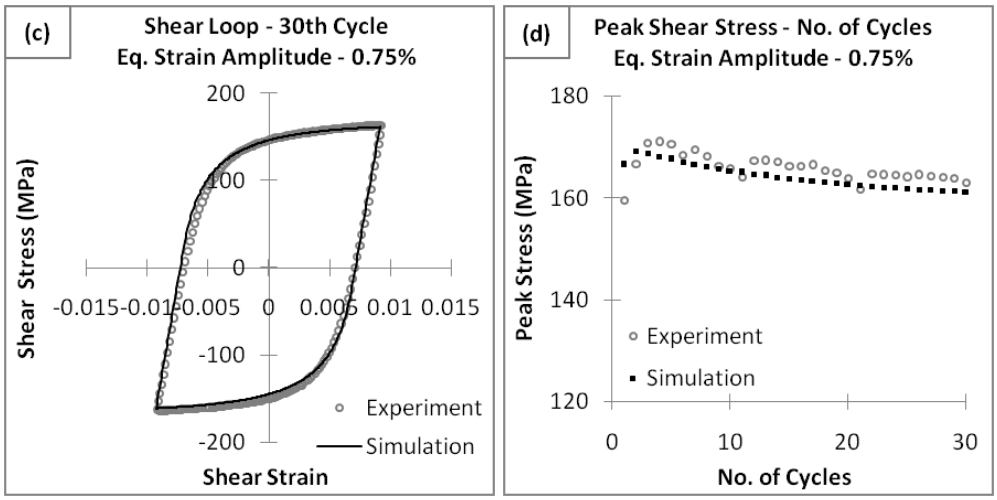

Figure 6: *Comparison of in-phase biaxial tension-torsion experimental and simulated results for 0.75% equivalent strain amplitude,* ***(c)*** *shear stress-strain hysteresis loops at 30th cycle* ***(d)*** *Peak shear stress vs. cycles.*

Changes in the strain-path can activate different slip systems. The built-up dislocation structure in the first deformation path becomes unstable when a sudden and abrupt strain-path change occurs (Barlat et. al., 2003; 2011), The starting of sub-cell formation under non-proportional loading for this material with adequate randomly distributed dislocations (figure 3a) can be delayed for a few initial cycles for a steady state events due to strain path change to occur.

It can be speculated that, a huge number of dislocations get immediately transferred from already active slip systems to the newly active slip systems. The transferred dislocations are usually piled-up to deliver an extra hardening and gradually get streamlined and mobile. The phenomena is called latent effect (Franciosi, 1985; Barlat et. al., 2003; 2011; Rauch et. al., 2011). The transferred dislocations are usually piled-up initially to deliver a sudden rise in flow stress as cross hardening and gradually get streamlined, mobile and naturally evolving. While the dislocations remain tangled in the matrix, all the mobile dislocations in every active slip systems experience constriction and overall manifestation is isotropic non-proportional hardening. Latent hardening can therefore be recognised as the micro-mechanism behind sudden cross hardening and gradually influencing non-proportional hardening as observed in the non-proportional experiments.

Fundamentally, the interactions of forward dislocations in the primary slip systems are incorporated in the KH rule as the hardening term. The interactions of reverse dislocation population is captured by the dynamic recovery mechanism (Kocks and Mecking, 1979). But, the KH rule remains insensitive to the interaction of the latent dislocations developed by the non-parallel strain-path changes.

To activate latent effect for non-parallel strain paths in the mathematical model, a non-proportionality trigger is required. The non-proportionality caused by the above reason, can be sensed by measuring the angle between deviatoric stress rate vector and plastic strain rate vector. The degree of non-proportionality is scaled from zero to one respectively for parallel

to orthogonal strain-path changes and introduced in numerical modelling as proposed by Benallal and Marquis (1987). This numerical parameter, if detects any differences in loading phases, triggers the latent hardening mechanisms and amplifies the non-proportional hardening effects according to the degree of non-proportionality. The forward dislocation density is calibrated by the size of the plastic strain memory surface (Chaboche et. al., 1979; McDowell, 1985) to capture the cumulative effect of plastic deformation and activation of new slip planes.

The simulation results are compared with experimental results and in the peak shear stress direction a considerable under-estimation is observed (figure 7 shows such comparison for one representative strain amplitude), which indicate the anisotropic behaviour of the non-proportional hardening. The transferability of the softening function in different loading conditions are validated by the good estimation of cyclic softening.

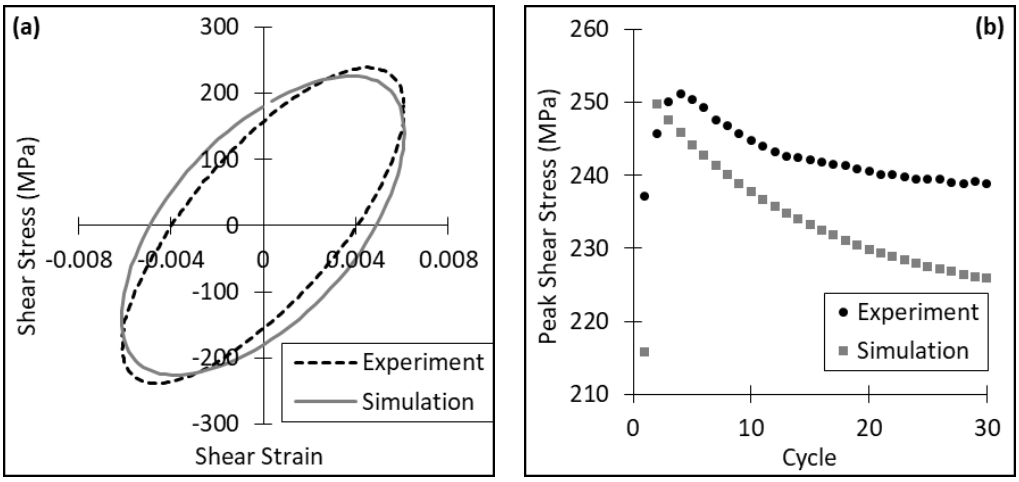

Figure 7: *90° out-of-phase tension-torsion experimental and simulated results for 0.35% equivalent strain amplitude,* ***(a)*** *shear stress-strain hysteresis loops at 30th cycle* ***(b)*** *Peak shear stress vs. cycles.*

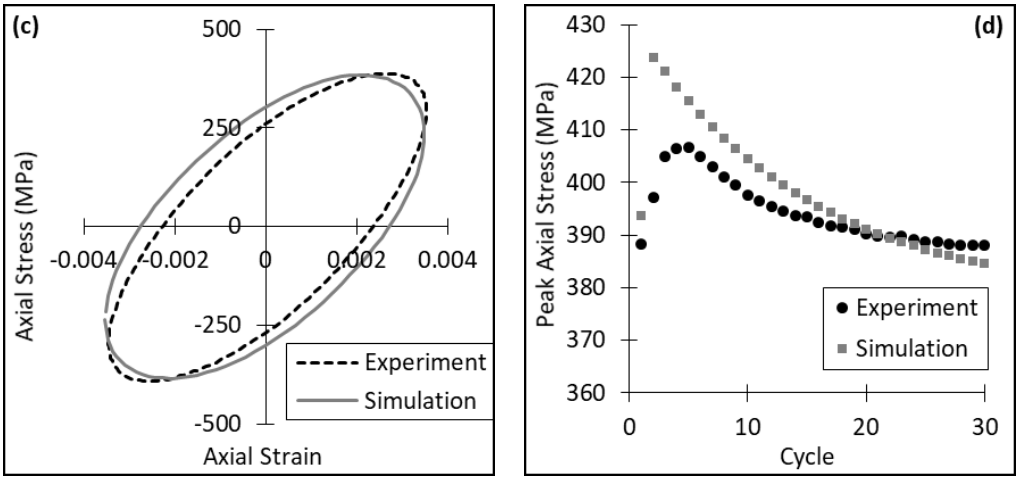

Figure 7: *90° out-of-phase tension-torsion experimental and simulated results for 0.35% equivalent strain amplitude,* ***(c)*** *axial stress-strain hysteresis loops at 30th cycle,* ***(d)*** *Peak axial stress vs. cycles.*

The Ohno-Wang (OW) multi-segmented kinematic Hardening rule amended with cyclic softening and non-proportional hardening mechanisms successfully simulates symmetric uniaxial, proportional and non-proportional stress-strain behaviour of the material well.

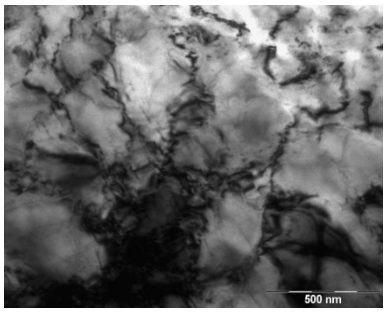

Figure 8a: *TEM micrograph of SA333 subjected to M80A310 ratcheting loading, after half lifetime (5000 Cycles).*

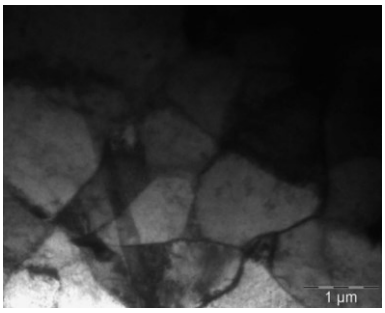

Figure 8b: *TEM micrograph of SA333 subjected to M80A310 ratcheting loading, after failure (longitudinal section).*

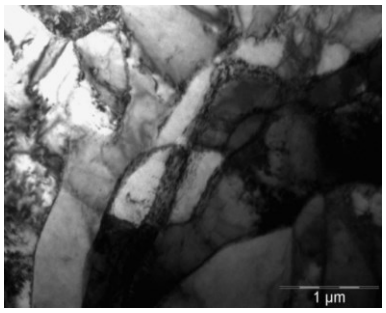

Figure 8c: *TEM micrograph of SA333 subjected to M80A310 ratcheting loading, after failure (cross section).*

But, for the asymmetric (unbalanced) cases, the sub-grain formation gets delayed, as observed in the TEM micrographs (figure 8), due to continuous generation of dislocation. The kinematic hardening rule alone cannot capture the material response and eventually over-predicts the as reported in the literature (Bari and Hassan, 2000).

The experimental results show accumulation of plastic strain per cycle for stress controlled cycling, popularly known as ratcheting. The ratcheting strain accumulation in the primary and secondary stages of ratcheting closely resembles with the hardening curve of a stress controlled analysis and can be described by the increment in the size of the plastic strain memory surface. Ratcheting strain gives rise to generation of new dislocations in the microstructure. The dislocations interact with themselves and other dislocations in the vicinity, ending up with only entanglement initially. Gradually they annihilate and reorient as well. Therefore, they influence hardening initially which is witnessed in the primary stage and is recovered by the course of time, manifested at the secondary stage.

The phenomena can be modelled by modifying the hardening part of the kinematic hardening rule. The instantaneous dislocation density due to ratcheting is used to develop an exponential scaling function. The function (Dong et. al., 2014) is employed to modify the kinematic hardening parameter related to hardening. Though, a phenomenological bound is also employed on the evolution of the parameter which is calibrated from the experimental results.

The modelling shows convincing results in uniaxial and in-phase multiaxial ratcheting response of the material. Figure 9 and 10 shows comparison of results for representative uniaxial and multiaxial cases respectively. The model provides a physical based single parameter approach to simulate the effect of mean stress and stress amplitude on ratcheting. The simulated ratcheting rate shows good agreement with the experimental results.

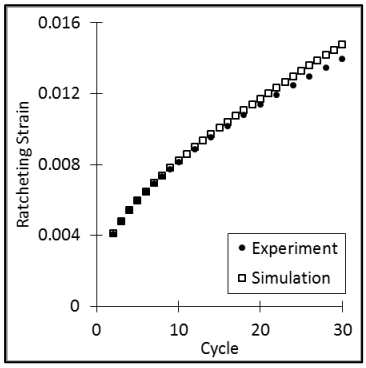

Figure 9a: *uniaxial ratcheting for mean stress 80MPa and stress amplitude 310MPa*

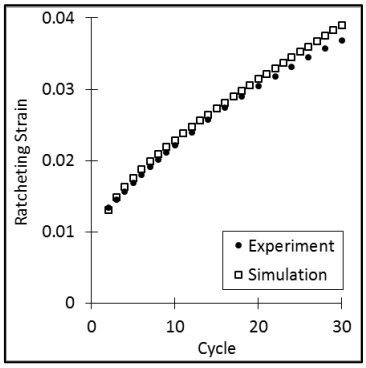

Figure 9b: *uniaxial ratcheting for mean stress 80MPa and stress amplitude 350MPa*

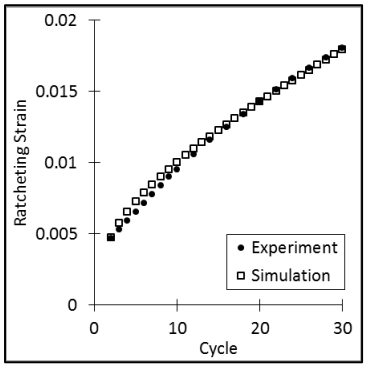

Figure 9c: *uniaxial ratcheting for mean stress 40MPa and stress amplitude 350MPa*

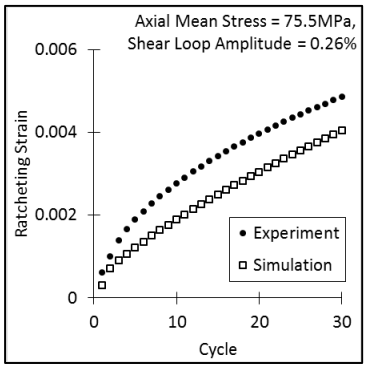

Figure 10a: *biaxial (tension-torsion) ratcheting for axial mean stress 75.5MPa and shear strain amplitude 0.26%*

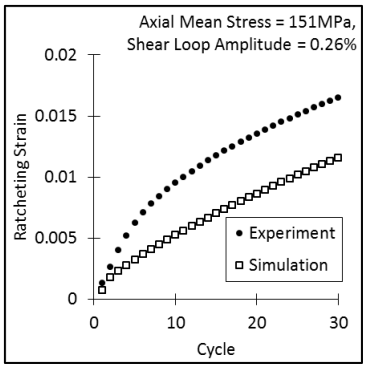

Figure 10b: *biaxial (tension-torsion) ratcheting for axial mean stress 151MPa and shear strain amplitude 0.26%*

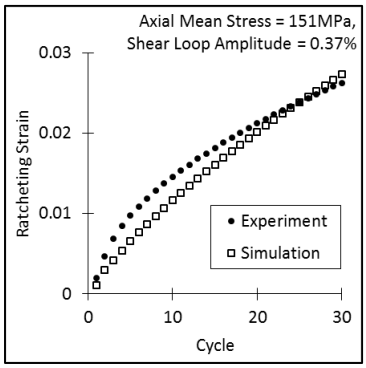

Figure 10c: *biaxial (tension-torsion) ratcheting for axial mean stress 151MPa and shear strain amplitude 0.37%*

The validation: the model integrated into 3DS SIMULIA ABAQUS CAE (v6.8) commercial finite element software in the form of user defined material subroutine (UMAT) for the simulations of the material behaviour under static (rate independent) cyclic loading conditions. Backward Euler (radial return) integration scheme is used in the subroutine to implicitly solve for stress components and plastic strain increments are determined through iterative search method. After convergence of the Newton-Raphson iterations for the plastic strain, the state of elastic strain is compensated by return mapping and the consistent material tangent is calculated from the constitutive stress-strain relations. The material tangent is required by the software (ABAQUS) to solve (convergence) the finite element governing equation. Care has been taken during discretizing the geometry, hexahedral elements with linear shape functions are selected with full integration avoiding hourglass problem. The boundary conditions are imposed in cylindrical coordinate system to maintain the symmetry and simplicity while loading is applied on a reference point which is tied with the cross-sectional surface through kinematic coupling. The finite element model itself and the material model are validated by comparing simulated results with experiments.

References:

3DS SIMULIA ABAQUS CAE (v6.8), User's Manual.

1934, Taylor, G. I., The mechanism of plastic deformation of crystals, part 1 – theoretical, Proceeding of the Royal Society of London, Series A, Volume 145, Issue 855, pp 362-387.

1940, Bragg, W. L., The structure of a cold worked metal, Proceedings of the Physical Society, Volume 52, Issue 1, pp 105-109.

1940, Burger, J. M., Geometrical considerations concerning the structural irregularities to be assumed in a crystal, Proceedings of the Physical Society, Volume 52, Issue 1, pp 23-33.

1949, Shockley, W., Read, W. T., Quantitative Predictions from Dislocation Models of Crystal Grain Boundaries, Physical Review, Volume 75, Issue 4, pp 692.

1950, Read, W.T., Shockley, W., Dislocation models of crystal grain boundaries, Physical Review, Volume 78, Issue 3, pp 275-289.

1958, Besseling, J. F., A Theory of Elastic, Plastic and Creep Deformations of an Initially Isotropic Material. Journal of Applied Mechanics, Volume 25, pp 529-536.

1966, Armstrong, P. J., Frederick, C. O., A Mathematical Representation of the Multiaxial Bauschinger Effect. CEGB Report No. RD/B/N 731.

1979, Chaboche, J. L., Dang Van, K., Cordier, G., Modelization of the strain memory effect on the cyclic hardening of 316 stainless steel, SMiRT-5, Berlin.

1979, Kocks, U. F., Mecking, H., in Strength of Metals and Alloys, (Edited by: P. Haasen, V. Gerald and G. Kostorz), Pergamon Press, Volume 1, pp 345-350.

1981, Meckings, H., Kocks, U. F., kinetics of flow and strain-hardening, Acta Metallurgica, Volume 29, pp 1865-1875.

1984, Ackermann, F., Kubin, L. P., Lepinoux, J., Mughrabi, H., The Dependence of Dislocation Microstructure on Plastic Strain Amplitude in Cyclically Strained Copper Single Crystals, Acta Metallurgica, Volume 32, Issue 5, pp 715-725.

1985, Franciosi, P., The concepts of latent hardening and strain hardening in metallic single crystals, Acta Metallurgica, Volume 33, Issue 9, pp 1601-1612.

1985, McDowell, D.L., A two surface model for transient nonproportional cyclic plasticity, Journal of Applied Mechanics, Volume 52, Issue 2, pp 298-302.

1987, Benallal, A., Marquis, D., Constitutive equation for nonproportional cyclic elasto-viscoplasticity, Journal of Engineering Materials and Technology, Volume 109, pp 326-336.

1990, Doong, Shiing-Hwa, Socie, D. F., Robertson, I. M., Dislocation Substructures and Nonproportional Hardening, Journal of Engineering Materials and Technology, Volume 112, Issue 4, pp 456-464.

1993, Ohno, N., Wang, J.D., Kinematic hardening rules with critical state of dynamic recovery, part I: Formulation, International Journal of Plasticity, Volume 9, Issue 3, pp 375-390.

2000, Bari, Shafiqul, Hassan, Tasnim, Anatomy of coupled constitutive models for ratcheting simulation, International Journal of Plasticity, Volume 16, pp 381-409.

2002, Sedláček, R., Blum, W., Kratochvíl, J., Forest, S., Subgrain Formation during Deformation - Physical Origin and Consequences, Metallurgical And Materials Transactions A, Volume 33A, pp 319-327.

2003, Barlat, F., Ferreira Duarte, J. M., Gracio, J. J., Lopes, A. B., Rauch, E. F., Plastic flow for non-monotonic loading conditions of an aluminum alloy sheet sample, International Journal of Plasticity, Volume 19, pp 1215-1244.

2003, Kocks, U. F., Mecking, H., Physics and phenomenology of strain hardening: the FCC case, Progress in Material Science, pp 171-273.

2005, Sauzay, M., brillet, H., Monnet, I., Mottot, M., Barcelo, F., Fournier, B., Pineau, A., Cyclically induced softening due to low-angle boundary annihilation in a martensitic steel, materials Science and Engineering: A, Volumes 400-401, pp 241-244.

2007, Rauch, E.F., Gracio, J.J., Barlat. F., Work-hardening model for polycrystalline metals under strain reversal at large strains, Acta Materialia, Volume 55, pp 2939-2948.

2008, Kubin, L., Devincre, B., Hoc, T., Modeling dislocation storage rates and mean free paths in face-centered cubic crystals, Acta Materialia, Volume 56, Issue 20, pp 6040-6049.

2011, Barlat, Frederic, Gracio, Jose J., Lee, Myoung-Gyu, Rauch, Edgar F., Vincze, Gabriela, An alternative to kinematic hardening in classical plasticity, International Journal of Plasticity, Volume 27, pp 1309-1327.

2011, Fournier, B., Sauzay, M., Pineau, A., Micromechanical model of the high temperature cyclic behavior of 9-12%Cr martensitic steels, International Journal of Plasticity, Volume 27, Issue 11, pp 1803-1816.

2014, Davoudi, K. M., Vlassak, J. J., Dislocation evolution during plastic deformation: equations vs. discrete dislocation simulations, arXiv preprint arXiv: 1408.6609.

2014, Dong, Yawei, Kang, Guozheng, Yu, Chao, A dislocation-based cyclic polycrystalline visco-plastic constitutive model for ratcheting of metals with face-centered cubic crystal structure, Computational Material Science, Volume 91, pp 75-82.

Blank Page

NOMENCLATURE

List of Subscripts and Superscripts

Subscripts

0	Initial (σ_0 = Initial yield stress)
c	Current (σ_c = Current yield stress) Critical (ρ_c = Critical dislocation density)
1	Softening
2	Hardening
ij	Second order tensor indices
eq	equivalent
mises	Von-Mises norm
Taylor	Taylor pile-up stress
CRSS	Critical resolved shear stress
n	Number of active slip systems
f	In forward family
r	In reverse family
l	In latent family
˜	In forward direction in latent system

Superscripts

i	Current or, i^{th}
1	Current
0	Previous
e	Elastic
p	Plastic
trial	Trial value or function
+	Incomplete Update
m	Number of segments of each back stress components
k	Current segment of each back stress components (also in subscript)

List of Prefixes, Operators and Indices

Δ	Increment Range
∂	Partial differential operator
d	Total differential operator
‘	Space derivative
˙	Time derivative or rate
δ	Kronecker delta $\left(\delta_{ij}\right)$
Tr()	Tress operator
H()	Heaviside function

List of Symbols

a	Power law coefficient
m	Power law exponent Mean stress
μ or G	Lame's parameter or Shear modulus
λ	Lame's parameter Non-negative plastic multiplier (dλ) Softening Coefficient (Marquis approach) Slip band width
E	Young's modulus
ν	Poisson's ratio
σ	Stress
ε	Strain
S	Deviatoric stress Number of active slip system (S_n)
α	Deviatoric back stress (α_{ij}) A strength factor for dislocation interaction
φ	Yield function
R	Isotropic hardening stress
h	Modulus of plasticity
n	Flow vector (n_{ij}) Number of possible annihilation sites within a slip band
n*	Normal direction to the plastic strain memory surface
C, r	Material parameters regarding Kinematic Hardening
χ	Power to the dynamic recovery term, usually = 0 for LCF and > 0 for ratcheting
K	Softening constant (Marquis approach) Interaction constant (dislocation bowing-out)
ω	Softening exponent (Marquis approach)
l	Back stress direction tensor (l_{ij})
L	Bowing out distance of a dislocation
y	Critical annihilation distance
ρ	Mobile dislocation density (m^{-2}) in the forward direction
Λ	Dislocation density at sub-grain boundary (m^{-1})
v	Velocity of edge dislocation
t	Small time
γ	Slip
b	Magnitude of Burger's vector

M	Average Taylor factor
D	Sub-grain diameter
p	Probability of total annihilation
θ	Sub-grain boundary 'misorientation' angle Loading phase angle
τ	Shear stress
F	Plastic strain memory surface
β	Centre of the plastic strain memory surface
q	Radius of the plastic strain memory surface
η	Expansion coefficient for plastic strain memory surface
ξ	Shift coefficient for plastic strain memory surface
A	Non-proportionality parameter (Benallal type)
K_l	Latent hardening coefficient
f	function
$\overline{\chi}$, χ_0 , χ_{sat} , B	Material parameter for the evolution of kinematic hardening parameter (r)

LIST OF FIGURES

LIST OF TABLES

Blank Page

Chapter 1

INTRODUCTION

In this chapter, a brief chronological review on the metal fatigue and related material behaviour is carried out. Several modelling attempt and simulation methodology are also surveyed in the available literatures. From the survey, a goal has been set and subdivided into several benchmarks. Necessary experimentation, tools and methods are also discussed.

Content **Page**

Blank Page

1.1 Introduction

Structural members and machine elements can fail to perform their functions in three possible ways. Most common and age old consideration is yielding causing excessive permanent deformation in the plastic regime of the material. Excessive deformations even in the elastic range can also be treated as failure, when the member or the machine element loses its necessary geometric accuracy temporarily. A design engineer can take care of such failure aspects by choosing right material and right geometry for simple loading conditions. But in reality, these components are mostly subjected to vibrations and other kind of repeated loading conditions and the material contains inclusions and flaws in microscopic levels. In this circumstances, it is observed that, no matter how carefully the component is designed after certain lifespan, the material failure is all but certain by progressive fracture or commonly known as fatigue failure.

The component eventually fails for a much lower operating stress than the corresponding static strength of material due to fatigue. The difficulty in fatigue is that it occurs without a visible sign caused by a critical localised tensile stress which is very difficult to locate and evaluate, though, the fatigue fracture occurs after a considerable period of service called 'fatigue life'. At some point in service, micro cracks initiate in the component at a localised spots, generally at the concentrated stress points and gradually spread through the cross-section until the member loses its load bearing capacity. Therefore, the study of fatigue behaviour of a material has gain interest.

Material undergoing cyclic plastic deformation, generally experience low cycle fatigue. In such cases, there are different stress-strain responses observed during the fatigue life. These material responses should be evaluated thoroughly to quantify and understand if any other underlying mechanism or damage is influencing the fatigue life.

The fatigue life is delicately structure sensitive. At macroscopic level, component geometry like size, shape and surface texture influence the fatigue life. It is observed that, even in the microscopic level the fatigue life is influenced by grain size, defects and inclusions, staking fault energy and dislocation structure. Therefore, a rigorous experimentation for different geometries and appropriate metallurgical investigations are critical aspects in characterising fatigue behaviour of a material. But sometimes, large and irregular geometry of components limit the practicability of physical experimentation. So, from the feasibility and economic point of view, the rigorous experimentation is better substituted by numerical simulations, ministered by carefully defined mathematical material model. For standard specimen geometries, observations from a few mechanical tests can set up the framework for the material model and metallurgical investigations can further substantiate its effectiveness. With the implementation of a capable material model factors like the size, shape and surface finish of the component/specimen results in factual fatigue behaviour in numerical simulations. Nowadays, powerful electronic computers and commercial numerical analysis software are readily available, making the simulation a fast, easy and accurate mathematical tool for the study of fatigue. Though the accuracy of the simulation

explicitly depend on the mathematical approximations and domain decomposition schemes.

The present work deals with a small part of the study of fatigue in design. This work intend to develop a micro-mechanism based material model for a specific material, subjected to specific loading conditions. The model is validated through the finite element simulations of standard specimen geometries with standard experimentations of the same. The transferability of the model is also checked for other specimen geometries and different loading arrangements. But, before getting into the technical details of the discussion, a brief account of progress on the subject should be discussed.

1.2 Literature Review

A brief chronological discussion on the understandings, recorded attempts and inventions related to fatigue and associated material behaviours are presented below, along with a brief account of the development of the different material models and numerical analysis. This general discussion converge the focus on the objective of the present work for better perspective and significance.

1.2.1 Chronology of fatigue research

Early in the 19th century the concept of fatigue draws the attention of researchers working mainly on mining and railway industries. The first known contribution is made by a German engineer, named W. A. J. Albert in 1837 (Pook, 2007) devised a testing machine for hoist chains used in mines and published the first article on fatigue. The first fatigue test results published in English appear to be those by Fairbairn (1864) on repeated bending fatigue tests on beams. Rankine (1842) recognised the importance of stress concentrations during investigation of the Versailles Train Crash incident. Braithwaite (1854) reported common service fatigue failures and coined the term ‘fatigue’. Ewing (1903) demonstrated the origin of fatigue failure in microscopic cracks. Basquin (1910) proposed a log-log relationship for S-N curves, using Wöhler’s (1870) test data. Miner (1945) popularised Palmgren’s (1924) linear damage hypothesis as a practical design tool for fatigue.

If applied load amplitude is low enough to deform the material only elastically, the material survives a large number of cycles, and known as 'High Cycle Fatigue' (HCF).Fatigue is the localised and progressive structural damage. The fatigue damage is cumulative and the materials do not recover when relieved (Palmgren, 1924; Miner, 1945). Eventually a crack will grow unto a critical size and then propagates suddenly to catastrophic fractures. The failure process is divided in the following stages (Laird et al., 1979):

- Crack initiation by microstructural damage, the early development of fatigue damage (Polakowski and Palchoudhuri, 1954).
- Slip-band crack growth involves the deepening of micro cracks on planes of high shear stress. This is frequently called Stage-I crack growth (Ritchie, 1979).

- Crack growth on planes of high tensile stress involves growth of well-defined crack in direction normal to maximum tensile stress. Usually called Stage-II crack growth (Paris, 1963; Laird, 1967; Walton and Ellison, 1972).
- Ultimate ductile failure occurs when the crack reaches sufficient length so that the remaining cross section cannot withstand the applied load.

The fatigue crack initiation at Stage-I is influenced by several factors like: Fatigue strength is seriously reduced by the introduction of a stress raiser (Neuber, 1946; Peterson, 1974; Makkonen, 1999 and 2003) and the size of the specimen (Horger, 1953; Kuguel, 1961). Surface quality (Seibel and Gaier, 1957) of the specimen is one of the important parameters to influence fatigue life of the specimen. The surface quality can be improved to resist crack initiation by smoothening and electroplating (Hammond and Williams, 1960), heat treating (Cameron et al., 1983) and imposing suitable residual stress (Almen and Black, 1963). Corrosive environments (McEvily and Staehle, 1979) often produce pits on the material surface making it vulnerable to surface crack generation. Fatigue properties are quite microstructure sensitive (Gensamer, 1942; Grosskreutz, 1972) and the dependence of fatigue life on grain size varies depending on the mode of deformation(Thompson and Backofen, 1971) not only that, the existence of micro-cracks, voids, inclusions, and other defects (Epremian and Nippes, 1948)can accelerate crack initiation and propagation. Below room temperature, fatigue strength increases with decreasing temperature (Allen and Forrest, 1956; Ellison, 1969) and if the temperature is increased well above the room temperature, creep will become important and at high temperature it will be the principal cause of failure. Fatigue failure can be produced by fluctuating thermal stresses (Coffin, 1954) under conditions where no stresses are produced by mechanical causes. With the increase of stress amplitude and the mean stress (Goodman, 1899; Soderberg, 1930), fatigue life gradually decreases.

Crack propagates in Stage-II. Striations arise on the fatigue failure surface via two primary mechanisms alternating slip (Neumann, 1969 and 1974a,b) and crack tip blunting and re-sharpening (Tvergaard, 2004), produced due to crack propagation. Alternating slip occurs when the crack tip plasticity is limited, so that dislocations only move on a few parallel planes. Upon loading, the initially sharp crack will blunt due to plastic deformation of ductile crack tip. When the crack is unloaded, the elastic stress field around the plastically relaxed crack tip will cause the crack to re-sharpen. As the crack is again loaded, it again blunts, leaving behind a ripple on the surface.

Further on, in Stage-III, static fracture modes are superimposed on the growth mechanism (Forman and Mettu, 1990), till finally it fails catastrophically. Shapes of hysteresis loops are not constant throughout the fatigue life for all materials. Generally, increment or decrement in stress amplitude with cycles take place only in initial stages of fatigue life, depending upon hardening-softening behaviour of materials and loading arrangement. Excluding those few initial cycles, it can be said that, the cyclic stress-strain response is independent with number of cycles. The peaks of saturated hysteresis loops at various strain ranges constitute the cyclic stress-strain curve (Ellyin, 1996). The concept of cyclic stress-strain curve has been introduced to characterize a material's cyclic plastic stress-strain

response for major part of its fatigue life, and is one of the most important fatigue characteristics. If the stabilized state is not satisfactorily defined, several cyclic stress-strain curves can be obtained, depending to a certain degree of straining history (Manson, 2006) and thus cyclic stress-strain curve can also be evaluated for stress controlled cycling.

1.2.2 Low cycle fatigue and material response

If the applied cyclic load is high enough to deform the material irreversibly (plastically), it survives relatively low number of cycles, and known as 'Low Cycle Fatigue' (LCF). LCF as a material failure process has received much attention since the early work of Manson (1953) and Coffin (1954) where they explained fatigue crack-growth in terms of plastic strain in the tip of cracks. Local stress concentrators like: the geometrical discontinuities, surface roughness, persistent slip bands, grain interfaces, inclusions, defects etc., may cause local cyclic plastic deformation even for small amplitude cyclic loadings (Paul, 2011c). Before the catastrophic failure or even crack initiation, unlike high cycle fatigue, different kind of stress-strain responses may be observed depending on loading sequence, symmetry, material properties etc. These material responses are of practical interest in design of power plant and other engineering components, as sometimes, they indicate the symptoms of any secondary damage mechanism evolved and influencing the fatigue life. Thus, considering the structural integrity aspect, understanding the material's cyclic plastic behaviour is very important. Extensive research work has been carried out in last a few decades by several researchers to understand the material behaviour for irreversible cyclic loading. However, a number of cyclic plasticity issues are yet to be fully understood (Suresh, 1998; Mughrabi, 2010). To carry out accurate modelling in cyclic plastic deformation behaviour of materials requires sound understanding. A brief account of the different behaviours causing the changes in the shape of hysteresis loops are presented below in figure 1.1:

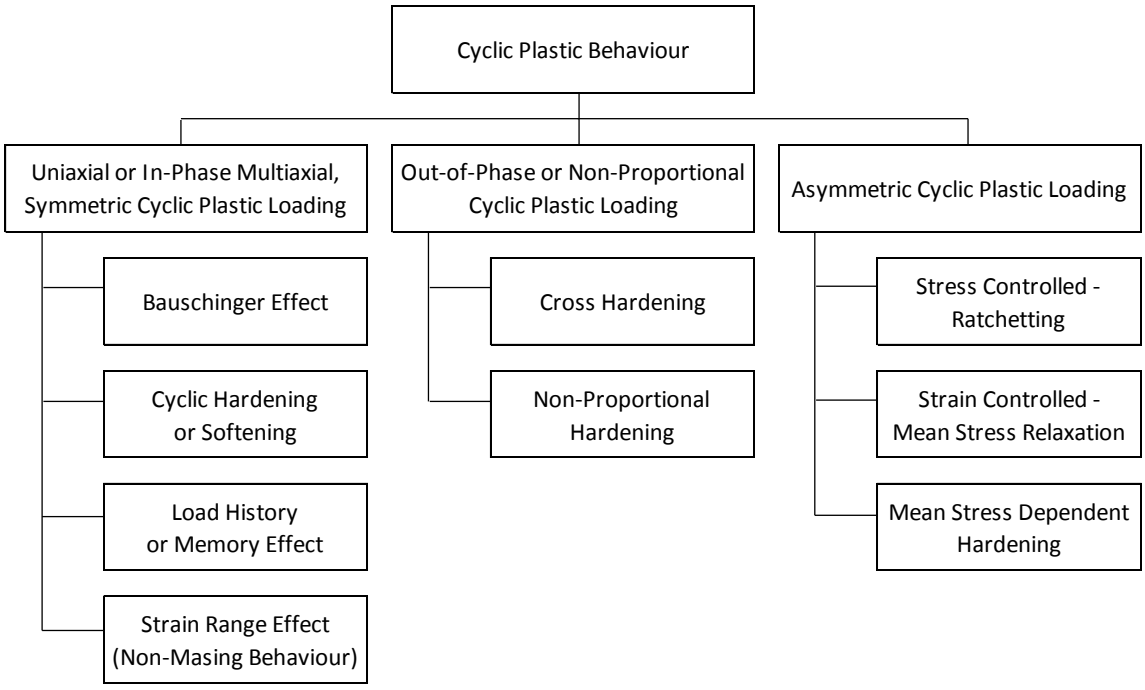

Fig. 1.1: *Commonly observed cyclic plastic behaviours in metallic materials.*

- Bauschinger effect (Bauschinger, 1881 and 1886) is a fundamental and well known cyclic plasticity behaviour. Figure 1.2 shows the schematic representation of the Bauschinger effect observed during cyclic plastic deformation. According to a 'standard' definition, the Bauschinger effect is ''the phenomenon by which plastic deformation increases yield strength in the direction of plastic flow and decreases it in other direction" (Bauschinger, 1886).

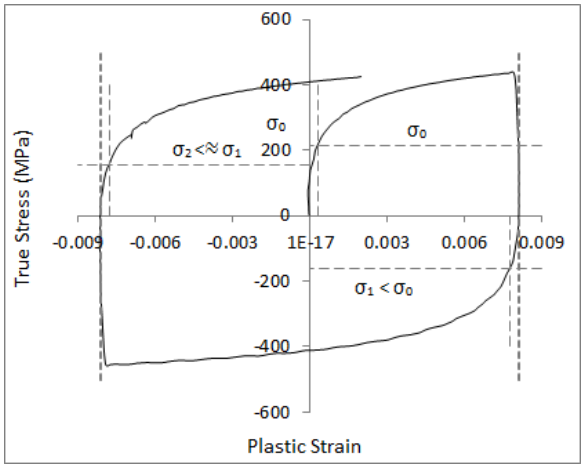

Fig. 1.2: *Typical experimental Results showing Bauschinger effect.*

- Cyclic hardening and softening (figure 1.3a,b) refers to the hardening or softening response of a material subjected to repeated loading (Boller and Seeger, 1987; Doong et al., 1990; Jiang and Kurath, 1997; Jiang, 2001; Zhang and Jiang, 2004). It is often reflected by testing the material under fully reversed strain-controlled loading. With controlled strain amplitude, a material is cited to display cyclic hardening or softening when the stress amplitude increases or decreases respectively with increasing loading cycle (Jiang and Sehitoglu, 1994a,b; Aubin et al., 2003; Jiang and Zhang, 2008; Sivaprasad et al., 2010; Paul et al. 2010, 2011b).

  Usually it has been seen that, hard materials (i.e. cold deformed, quenched and tempered) cyclically soften and soft materials (i.e. annealed) cyclically harden (Suresh, 1998; Mughrabi et al., 2004; Lu et al., 2009).

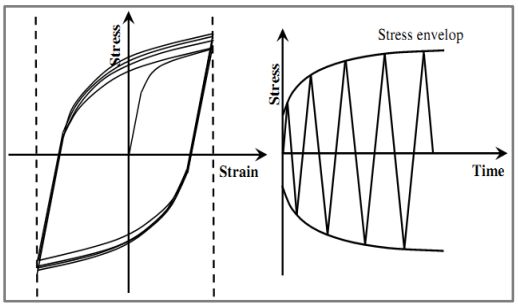

Fig. 1.3a: *Strain controlled cyclic hardening.*

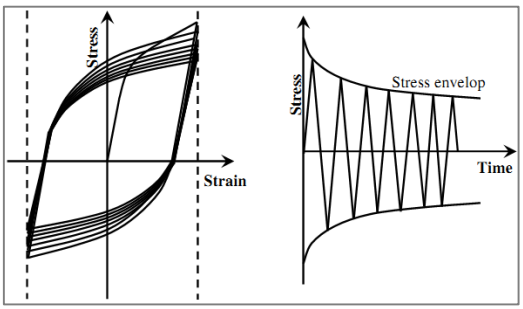

Fig. 1.3b: *Strain controlled cyclic softening.*

Cyclic hardening/softening is influenced by number of factors like prior deformation histories(i.e. initial dislocation density and arrangement)like cold

deformation (Estrin et al., 2013), chemical composition and heat treatment (materials phase i.e. planner slip or wavy slip), (Mughrabi et al., 2004; Lu et al., 2009; Pan et al., 2014), applied stress state (mean stress and stress amplitude), (Mughrabi et al., 2004; Lu et al., 2009), and environment temperature, (Mughrabi et al., 2004) etc.

- Cyclic hardening or softening of materials depends on the initial dislocation population and structure. As previous loading (i.e. pre-straining, pre-cycling at high strain amplitude, etc.) on material alters the initial dislocation structure and thereby changes its initial cyclic hardening/softening response (Estrin et al., 2013).

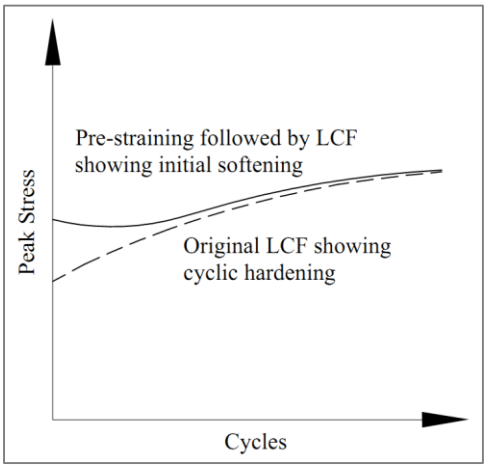

Fig. 1.4: *Effect of previous loading history on subsequent cycling schematic.*

Figure 1.4 schematically shows initial cyclic softening due to pre-straining followed by LCF loading. After a few cycles, the cyclic stress-strain response is very similar to pure LCF. Like pre-straining, material also shows very similar kind of responses in high-low loading sequence (Jiang and Zhang, 2004).

- The material is said to have Masing behaviour when the loading branches of the stress-strain hysteresis loops follow a common curve which is known as master curve, with the lowers tips being tied together for different strain amplitudes (Masing, 1923; Elline and Kujawaski, 1984; Wang and Laird, 1988). Figure 1.5a and 1.5b schematically shows Masing and non-Masing behaviour respectively.

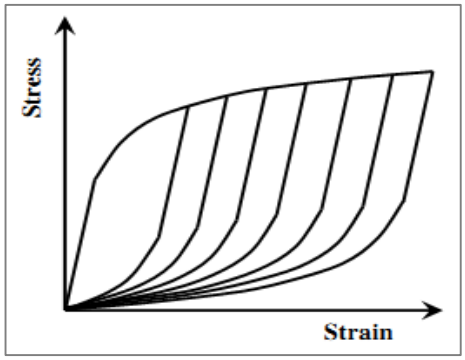

Fig. 1.5a: *Schematic Masing behaviour.*

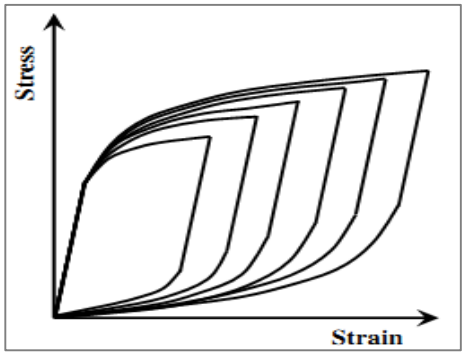

Fig. 1.5b: *Schematic non-Masing behaviour.*

Some engineering materials display Masing behaviour under certain conditions like pressure vessel steel at 300°C and 420°C (Fan and Jiang, 2004), ultra-fine grained copper (Maier et al., 2006), polycrystalline copper under ramp loading (Wang and Laird, 1988), 304LN stainless steel which had been cold worked for 30% prior testing (Raman and Padmanabhan, 1996) etc. Normally, metals with finely dispersed particles and single phase low stacking fault energy exhibited Masing behaviour (Plumtree and Abdel-Raouf, 2001). For high stacking fault energy metals where the cyclic deformation was matrix controlled, the cyclic stress-strain response was non-Masing. However, masing behaviour was observed below a threshold strain level. Above the threshold, non-masing behaviour occurred, which was accompanied with the formation of a dislocation cellular microstructure (Plumtree and Abdel-Raouf, 2001).

- The effect of hydrostatic stress in flow stress is observed in mostly porous materials after a few cycles. This produces higher flow stress in compression than that in tension and is known as strength differential (SD) effect (Casey et al., 1985; Kim et al., 1987).

A brief account of different behaviour causing the changes in shape of hysteresis loops are presented below for non-proportional but symmetric loading conditions:

- Cross hardening (figure 1.6) is manifested as sudden raise in stress value when a material is loaded in a different direction after certain loading in a particular direction (Krempl et al., 1984; Cailletaud et al., 1984; Ohashi et al., 1985; Benallal et al., 1987; Tanaka et al., 1985). For the same equivalent strain range, a change in the loading direction leads to a strengthening during the first subsequent cycle (Benallal et al., 1987).

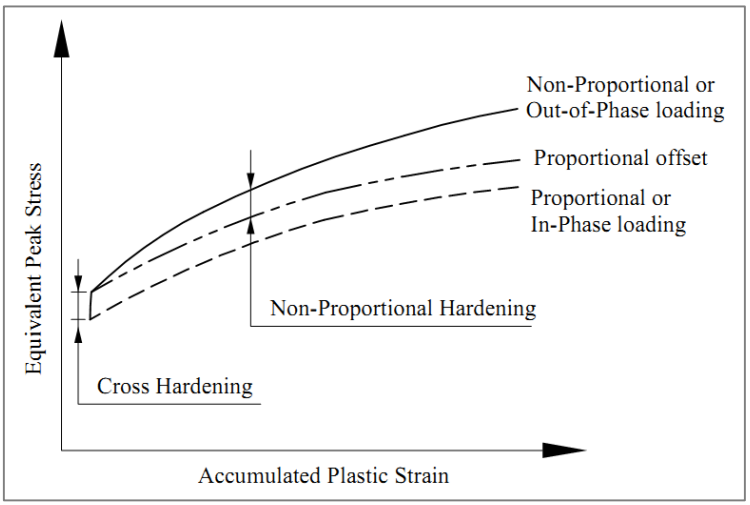

Fig. 1.6: *Schematic representation of cross hardening and non-proportional hardening.*

- Out-of-phase or non-proportional multiaxial loading results in the rotation of principal axes with time. Rotation of maximum shear plane under non-proportional

loading causes change in the slip plane from one crystallographic slip system to another and which is thought to be the basis of non-proportional hardening (fig.1.6).

Rotation of principal stress axes during non-proportional cyclic loading hinders the formation of stable dislocation sub-structure in the material. Due to cross slipping and activation of multiple slip system in non-proportional loading, more amount of energy should be spent for achieving the specified strain level. Materials can be divided into three groups to establishing the correlation between additional hardening and staking fault energy (SFE) under non-proportional loading. The first group includes metals with a high level of the SFE (like - Al, Ni, metals with bcc lattice) that exhibit low additional hardening or not at all (Doong et al., 1990). The metals with a medium level of the SFE (like - Cu) fall into the second group. They are characterized by the appearance of additional hardening under conditions of non-proportional loading and the constancy of the attained level of hardening in the reverse transition to proportional loading (Doong et al., 1990). The third group incorporates the materials with a low level of the SFE (like - stainless steels, alloys), which exhibit the largest additional hardening on the one hand, and partial cyclic softening in the reverse transition on the other (Doong et al., 1990; Li and Almazouzi, 2009).

The level of non-proportional strain hardening depends on the shape and amplitude of the strain or load path (Tanaka et al., 1994; Borodii and Shukaev, 2007; Shamsaei et al., 2010) and the material microstructure (Shamsaei and Fatemi, 2010). Generally, there are two broad categories of approaches for estimating the stress response under general multiaxial loading: plasticity (or constitutive) models as proposed by Benallal and Marquis (1987) or Tanaka (1994), and empirical formulations (Borodii and Shukaev, 2007; Shamsaei et al., 2010). Maximum level of non-proportional hardening occurs for 90° out-of-phase strain path (Tanaka, 1994), which results in complete rotation of principal axes and activation of slip systems in all directions.

The saturated or stabilized hysteresis loops sometimes may not be found like in the case of asymmetric loading, and thereby cyclic stress-strain curve cannot be obtained for fatigue life estimation. Asymmetric loading causes plastic strain accumulation per cycle and thereby accelerate the failure. A brief account of different behaviour causing the changes in shape of hysteresis loops are presented below for asymmetric loading conditions:

- Materials and structures are often subjected to cyclic stressing with non-zero mean stress, cyclic accumulation of inelastic deformation will occur if the applied stress is high enough (ensuring that a yielding occurs), and the phenomena is called ratcheting (schematically shown in figure 1.7). The ratcheting is very important and should be addressed in the safety assessment and fatigue life estimation of such structural components. For example, in early 1990s, the ratcheting behaviour of the nuclear pipes and its detrimental effect on the nuclear reactor structure were contained in the American ITER design code and ASMENB 32xx code.

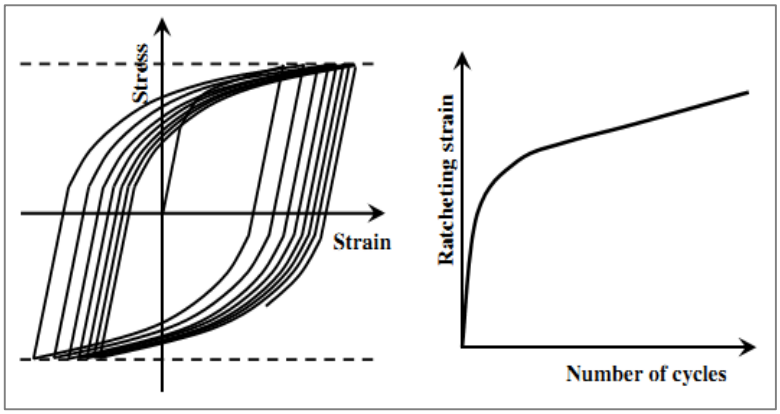

Fig. 1.7: *Schematic illustration of ratcheting.*

Radhakrishnan and Baburamani (1975) observed multiaxial ratcheting in Aluminium and steel at room temperature, Lorenzo and Laird (1984) summarised uniaxial cyclic creep retardation caused by glide exhaustion of the available dislocations while testing polycrystalline copper at room temperature. Uniaxial tests on SUS304 stainless steel at room temperature done by Yoshida (1990) shows cyclic stressing with a peak stress hold yield more ratcheting strain. Uniaxial experiments by Hassan and Kyriakides (1994) on stainless steel 304 and carbon steel 1018 at room temperature concludes Cyclic softening causes acceleration in the rate of ratcheting and cyclic hardening causes reduction in the rate. His experiments on biaxial loading (axial and internal pressure) also concludes circumferential ratcheting rate increases with cycles. Jiang and Sehitoglu (1994) performed uniaxial and multiaxial tests on 1070 steel at room temperature and found the ratcheting direction is coincident with the mean stress direction for proportional loading. There is no unequivocal relation between the mean stresses and ratcheting directions when the loading is non-proportional. Under multiple step loadings, the material exhibits a strong memory of previous loading history, and such memory has a great influence on the subsequent ratcheting. The material could ratchet in opposite direction to the mean stress or could reverse ratcheting direction with time. The ratcheting rate decreases with increasing loading cycles for both proportional and non-proportional loadings. Kang and his co-workers (2002) concludes from the uniaxial and multiaxial tests on SS304 stainless steel at elevated and room temperature that ratcheting strongly depend on the history of mean stress, amplitude and temperature. He also found that dynamic strain aging offers high deformation resistance at particular temperature window. Kulkarni (2003) and Gupta (2005), with their co-workers, worked on SA333 Grade-6 C-Mn steel with internal pressure the specimen suffers significant bulging and cross-sectional distortion. Negative stress ratio and low stress rate increase the ratcheting behaviour. Yang (2005) experimented on carbon steel 45 at room temperature and concluded increase in the mean stress decreases ratcheting failure life for constant stress amplitudes. Yaguchi and Takahashi (2005) performed uniaxial and multiaxial tests on modified 9Cr-1Mo steel at high temperature and found the ratcheting depended on the steady stress, cyclic strain range and strain rate. Khan (2007)

worked on OFHC copper 593°C, multiaxial tests results Pre-cyclic hardening reduced multiaxial ratcheting through the first few cycles but it did not eliminate it or its rate. Date (2008) observed for 316FR at room temperature that tensile ratcheting decreased the failure life, while compressive ratcheting did not.

It can be concluded that, Ratcheting is a secondary deformation process and its evolution is greatly dependent upon many loading factors, such as stress level, loading history, stress rate and loading path (Jiang and Sehitoglu, 1994).

- Mean stress relaxation (fig. 1.8) can be defined as gradual decreasing of mean stress during asymmetric strain cycling where, a constant mean strain is maintained. A mean stress will build up because of mean strain, but the mean stress progressively come down to almost zero value (Valiev et al., 2000; Arcari et al., 2009).

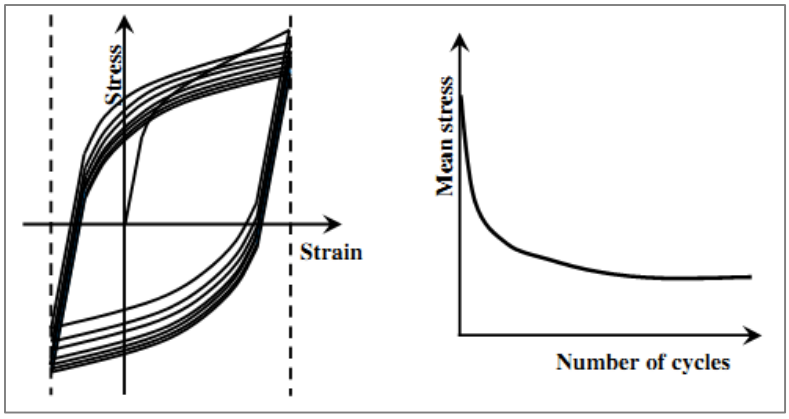

Fig. 1.8: *Schematic illustration of mean stress relaxation.*

- Material shows an extra hardening character depending on mean stress during stress cycling (figure 1.9). Decreases in plastic strain amplitude with increasing mean stress were also reported by others in engineering stress controlled ratcheting experiments for carbon steel by Kliman and Bílý (1980), 304 stainless steel by Turner and Martin (1980), Lorenzo and Laird (1984), Mughrabi et al. (1997), polycrystalline copper by Eckert et al. (1987), Lukas and Kunz (1989), and for polycrystalline nickel by Holste et al. (1994).

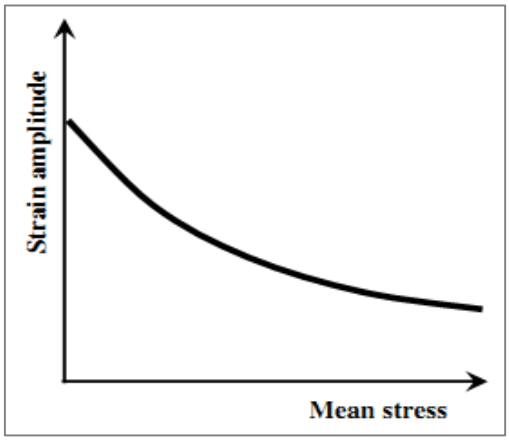

Fig. 1.9: *Schematic representation of mean stress dependent hardening.*

The stress-strain behaviours during the cyclic plastic loading for a material are required to be understood and modelled accurately in order to compute the fatigue life.

1.2.3 Physical explanation

Dislocation motion and lattice rotation are supposed to be the prime cause of plastic deformation. Through decades, several researchers were trying to find micro-mechanism based explanations behind the cyclic plastic phenomena as well. The work of Gough (1933) established that a metal deforms under cyclic strain by slip on the same atomic planes and in the same crystallographic direction as occur in the unidirectional case. Contemporary scientist, Orowan (1934), correlated dislocation density and slip. Taylor (1938) proposed the correlation between dislocation density and shear stress. The relation uses parameter α (Mughrabi, 2016) and the average Taylor factor M (Estrin, 1998; Kassner, 2003). Relation between slip and strain was established (Kocks, 1970; Mecking and Kocks, 2003).Later, Rauch et al. (1989) have pointed out that plastic strain can evolve based on dislocation.

It is the nature of the dislocation interactions that differentiate macroscopic material behaviour. Years of meticulous study of the dislocation dynamics by several researchers in different polycrystals revealed more facts. In the work of Kubin et al. (2008), the possible interactions of dislocations are classified in six kinds. Three of them are accounted for forest interactions between non-coplanar slip systems, resulting in the formation of junctions or locks, namely the Lomer–Cottrell lock, the Hirth lock and the glissile junction. There are two non-contact interactions for dislocations gliding in parallel slip planes with same or different Burger's vectors, known as the self-interaction and the coplanar interaction. And the last interaction is the collinear interaction, produces annihilations. The hardening responses are mainly the manifestation of dislocation entanglements while annihilation results in softening.

By the course of time, the work of Wood (1955) suggested a mechanism of slip band extrusion and intrusion for the understanding of fatigue. Plumbridge and Ryder (1969) studied the basic structural changes occur in the material subjected to cyclic loading. Ashby (1970) reported deformation modes are complex in polycrystals than single crystal, and understanding of dislocation dynamics for polycrystals during large deformation became critical.

In BCC and FCC crystals, there are twelve such slip systems exist, which can be activated easily. The total possible interactions between mobile dislocations in a B.C.C crystal can be captured by a matrix of 144 (12×12) interaction coefficients (Franciosi, 1985). This interaction matrix actually designates the generalised hardening character of the material. It is reported (Kubin et al., 2008) that, there are only six independent coefficients can represent the matrix considering symmetry assumptions, which are associated with six different types of dislocation interactions. Apart from dislocation interactions, some reorganisations of the lattice structures continue to occur while deforming in the plastic regime. These reorientations can create and/or destroy many opportunities for further interactions, increasing the complexities in the imminent state of affairs.

During cyclic plastic deformation, continuous generation and annihilation of dislocations simultaneously occur and, the remaining dislocations at any instance, try to align themselves such as to reduce their individual contribution to the stored energy. The reorganisation of dislocations can resolve through entanglements quickly within a few cycles. The rearrangements of dislocations are resulting from the dissimilar rotations of the neighbouring lattices (Read and Shockley, 1950). These reorientations of the dislocations continue to occur to a certain extent of plastic deformation, and by the time, the stable dislocation substructures are fully developed (Sedláček et al., 2002). The substructures are cellular and surrounded by walls consist of rough tangles of dislocations and the interiors of the cells have a correspondingly much lower dislocation density. The sub-cells often disoriented during initial stages of plastic deformation. The simplest case of 'misorientation' can be tilted sub-grains forming low angle tilt boundary (as sub-grains are tilted symmetry of one another – Bragg, 1940; Burger, 1940;Shockley and Read, 1949; Read and Shockley, 1950) with an array of edge dislocations and with misorientation angle less than 15°. The orientation of dislocations in their minimum energy positions leave traces may be manifested as memory effect.

A moving dislocation, in the vicinity of sub-structure, takes part either by pilling-up at sub-grain walls reinforcing the wall entanglements or, by getting annihilated with its compatible pair relieving some stored energy (Sauzay et al., 2005). Obviously, entanglements resist the easy glide of remaining dislocations and thereby, cumulatively raise the macroscopic hardness and annihilations make free passages for the remaining dislocations thus reduce the hardness. The interactions of moving dislocations are direction dependent and may result in directional behaviour like ratcheting.

Though the overall manifestation of the annihilation is softening, the dissimilar kinematics of the dislocations involved, have different macroscopic response of the material. The reductions of boundary dislocations primarily resolve the boundary misorientation (Sauzay et al., 2005; Fournier et al., 2011) and eventually cause the dissolution of the boundary itself. The effect of annihilations of boundary dislocations can be a reasonable phenomenon to justify isotropic cyclic softening in cyclic plastic loadings.

In cyclic plastic loading, strain path change occurs due to load reversal or due to non-proportional loading. Strain path change can activate new slip systems. The built-up dislocation structure in the first deformation path becomes unstable when a sudden and abrupt strain path change occurs (Barlat et al., 2003; 2011), though, only a single event of sudden strain path change cannot hinder the obvious sub-structure formation for a long time. Strain-path change transfers total or a part of the available dislocations, sensitive to the polarity of the stress, into the newly activated slip systems. This transfer causes a sudden dislocation crowd in the slip system and may disappear gradually (Rauch et al., 2007) due to strong collinear interactions. This is commonly observed in case of reversed loading. The disappearance of the polarized fraction of the dislocation is manifested as the Bauschinger effect. Another possible phenomena is, the transferred dislocations entangle in the newly active slip systems producing a non-proportional hardening effect in those slip systems.

Mughrabi et al. (1987) researched Masing behaviour in polycrystalline copper. They proposed the hypothesis that hysteresis loops reveal Masing behaviour when the dislocation arrangements do not change during cyclic deformation. It was found in the work of Li and Laird (1993) that Masing behaviour is not a saturation phenomenon, but simply requires that no changes occur in dislocation structure under variable loading. Investigations by Watanbe et al. (2013) reveals that dislocation structures are not always the same during Masing behaviour.

1.2.4 Chronology of Modelling

Different cyclic behaviours are observed and documented in the last a few decades of rigorous research for different materials. At the same time, an even more meticulous effort was given to model the phenomena mostly from mathematical and thermodynamic point of view. Contemporary researchers have been trying to propose simple and physically sound constitutive models for cyclic plasticity simulation (Bari and Hassan, 2002).

Cyclic plasticity is considered as one of the most critical structural problems to be simulated. And in the context of constitutive modelling, the development of kinematic hardening rule is enormous benchmark in the history of cyclic plasticity modelling. The most of the cyclic plasticity phenomena are modelled by modifying the kinematic hardening rule. In the following section, a brief history of such modifications are presented.

Translation of the yield surface in the deviatoric stress space known as the kinematic hardening mechanism. The standard kinematic hardening rules include the forest pile-ups of dislocations as 'back stress' and the effect of annihilated mobile dislocations causing some recovery of the back stress is generally included in the ‘dynamic recovery’ term. The concept of KH rule is materialized first in the work of Prager (1956).

- Prager (1956) proposed the linear type kinematic hardening (KH) rule suggesting a proportional stress raiser by dislocation pile-ups may be apprehended. When a material is loaded beyond its yield limit, microscopically, a large number of dislocations are activated by generation and multiplication at different sources, like, grain and sub-grain boundaries, pinned dislocations, impurities, and other kind of defects etc. As plastic deformation continues, the probability of mobile dislocations being tangled with each other and caught up in the dislocation forest increases exponentially as more slip systems get activated. The entanglement of mobile dislocations at different sites resist the easy glide of dislocations, cumulatively resulting the macroscopic hardening.

- Improvement to the linear kinematic hardening model was proposed by Mroz (1967) as a multi-surface model, where each surface represents a constant work hardening modulus in the stress space. Besseling (1958) introduced a multilayer model without any notion of surfaces. In uniaxial loading, all these models essentially divide the stress-strain curve into many linear segments. When a sufficient number of segments are chosen, the hysteresis loop simulations by these models are very good. Unfortunately, like the linear kinematic hardening model,

multi-linear models also predict a closed loop when subjected to a uniaxial stress cycle with a mean stress and hence produce no uniaxial ratcheting.

- From the metallurgical point of view, Li (1960, 1963) proposed a model for local kinematic stress as a function of sub-grain size and low angle misorientation angle. In this model, no clear information was given about the source of the kinematic stress in the material.

- The linear hardening law was successful to simulate the Bauschinger effect but rudimentary to imitate the stress-strain hysteresis due to the linearity. The development of non-linear KH rule consisting of a dislocation annihilation based non-linear 'Recovery' or 'Recall' term was first introduced by Armstrong and Frederick (1966). In support, Transmission Electron Microscope (TEM) micrographs can show, other than entanglement, when dislocations of opposite signs interact, they both get annihilated (Essmann and Mughrabi, 1979) reliving the stored energy and space for remaining dislocations to glide easily without barrier. Movable dislocations within a slip system (slip direction and plane) when interact with each other and dislocations of opposite signs annihilate, the process is designated as 'dynamic recovery'. Any kinematic hardening (KH) rule used in the material modelling, now a days, are equipped with the hardening term that handles the dislocation generation and pile ups and a recovery term mainly capture the annihilation of movable dislocations within the active slip systems.

- The Armstrong and Frederick (AF) (1967) model incorporates a dynamic recovery term and was successful to simulate balanced non-linear cyclic loading. The incorporation of the recovery term in kinematic hardening rule is another landmark in the history of cyclic plasticity modelling. For unbalanced loading, the AF rule showed over-prediction might be due to lesser hardening and further modifications of KH rule are focussed mainly on dynamic recovery of the back stress. To get proper hardening effect, the recovery term needs to be understood and modelled properly because, the annihilations of dislocations are 'not so controlled' physical phenomena.

- Chaboche and his co-workers (1979, 1986) proposed a 'decomposed' nonlinear kinematic hardening rule. Chaboche kinematic hardening rule is a superposition of several Armstrong-Frederick hardening rules. Each of these decomposed rules has its specific purpose. A stable hysteresis curve can be divided into three critical segments where the Armstrong-Frederick model fails: the initial high modulus at the onset of yielding, the constant modulus segment at a higher strain range and the transient nonlinear segment. And accordingly, they suggested that the first rule (α_1) should start hardening with a very large modulus and stabilizes very quickly. The second rule (α_2) should simulate the transient nonlinear portion of the stable hysteresis curve. Finally, the third rule (α_3) should be a linear hardening rule ($\gamma_3 = 0$) to represent the subsequent linear part of the hysteresis curve at a high strain range. If this scheme is followed, the simulation for a stable hysteresis loop

improves. Chaboche model has a tendency to over-predict uniaxial ratcheting rates during initial cycles and over-predicts the biaxial cases to a large extent. Chaboche (1991) added a fourth hardening rule with a concept of 'threshold' in his model. This kinematic hardening rule grows linearly to a certain 'threshold' stress level and subsequently hardens according to the Armstrong-Frederick rule. It is observed that the incorporation of a fourth rule improves the stable hysteresis loop simulation, but the ratcheting simulations for both uniaxial and biaxial experiments do not improve that much.

- Guionnet (1992) proposes a model which uses some parameters that are determined from biaxial ratcheting experiments. The Guionnet model basically modifies the original Armstrong-Frederick hardening rule by incorporating the effect of accumulated plastic strain in it. The simulations of hysteresis loops and ratcheting response are not upto the mark, and the model has numerical divergence problem for higher uniaxial ratcheting rate responses as reported by Bari and Hassan (2000). For the bow-tie loading case, this model over-predicts with constant rate of ratcheting, whereas for the reverse bow-tie, it under-predicts the ratcheting. Similar erratic behaviour is also observed in the simulations for bow-tie and reverse bow-tie loading cycles obtained by the Dafalias-Popov (1976) uncoupled model with Armstrong-Frederick kinematic hardening rule (Corona et al., 1996).

- One of the popular models, following the Besseling type multi-linear formation was proposed by Ohno and Wang (1993a). The model like other linear models, simulates closed hysteresis loops resulting no ratcheting response. Later, to rectify this error, they extended their model (Ohno and Wang, 1993b) to have non-linearity and thus conforms the AF format, showing improvements in simulating non-linearity in the stabilized hysteresis loops and uniaxial ratcheting curves than Chaboche model with threshold term. Though there are further modifications to the OW model mainly targeting the ratcheting response. In 1994, they extend the model further and replaced plastic strain increment with accumulated plastic strain in the dynamic recovery term. This rule (Ohno and Wang, 1994) becomes a direct modification of AF rule, where the contribution of the dynamic recovery term is modulated by a constant χ.

- McDowell (1995) and Jiang and Sehitoglu (1996a) modified the dynamic recovery power term χ as functions of non-proportionality parameter but the simulations were conducive to portray the experimental biaxial ratcheting curves.

- The kinematic hardening rule proposed by Voyiadjis and Sivakumar (1991, 1994) is a combination of the Phillips (Phillips and Tang, 1972; Phillips and Lee, 1979) and Tseng-Lee (1983) rules. They reason that the Phillips rule, which stipulates the evolution of the back-stress along the stress rate direction, follow the experimental trend better, but it does not ensure the tangential nesting of the yield and other surfaces in a multi-surface plasticity model. In contrast, the Tseng-Lee rule invokes the desired nesting feature for both the proportional and non-proportional loading.

Hence, Voyiadjis and Sivakumar (1991) propose a rule to appropriately blend the deviatoric stress rate and the Tseng-Lee rules, to include both the requirement of surface nesting and the experimental observation of the yield surface movement. Note that, in the improved Dafalias-Popov model, the surface nesting is inherently ensured with any kinematic hardening rule. The model fails to simulate biaxial ratcheting responses.

- Voyiadjis-Basuroychowdhury (1998) and Basuroychowdhury-Voyiadjis (1998) attempt to improve the Chaboche (1991) kinematic hardening rule by adding the direction of the stress rate. But could not achieve more than the mother model.

- Abdel-Karim and Ohno (2000) propose a new kinematic hardening rule combining the initial multilinear version of the Ohno-Wang and the Armstrong-Frederick rule. This model produces a better biaxial ratcheting simulation, especially in reproducing the recorded steady rate of ratcheting, but, under predicts the ratcheting in uniaxial loading cases.

The modifications in KH rule are focused on making the model compatible for both balanced and unbalanced, proportional or non-proportional multiaxial loadings. Exponential isotropic hardening rule (Zaverl and Lee, 1978) also employed alongside the KH rule in the model to capture several hardenings or softenings manifested during irreversible cyclic loading. But these mathematical theories are mainly based on loading functions and justified over experimental observations.

The recent trend is directed towards constitutive modelling based on dislocation dynamics. Dislocation based modelling delivers physically justified and more accurate hardening functions (both Kinematic and Isotropic), which can be effective tools for simulation of monotonic and cyclic loading conditions with or without considering the rate effects. Anisotropic material properties are also completely compatible with this type of formation. Furthermore, any orthodox numerical scheme can easily fit in to incorporate the hardening function, though some complexity may be costly in terms of numerical computations.

The Effect of the six possible dislocation interactions are incorporated in the simplified mathematical model broadly generalised by three families of moving dislocations namely forward, reverse and latent dislocations depending on their origins. For simplicity, Rauch and his co-workers (2011) considered the idea that different loading conditions including forward loading, reverse loading and loading in any arbitrary direction, may result in three distinct ‘families’ of dislocations. These families are sufficient to produce the essential mechanical features observed for pre-strained samples. Therefore, the average dislocation density can be additively decomposed into three families respectively associated with the forward, reverse and latent interactions.

For monotonic loading, the net dislocation density available at any instance can be regarded as the forward dislocation density. This mainly contributes to the hardening by forest pile-up according to the Taylor model. Any dislocations with opposite Berger's vector originate the reverse dislocation family even during the monotonic forward loading. The dynamic

recovery terms of any standard kinematic hardening rules in Armstrong-Frederick (1966) format, is designed to reproduce the reverse dislocations interactions in mathematical material models. The change of strain-path in any other direction (between 0° to 180°) is classified as non-proportional loading. The part of the dislocation density to be transferred is related on the degree of non-proportionality and causes the latent hardening effect. The kinematic hardening rules do not incorporate the additional (latent) hardening due to non-proportional strain-path change.

Dislocation based constitutive modelling is done by Peeters et al. (2001a,b), Chia et al. (2005), Bouvieret al. (2006), Sinclair et al. (2006), Rauch et al. (2007) Bergstrom et al. (2010), etc. for different materials. The basic theory of the modelling is, at moderately large strains microstructural evolution contribute to work hardening. Rauch et al. (2011) discussed strain-path based hardening in terms of dislocation densities. Exhaustive research which are versatile in respect of materials like DP steel, IF steel, and SS has been conducted by Carvalho-Resende et al. (2013) and showed dislocation-based prediction of the behaviour of BCC materials by modelling grain size and train path effects. At initial cycles, for BCC material the dislocation structure are planar and entangled (Schayes et al., 2015). The 'homogeneous anisotropic hardening' approach extended to cross-loading cases with latent hardening effects. This continuum approach is based on the physical understanding of dislocation structure evolution during strain-path changes and not included in the concept of kinematic hardening (Barlat et al., 2013).

1.2.5 Evolution of simulation technique

The rigorous experimentation reveals different material behaviour for small specimens with uniform geometries. But the size and shape of the specimen are found to be influencing the fatigue life (Putatunda and Rigsbee, 1985; Frost, 1999). Due to the limitations in physical experimentations, scientists have devised a mathematical domain, which is a virtual reality for physically impossible experimentations. In this domain, all physical objects, actions and responses can be formulated and quantified, where a physical material becomes material model, and a physical experiment becomes simulation. Though, there are some hypotheses to simplify the complexities associated in one or many aspects, the mathematical tool almost accurately imitates the material responses using a material model for its complicated structure, loading arrangements and atmospheric conditions. The entire process is known as 'Mathematical Simulation'. The most popular simulation tool used in structural and engineering analyses is 'Finite Element Method'.

All these models are intended to simulate actual material behaviour mathematically. Numerical methods are the tools that make that possible. Unlike discrete mathematics, the method uses numerical approximation to solve differential and integral equations, linear algebra, stochastic analysis, optimization, interpolation-extrapolation and other applied mathematical problem. Till the latter half of 20^{th} century, the numerical analysis was not so powerful tool due to heavy computation. Numerical analysis on electronic computers can solve any complex problem with a great number sensibly faster.

Finite Element analysis is a package that create and solve structural and other differential and integral equations numerically (Strang, 1971; Bathe, 1976). It requires appropriate problem definition and correct numerical approach to solve the same. The global geometry is discretised and solved locally and validated with global response. During structural analysis through finite element method, local and global level numerical integrations should be carried out simultaneously (Rahaman, 2006). The material subroutine used in structural analysis named it 'Radial Return' or 'Return Mapping' algorithm, which consists of an elastic predictor and a plastic corrector (Nagtegaal, 1982; Simo and Taylor, 1985 and 1986; Kobayashi and Ohno, 2002).

1.3 Goal-setting and Benchmarking

A brief and contextual survey of the existing literature is presented above. From the literature review, it is observed that the cyclic plastic behaviour of the commonly used metallic materials are versatile. Significant efforts were given to model those behaviour from the phenomenological perspective. The efficiency and the effectiveness of the model was validated by comparing the experimental results with numerically simulated results using the model. By the course of time, the numerical simulation techniques are also developed to the present form.

From last a few decades, a parallel study was carried out simultaneously to physically justify the physically observed phenomena in the context of micro-mechanism like dislocation interaction. The present work emphasizes on this area and attempts to incorporate it in the material modelling for cyclic plasticity. The following points can clearly visualise the objective of the present:

1) Cyclic Plastic Behaviour of steel
    a. Steel is commonly used structural material which shows versatile behaviour while subjected to cyclic plastic loading.
    b. Steel generally shows Bauschinger effect which saturates within first a few cycles.
    c. Steel generally shows non-Masing behaviour (strain range effect) in the initial cycles.
    d. Steel can show cyclic hardening or softening in the initial transitional cycles,
    e. Steel generally shows non-proportional hardening and cross hardening in appropriate out-of-phase loading, though, cyclic hardening or softening may be predominant.
    f. Shows uniaxial and multiaxial ratcheting, mean stress relaxation and mean stress dependent hardening.

The various field of application of the material and its versatile responses when subjected to cyclic plastic loading, makes the material suitable for the present study. SA333 Grade-6 C-Mn steel is the specific material chosen for the job. The details of the material and are discussed in the ensuing section.

2) Classical approach of material modelling
    a. Kinematic Hardening:
        i. Kinematic hardening rules of Armstrong-Frederic format have a hardening part and a dynamic recovery part which incorporates the contributions of the reverse dislocation family and widely studied.
        ii. Multi-segmented kinematic hardening rules can capture the hysteresis hardening character more efficiently.
        iii. Bauschinger effect can be modelled by kinematic hardening rules.
        iv. Strain range effect (non-Masing) can be captured using different KH parameters for different plastic strain amplitudes.
        v. Ratcheting is still considered as one of the most critical structural problems to be simulated comprehensively and modifications to the kinematic hardening rule is the popular way to simulate ratcheting.

    Six segmented nonlinear Ohno-Wang (1993a,b) KH rule, with its modifications, is found to be acceptable in all loading conditions and it is reasonably simpler.

    b. Isotropic Hardening:
        i. There are many direction independent hardening behaviour observed and can be easily modelled by isotropic hardening rules.
        ii. The modelling of cyclic softening by phenomenological isotropic hardening rules are not quite physically justified without indulging damage mechanics.

    There are plenty of scopes to cultivate the isotropic cyclic properties of the material. The present work solely focus on the physical micro-mechanism based modelling of the same.

    c. Plastic strain memory surface:
        i. Loading history effect can be captured by a plastic strain memory surface as introduced by Chaboche and his co-workers (1979).

    The significance of the memory surface is more profound, as it can estimate the plastic strain as a cumulative outcome of activation of slip systems and net effective slip.

The well-established classical approach is supported by thermodynamic principles. Recent advancements in the metallurgical investigations found the physical micro-mechanism behind the mathematical models.

3) Recent trend in material modelling:
    a. Dislocation based theories:
        i. Dislocation entanglement, orientation and annihilations are basic physical phenomena governing any macroscopic cyclic plastic behaviour.
        ii. interacting dislocations with different dynamics may explain different macroscopic phenomena,

iii. Non-parallel strain-path change causes latent hardening where, hardening may be observed in the inactive slip systems.
iv. There are direct relations in dislocation density, slip and shear stress.

Cultivating through the decades of comprehensive studies and enormous experimental database as discussed above, the objective of the present work is set to develop a physically justified material model that can simulate cyclic plastic behaviours shown by SA333 C-Mn steel in symmetric and asymmetric cyclic plastic loading under static loading conditions. To do so, the material model should incorporate micro-mechanism dislocation based hardening mechanisms in which Ohno-Wang (1993a,b) kinematic hardening rule and plastic strain memory surface together with dislocation annihilations at low angle grain boundary find their rightful places.

1.3.1 Benchmarking:

To achieve the goal set above, a systematic and step by step approach is required. The development of the material model starts from a simple loading condition and progressively modified to accommodate the complex ones. Though, the present study formally begins with the symmetric uniaxial cyclic tests and further developments are reflected in the subsequent chapters, some primary investigations are important and discussed in the following section. In this subsection, the entire works can be organised as:

1. Primary Investigations
    a. Basic metallurgical investigations on the material at 'as received' condition are carried out before the commencement of any mechanical tests for identification and quantification of Phases and initial state of dislocations (density and structures, if any) respectively from the optical and TEM micrographs.
    b. Simple (uniaxial) tensile tests were done before the cyclic tests and mechanical properties are extracted following standard procedures.

2. Symmetric uniaxial cyclic plastic loading
    a. Symmetric or balanced uniaxial low cycle fatigue tests were done in different strain amplitudes under static loading in standard environmental condition.
    b. Metallurgical (TEM) investigations are carried out to understand the evolution of the dislocation structures and their influences on macroscopic behaviour. And appropriate material parameters are extracted. Cyclic yield stresses and kinematic hardening parameters are identified from the experimental raw-data.
    c. Material modelling is done based on Ohno-Wang kinematic hardening rule and dislocation based softening mechanism.
    d. The material model is plugged into ABAQUS CAE v6.8 through user material subroutine and simulated for respective loading conditions. The results are compared with experimental results to validate the model.

3. Symmetric biaxial (tension-torsion) cyclic plastic loading
    a. In-phase or proportional biaxial experiments are carried out under symmetric biaxial (tension-torsion) low cycle fatigue loading in different strain amplitudes in static loading condition and standard environmental.
    b. The transferability of the model can be checked through Finite Element Analysis for different loading conditions where no non-parallel strain-path changes occur.
    c. 90° out-of-phase or non-proportional biaxial experiments are carried out under symmetric biaxial (tension-torsion) low cycle fatigue loading in different strain amplitudes in static loading condition and standard environmental.
    d. Material model is modified for additional hardening observed during the experiments, with dislocation based latent hardening
    e. Appropriate material parameters are calibrated from the experimental data and primary metallurgical investigations.
    f. The model is validated comparing the FE simulation results to the experiments.

4. Asymmetric uniaxial and biaxial cyclic plastic loading
    a. Mainly stress controlled ratcheting tests were done under uniaxial and multiaxial (tension-torsion) asymmetric loading conditions, with different stress amplitude and mean stress combinations.
    b. Metallurgical (TEM) investigations are done to realise the dislocation behaviour.
    c. Dislocation density dependent modification of the kinematic hardening parameters is proposed.
    d. The modified model is used to simulate the experiments and the results are compared to validate the model.

The objective of the present work can be achieved by obtaining the three main benchmarking. The work is further subdivided in the benchmarks, the experimental observations are justified by existing theories and metallurgical investigations focusing mainly on dislocation interactions and accordingly modelled. Finally, the material model is validated with the experiments through Finite Element Analysis after each modifications and discussed in details in the respective chapters.

1.4 The Material and Some Primary Investigations

SA333 Grade-6 C-Mn steel is commonly used in primary heat transport (PHT) pipes at nuclear power plants where, during Start-Up and Shut-Down or, due to fluctuations in operating conditions or, seismic activities can trigger cyclic loading, which is most likely multiaxial and may be non-proportional in nature. Depending on the amplitude of loading and/or geometric or microstructural discontinuities, the cyclic deformations may reach beyond the elastic range locally. From the safety point of view, the knowledge of different

cyclic plastic behaviour of the material and their contribution to the failure mechanism must be accurately known.

The material SA333 Grade-6 C-Mn steel, as reported in the literature, has shown a wide variety of cyclic plastic behaviour, what makes it a perfect choice for the present study. Rigorous experiments by Paul et at. (2010, 2011a and 2011b), Khutia et al. (2013), Sivaprasad et al. (2014) on monotonic, uniaxial and a few multiaxial behaviour of the material reports variations of its cyclic behaviours. Depending mainly on heat cycles and loading history the hardening characteristics of the material have changed. After substantial literature survey on the material, the cyclic plastic character of the material can be statistically summarised as: the material shows Bauschinger Effect, with most likely the non-Masing behaviour, followed by cyclic hardening or softening depending on the previous heat cycle and loading history. The material is reported to show non-proportional hardening response and ratchetting when accordingly loaded. The experimental observations are discussed in details later.

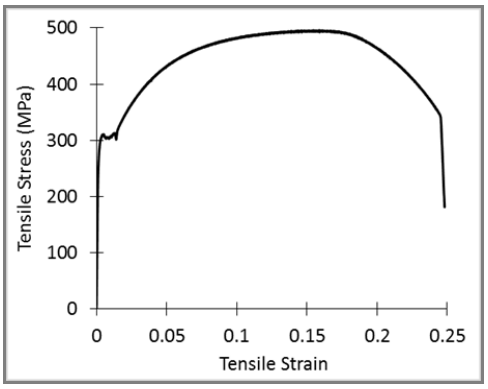

Fig. 1.10: *Tensile plot for SA333 C-Mn steel.*

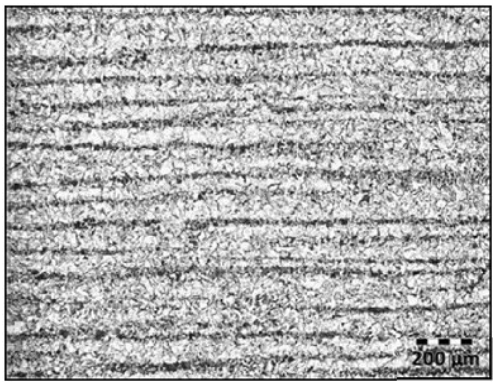

Fig. 1.11: *Optical microstructure of SA333 (Scale: 200µm).*

Typical tensile plot of the same material is presented above in figure 1.10. Elastic modulus 210 GPa, Poisson's ratio 0.3 is typical for the material. It is a steel of moderate strength (YS = 304 MPa, UTS = 495 MPa) and ductility (% elongation 24.5). There is about ±5% strength variation observed, changing the heat number alone. It is important to note from the tensile plot for the material is that, it has shown a long Luders Band upto about 1.4% strain.

Basic metallurgical investigations are also carried out to understand the experimentally observed phenomena. The typical microstructure of the material is presented above in figure 1.11 showing pearlite bands (volume fraction 30%) over ferrite matrix (volume fraction 70%) with average ferrite grain size of $22\,\mu m$. It is assumed that all the deformations are occurring mainly on the ferrite grains because ferrite is softer and susceptible to deformation than pearlite.

The typical chemical composition of the material is shown in table 1.1. SA333 steel is a low alloy steel. The two major alloying elements Carbon and Manganese are austenite stabilizers. Carbon has a strong tendency to segregate at the defects in steels (such as grain

boundaries and dislocations). Elements like – Fe, Mn may interact with carbon and form carbides.

The strengthening effect of Carbon in steel consists of interstitial solid solution strengthening and carbide dispersion strengthening. Carbon, simultaneously, decreases the ductility and weldability of the material (Sinha, 1989; Zhang and Wu, 1992). 0.18% Carbon in the steel generally deteriorates the surface quality (Totten, 2007).

Table 1.1: *Chemical composition of SA333 C-Mn Steel.*

Element	C	Mn	Si	P	Fe
Qty. by wt. (%)	0.18	0.90	0.02	0.02	Rest

Manganese, 0.90% by wt. present in SA333, is another major alloying element in this material. It is essentially used as a deoxidizer and a desulfurizer (Ross, 1992). Manganese, unlike Carbon, has favourable effect on weldability and improves surface quality. Manganese forms stable carbides in steel but cannot form in competition with Iron (Cementite), or even alter the microstructures formed after transformation (Maalekian, 2007). However, Manganese can infuse into solid solution Cementite at low as well as high concentrations. The presence of Manganese may enhance the segregation of Phosphorous to grain boundaries and induce temper embrittlement (Zhang and Wu, 1992).

Silicon and Phosphorus do not form Carbide and normally found in the matrix. Silicon, which is the principal deoxidiser, dissolves completely in ferrite increasing its strength without greatly decreasing ductility when the amount is low (Sinha, 1989). If combined with Manganese, Silicon may produce greater hardenability. Silicon can eliminate stress-corrosion, and improves wear resistance of the material. Phosphorus segregates during solidification, but to a lesser extent than Carbon. Phosphorus dissolves in ferrite and increases the strength of steels. Phosphorus has a very strong tendency to segregate at the grain boundaries, and causes the temper embrittlement of Mn-steels (Totten, 2007). The effect of Silicon and Phosphorous are hardly observable macroscopically as their presence is negligibly.

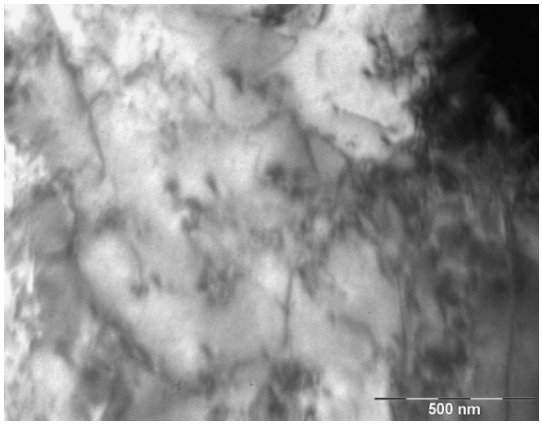

Fig. 1.12a: *TEM micrograph for SA333 C-Mn steel at 'as received' condition.*

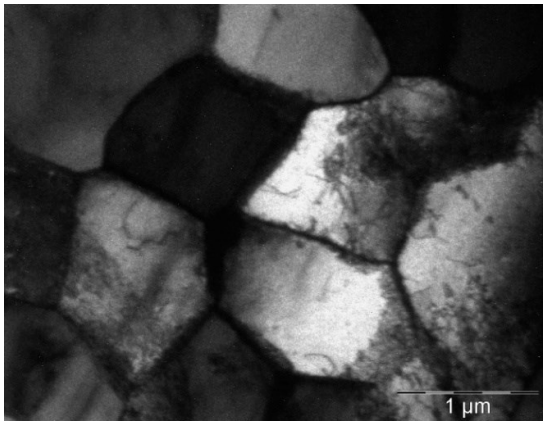

Fig. 1.12b: *TEM micrograph for SA333 C-Mn steel after failure (1.0% Strain amplitude, 16000 cycles).*

TEM imaging is done in Philips CM200 operated at $200\,kV$, for the material at 'as received' condition and 'after failure' of the samples, are displayed in figure 1.12a and 1.12b respectively. Though the TEM micrographs show no definitive dislocation structure for the material in 'as received' condition, there are traces (memory?) of obscure dislocation veins, formed during previous extensive plastic deformation like rolling. TEM micrographs after the failure of the samples show clear $1.2\,\mu m$ cellular substructures with dense wall made of dislocation tangles and practically clean interior.

1.5 Tools and Methods

The literature survey helps the researchers to do what is exactly needed to be done, which saves his time and resources. The literature survey also may direct the way how to proceed. Extensive literature survey on cyclic plastic behaviour and its modelling for different material shows a systematic and thorough investigation is required on the selected material and for that, different methods are standardized and standard tools are used. In this section, microstructural characterization, experimentation and finite element simulation as validation tool are discussed.

1.5.1 Metallurgical Investigation

Material microstructural and sub-structural features continuously evolve with cyclic plastic damage. To track this evolution and develop a deeper understanding of cyclic plastic deformation response, microstructural characterization is necessary. Appropriate preparation of samples is essential to properly study and capture high quality images of the microstructures. Details of sample preparation and microscopy are discussed in the sub-sections that follow.

1.5.1.1 Optical Microscopy

Optical microstructures are obtained by etching mirror polished sample surfaces by appropriate chemical reagent. Preparation of optical samples are thus two-step process: mechanical polishing and chemical etching. For mechanical polishing, the following steps are followed:

a. Cutting the sample through ISOMET 4000 slow speed diamond cutter,
b. Mounting sample in conductive copper mould,
c. Grinding the mould to remove surface irregularities,
d. Emery paper polishing to remove surface scratches,
e. Cloth polishing by alumina powder and colloidal silica to get mirror polished surface.

Material dependent chemical etchants are used for etching the smooth samples. A 4% NITAL solution (96% C_2H_5OH + 4% HNO_3) is to be used for SA333 C-Mn steel. The samples are submerged in etchant solution for a few seconds (typically 30 to 40 seconds) until the surface became dull. After cleaning and drying, samples are placed under an OLYMPUS 1000X optical microscope for microstructural study.

1.5.1.2 Transmission Electron Microscopy

Thin foils are prepared for examination in the Transmission Electron Microscopy (TEM). Thin slices of 0.2 mm to 0.3 mm thickness are cut off by a slow speed precision diamond cutter (ISOMET 4000). Thickness of slices are reduced to 0.1 mm by careful manual grinding on silicon carbide emery papers of 800 grits with intermittent cooling to avoid any rise in temperature. Coupons of 3 mm diameter are punched by a Gatan precision punching system. The coupons of SA333 C-Mn steel are finally thinned in a twin jet electro-polishing unit (Tenupol-III) at 40 V using a mixture of 10% Per-Chloric acid and 90% Acetic acid. Specimens are washed thoroughly in alcohol and dried properly. The electro-polished thin foils are examined in a TEM (Philips CM 200 with EDAX) at 200 kV operating voltage.

1.5.2 Mechanical Testing

Uniaxial monotonic and cyclic and, multiaxial cyclic tests are carried out on servo-hydraulic universal testing machine with automatic data acquisition system. The details of the tests are provided below:

1.5.2.1 Monotonic test

Uniaxial monotonic (tensile) tests are conducted for basic material properties. Tensile tests are performed according to ASTM E8M. Smooth round specimen with gauge length 30 mm and diameter 6 mm are used. A brief account of the tests are presented in table 1.2:

Table 1.2: *Overview of the monotonic tests.*

	Details	**Specification**	**Standard/ Grade**	**Maker**	**Remarks**
Testing Machine	Servo-Hydraulic Universal Testing Machine	100 kN Grip Capacity, 8800 Controller		Instron	'Blue Hill 2.0' software used
Measuring Instrument	Vernier Calliper	0 – 200 mm L.C. – 0.02		Mitutoyo	
	Extensometer	Static, 25 ± 5 mm		Instron	
Test Specimen	SA333 Grade-6 C-Mn Steel, Round tensile bar	Gauge diameter 6 mm, Gauge length 30 mm, Threaded specimen	ASTM E8M	Local Vendor	Dimensions are in 'mm'
Test Procedure	Tests are done in Room Temperature (300 K), in Displacement Controlled mode, for quasistatic Strain rate (10^{-3} per second)		ASTM E8M	As per ASTM	Current strain rate and temperature do not produce any rate effects

1.5.2.2 Cyclic plastic deformation experiments

Multiaxial conditions of loading are often experienced in service conditions. However due to limitations of equipment, complexity of testing and higher cost of testing, uniaxial mode of loading is often used for tests in the laboratory and the results are usually extrapolated or correlated with the actual operating conditions. In this work, both uniaxial and multiaxial tests are conducted and analysed.

1.5.2.2.1 Uniaxial testing

Cylindrical specimens of 8 mm gauge diameter and 20 mm gauge length are fabricated from the pipe stock available with their axes parallel to the pipe axis. The specimen geometry is as shown in figure 1.13a. All uniaxial and multiaxial strain controlled experiments (Tensile and LCF) are conducted at a strain rate of 10^{-3} s^{-1} and accordingly the displacement rates and the data extraction frequencies (200 pts. per cycle) are adjusted to achieve constant strain rate and accurate results without losing valuable information as far as possible. Similarly, all stress controlled experiments (Engineering and True Stress Controlled Ratcheting) are to be conducted at frequencies such that a constant stress rate of 50 MPa-s^{-1} is to be maintained throughout the investigation. Uniaxial experiments are to be carried out using a servo-electric test machine in laboratory environment (27 °C, 50% Relative Humidity). A close-up of the experimental setup is shown in figure 1.13b.

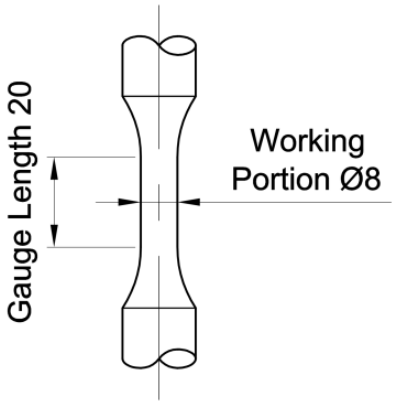

Fig. 1.13a: *Uniaxial specimen geometry (dimensions are in 'mm').*

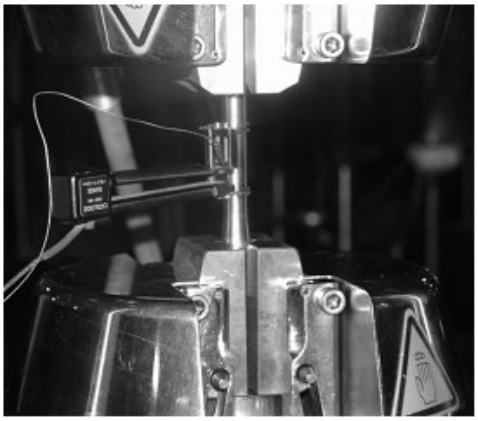

Fig. 1.13b: *Uniaxial testing system (INSTRON 8800).*

A 12.5 mm gauge length extensometer is to be used to measure the strain during tests. Tests are to be continued till failure and stress-strain data acquired throughout the test so as to obtain ~200 data points in each stress cycle for cyclic tests. Tests are to be conducted under software control using a computer interfaced to the control system of the testing machine and capture data automatically. For true stress controlled tests, the feedback from the extensometer was used to compute true strain and there from the true stress continuously. Applied loads were instantaneously altered to maintain true stress amplitude and mean stress as per the test specification ASTM E606M.

1.5.2.2.2 Multiaxial testing

Tubular specimens of 25 mm gauge length, 25.4 mm outer diameter and 1.7 mm wall thickness in the gauge portion are to be fabricated as per this geometry shown in fig. 1.14.

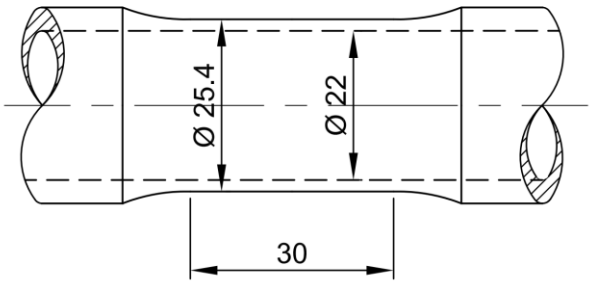

Fig. 1.14: *Multiaxial specimen geometry (dimensions are in 'mm').*

Multiaxial experiments are conducted using a 100 kN axial and 1 kN-m torsional capacity servo-hydraulic closed loop testing system (Instron 8800). The test setup employed is illustrated in figure 1.15a.

Fig. 1.15a: *Multiaxial testing system (INSTRON 8800).*

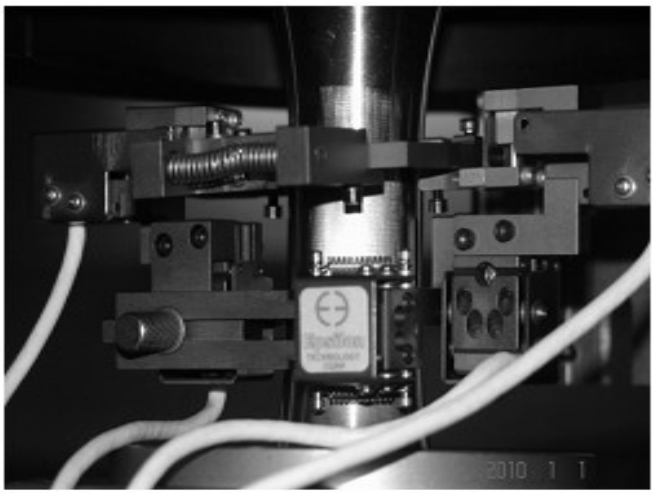

Fig. 1.15b: *Biaxial Extensometer.*

A 25 mm gauge length biaxial extensometer (figure 1.15b) with capacity of ±10 % axial strain and ±2.5 % shear strain (Epsilon made) is used to measure axial and shear strains on the outer surface of the hollow cylindrical specimen.

1.5.3 Validation Tool

Mathematical material model is validated through finite element analysis. Simulation results are compared to the experimental results to conform the validity of the model. A commercial FEA package - SIMULIA ABAQUS CAE v6.8 is used for accountability of the validation process. The steps for formulating and solving a finite element problem using commercial finite element software package like ABAQUS are described as follows:

a) Pre-processing,
   The pre-processing consists of defining: (i) the system geometry, (ii) employed material properties, (iii) the elements, (iv) meshing, (v) application of boundary conditions, (vi) defining the loading scheme.
b) Solution of finite element model defined in per-processing,
c) Post-processing to analyse and evaluation of the solutions obtained.

The finite element method is widely used for analysis of elastic-plastic response of structures. The finite element method employs constitutive modules to capture the material stress-strain response at each integration point. Structural response is the integrated output from all integration points. During structural analysis through finite element method, local and global level numerical integrations should be carried out simultaneously (Rahaman, 2006). Local integration performs numerical calculations using constitutive equations for finite increments of loading at integration points in each element. Global integration solves for the nodal force equilibrium equations in an iterative manner. The accuracy of a structural solution is dependent on the accuracy of calculation at the integration points. The structural stiffness matrix in turn depends on the tangent modulus calculated for each integration point. Thus, efficient global solution is dependent on consistency between the local numerical scheme and tangent modulus at each integration point. In this study, constitutive models have been implemented through the user material subroutine (UMAT for static analysis) facility with radial return method as the local numerical scheme.

The working (gauge length) portion of the specimen i.e. three dimensional Solid cylindrical and tubular specimen geometries for uniaxial and multiaxial cases respectively are required to be analysed. Geometries would be as per the dimensions shown in figure 1.13a and figure 1.14. Specimens are to be discretised adopting structural meshing. In case of solid cylindrical geometry, 8-noded linear hexahedral elements with 6-noded linear triangular prism elements at central zone are to be used to make a radial orientation. The hollow cylindrical specimen should use 8-noded linear hexahedral elements to get radially oriented. The elements are allowed to perform full integration (8 integration points in the brick and 2 on the wedge) with linear shape functions.

In this present study, a uniform loading distribution is considered on a regular and symmetric geometry, and the stress analysis of such a case results in no major strain or stress gradient. Therefore, no significant mesh sensitivity is expected.

Yet again, a mesh-sensitivity analysis is carried out for the cylindrical (Ø7 mm and gauge length 13 mm) specimen geometry and discretised it by 3D linear hexahedral elements with 8 integration points. The part is subjected to axial cyclic loading (one complete cycle) uniformly distributed over the cross-section for a particular strain amplitude. The material and other operating conditions are kept alike for the study.

The mesh tool in ABAQUS has its own algorithm that may restrict the user to select any arbitrary mesh sizes. In this case, the mesh size above 3 mm shows no variation in mesh sizes on the cross-section of the geometry. The present analysis within the feasible range of the mesh sizes is presented in the table 1.3 below. For different mesh sizes, the variations in the calculated stress and strain values at a representative time are noted along with the corresponding solution times.

At any time increment, it is observed that, the calculated strain and stress values show insignificant variation for different mesh sizes (for example, the stress strain values at time increment = 0.323 s, near peak stress, are presented in table 1.3).

Table 1.3: *The variation in solution times, calculated stress and strain values for mesh size variation.*

Shape function	Linear				
Number of integration points	8				
Global mesh size (mm)	4	3	2	1	0.5
Mesh size variation on the curved surface (mm)	2.68 - 3.25	2.68 - 3.25	1.8 - 2.16	0.91 - 0.93	0.5
Mesh size variation on the cross-section (mm)	1.45 - 2.68	1.45 - 2.68	1 - 1.8	0.57 - 0.91	0.2 - 0.5
Total Number of elements	48	48	120	840	5408
Total number of nodes	85	85	189	1095	6237
Computational time (s)	61	61	61	174	1057
Calculated strain at step time = 0.323 s	0.00318423	0.00318423	0.00318423	0.00318421	0.00318422
Calculated stress at step time = 0.323 s	327.78	327.78	327.78	327.779	327.779

On the contrary, the calculation time increases significantly when mesh size further reduced below 2 mm (table 1.3). From the observations it can be said that, 2 mm mesh size is the optimum choice for all the present simulations which provides sufficiently accurate results with minimal computation time.

Displacement boundary conditions are to be given according to the strain amplitudes using balanced triangular or sinusoidal amplitude function at reference points, conforming test conditions. Reference points are to be connected to the specific parts of the body through kinematic coupling. The coupling equation should allow tangential and axial displacements to avoid being over-constraint. The axial displacement and angular twist (in case of multiaxial loading) are to be applied on the reference points set on the axis of the cylindrical specimen. The boundary conditions (essentially the angular twist) are employed in cylindrical coordinate system, as the geometries are axisymmetric. Figure 1.16a and 1.16b respectively shows such discretised models created in ABAQUS FE platform.

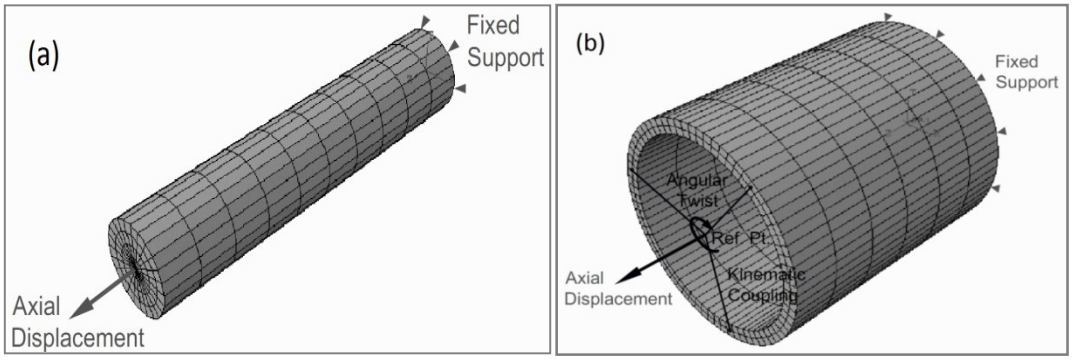

Fig. 1.16: *Discretised specimen with loading arrangements,* ***(a)*** *solid cylindrical, and* ***(b)*** *tubular with kinematic coupling.*

The major task, in the finite element analysis, is to devise the integration schemes for the constitutive mathematical material model.

1.5.3.1 Constitutive relations and backward Euler integration method

Backward Euler integration scheme is same as Euler method, only it is implicit. A step forward in time takes the updated trial state of stress outside the yield surface by elastic prediction, and then the state of stress is updated by plastic correction and brought back onto the yield surface in that particular time step. The function of the scheme named it 'Radial Return' or 'Return Mapping' algorithm, which consists of an elastic predictor and a plastic corrector (Nagtegaal, 1982; Simo and Taylor, 1985 and 1986; Kobayashi and Ohno, 2002). A schematic flow chart of the integration algorithm is shown in figure. 1.17:

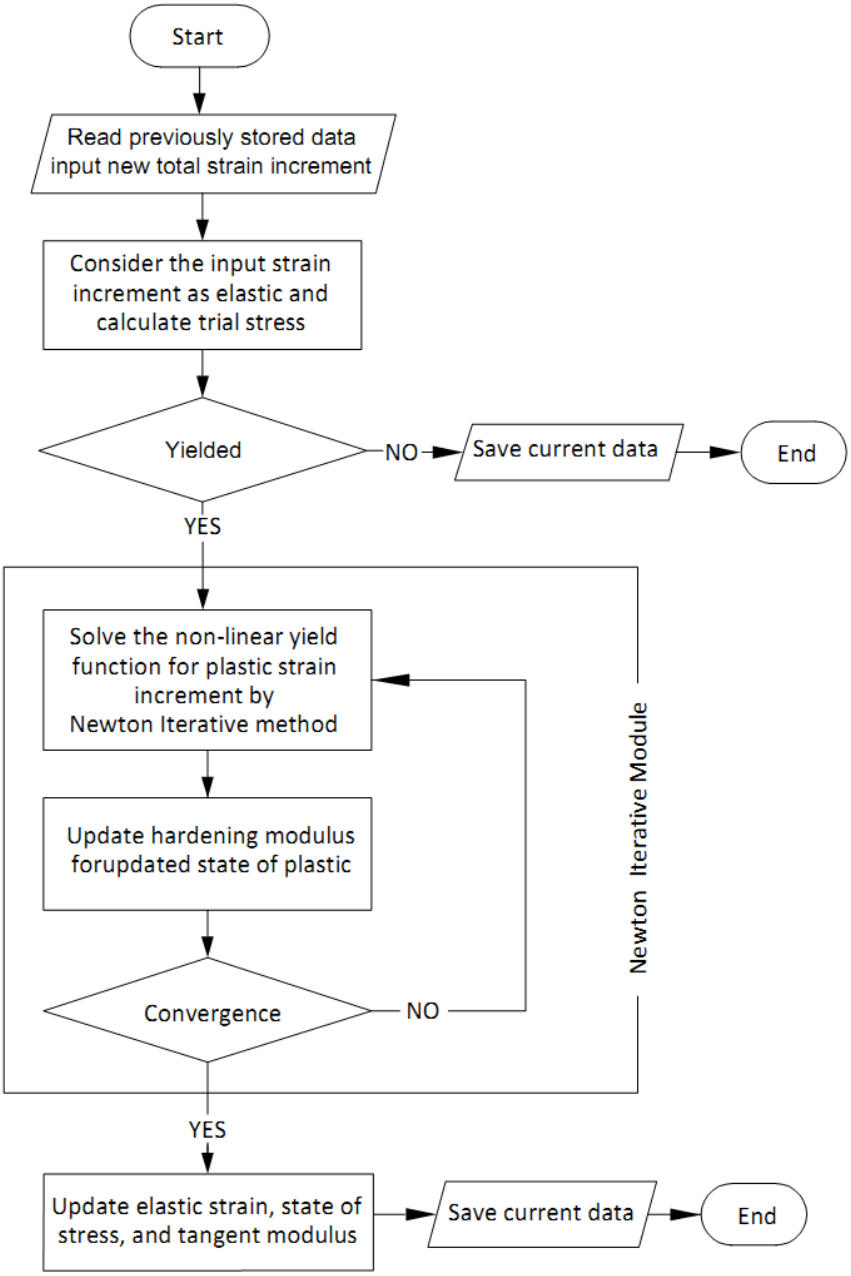

Fig. 1.17: *Schematic flow chart of the semi-implicit material algorithm.*

The integration scheme adopted in the present coding can be precisely named as semi-implicit integration scheme. Elastic prediction and radial return (plastic correction) makes the scheme implicit. Initially, the components of the total strain increment ($\Delta\varepsilon_{ij}$) fed into UMAT are assumed completely elastic and the elastic predictor stresses are calculated using generalised Hooke's law by elastic stiffness matrix.

But the incremental plastic strain components within the total of strain increment modify the stress value to the correct ones.

$$ {}^{1}\sigma_{ij} = {}^{0}\sigma_{ij} + \underbrace{\boxed{\mu\Delta\varepsilon_{ij} + \lambda Tr\left(\Delta\varepsilon_{ij}\right)}}_{\text{Elastic Predictor}} - \underbrace{\boxed{\mu\Delta\varepsilon_{ij}^{p}}}_{\substack{\text{Plastic}\\ \text{Corrector}}} \tag{1.1} $$

Where, prefix 1 and 0 signifies current and previous values respectively. μ and λ are Lame's constants, required to construct elastic stiffness matrix. $\Delta\varepsilon_{ij}$ is the total strain increment in that time step, $Tr()$ expresses the function $Tr(\Delta\varepsilon_{ij}) = \Delta\varepsilon_{ii}$ represents the volumetric strain increment.

Introducing equivalent plastic strain increment with flow vector current state of stress can be expressed as:

$$ {}^{1}\sigma_{ij} = {}^{trial}\sigma_{ij} - 2G\Delta\varepsilon_{eq}^{p}\frac{3}{2}\frac{S_{ij}-\alpha_{ij}}{S_{mises}} \tag{1.2} $$

Where, previous stress and elastic predictor stress cumulatively known as trial stress, and G is the shear modulus ($=\mu$). The yield function, using the trial stress, would be:

$$ \Phi = S_{mises} - R - \sigma_0 = S_{mises}^{trial} - 3G\Delta\varepsilon_{eq}^{p} - R - \sigma_0 = 0 \tag{1.3} $$

The above expression can be identified as a non-linear function of $\Delta\varepsilon_{eq}^{p}$. To maintain the consistency condition $d\phi$ should be equal to zero, i.e.

$$ d\phi = \frac{\partial\phi}{\partial\Delta\varepsilon_{eq}^{p}} d\Delta\varepsilon_{eq}^{p} = 0 \tag{1.4} $$

And together, in conjunction with the yield function (i.e. $\phi = 0$), the expression below can be solved for $\Delta\varepsilon_{eq}^{p}$ by Newton's iterative method.

$$ \phi + \frac{\partial\phi}{\partial\Delta\varepsilon_{eq}^{p}} d\Delta\varepsilon_{eq}^{p} = 0 \tag{1.5} $$

Where,

$$ \frac{\partial\phi}{\partial\Delta\varepsilon_{eq}^{p}} = h = n_{ij}\frac{\partial\Delta\alpha_{ij}}{\partial\Delta\varepsilon_{eq}^{p}} + \frac{\partial\Delta R}{\partial\Delta\varepsilon_{eq}^{p}} \tag{1.6} $$

Substituting above expressions into Newton-Raphson formulation and rearranging after i[th] iteration, the value of current back stresses will be:

$$\alpha_{ij}^{(i)} = \alpha_{ij}^{(i-1)} + \Delta\alpha_{ij}\left(\Delta\varepsilon_{eq}^{p\,(i)}\right) \tag{1.7}$$

As the value of back stresses changes depending on the equivalent plastic strain increment, the von-Mises equivalent trial stress will also change. Similarly, the value of the current isotropic hardening stress will be:

$$R^{(i)} = R^{(i-1)} + \Delta R\left(\Delta\varepsilon_{eq}^{p\,(i)}\right) \tag{1.8}$$

And, correspondingly the increment of plastic strain increment is expressed as:

$$d\Delta\varepsilon_{eq}^{p} = \frac{S_{mises}^{trial\,(i)} - 3G\Delta\varepsilon_{ea}^{p\,(i)} - R^{(i)} - \underline{\sigma_0}}{3G + \tilde{H}} \tag{1.9}$$

Where, '~' signifies that, H is not completely modified within a time step for every iterations. The isotropic part of it remains unaltered and be updated after the time step. This is the reason why the process is called semi-implicit integration. For stability, this semi-implicit scheme is adopted.

Yield criterion is employed as the convergence criterion with some numerical tolerance. For convergence, if not attained, the equivalent plastic strain increment will be further adjusted by accumulating calculated increment $(d\Delta\varepsilon_{eq}^{p})$ for the next iteration (say i+1[th]) in that time step as:

$$\Delta\varepsilon_{eq}^{p\,(i+1)} = \Delta\varepsilon_{eq}^{p\,(i)} + d\Delta\varepsilon_{eq}^{p} \tag{1.10}$$

1.5.3.2 Newton iterative method

Newton's method or Newton-Raphson method (Ypma, 1995) is an iterative technique for finding successively better approximations to the roots of a real valued function. This is a very fast method involves the slope or the function derivative to search the root.

$$x^{i+1} = x^{i} - \frac{f\left(x^{i}\right)}{f'\left(x^{i}\right)} \tag{1.11}$$

Newton method is applied in the implicit plasticity algorithms to find plastic strain increments for a particular time step solving the non-linear yield function of equivalent plastic strain increment.

1.5.3.3 Consistent tangent modulus

After convergence of the local iteration for the numerical scheme, it is important to calculate the consistent tangent modulus to preserve the quadratic convergence rate at global level of finite element calculation. Numerical method is said to be consistent with

the tangent modulus when prescribed stress increment for given strain increment from tangent modulus is consistent with stress calculated by local numerical scheme. Such tangent matrix is termed as consistent tangent modulus for the numerical scheme adapted. The consistent tangent modulus is prescribed in a general form for the Armstrong and Frederick model with radial return algorithm by Kobayashi and Ohno (2002), and Rahaman (2006).

1.6 Closing Remarks

Careful scrutiny of the existing literature, lay the stepping stone of the entire work. Modelling of cyclic plastic deformation behaviour is quite complex, and therefore a systematic approach is required. The objective of the work, benchmarked into small goals, is set after the survey. SA333 Grade-6 C-Mn steel is selected as suitable material after literature survey. Necessary experimentation, analysis, etc. are sequentially planned in the goal-setting section. Methodology, tools and software required are also discussed briefly in the previous sections.

The thesis follows the chronological development of the work and consists of four chapters. The next chapter (second) addresses the material behaviour of SA333 subjected to balanced uniaxial cyclic plastic loading. The third chapter deals with necessary experimentation and modelling aspects for balanced non-proportional loading and the fourth chapter concentrate on the unbalanced uniaxial and multiaxial cyclic plastic loading on the material. The conclusion and the scope of future work have been presented in the final chapter of this thesis work.

Present work includes extensive mechanical and metallurgical investigations. Some of them might need to be outsourced. Bhabha Atomic Research Centre, Mumbai and National Metallurgical Laboratory, Jamshedpur are acknowledged in this regard. Some analytical parameters and ideas might be borrowed from literature and are cited in respective section.

1.7 References

ASTM E8M

ASTM E606M

3DS Simulia Abaqus v6.8, Users' Manual

1842, Rankine, W. J. M., On the causes of the unexpected breakage of the journals of railway axles, and on the means of preventing such accidents by observing the law of continuity in their construction, Institution of Civil Engineers, Minutes of Proceedings, p105-108.

1854, Braithwaite, F., On the fatigue and consequent fracture of metals, Institution of Civil Engineers, Minutes of Proceedings, p463–474.

1855, Wöhler, A., Theorierechtekigereiserner Brückenbalkenmit Gitterwänden und mit Blechwänden, Zeitschriftfür Bauwesen, vol. 5 pp121-166.

1864, Fairbairn, W., Experiments to determine the effect of impact, vibratory action and long continued changes of load on wrought iron girders, Philosophical Transactions of the Royal Society, volume 154, pp311.

1870, Wöhler, A., Über die Festigkeitsversuchemit Eisen und Stahl, Zeitschriftfür Bauwesen, vol. 20 p73-106

1874,Gerber, W. Z., Calculation of the allowable stresses in iron structures, Z. Bayer ArchitIng Ver, volume 6, issue 6, p101–110.

1886, Bauschinger, J., Mechanisch-Techanischen Laboratorium. Materials Forum, 1886.

1899, Goodman, J., J. Mechanics Applied to Engineering, 1st ed., Longmans, Green, New York.

1903, Ewing, J.A., Humfrey, J.C.W., *Phil. Trans. Roy. Soc.*, vol. 200, p241.

1910, Basquin, O.H., Proc. Am. Soc. Testing and Materials 10, p. 625.

1923, Masing, G., ZurHeyn'schen Theorie der Verfestigung der Metalledurchverborgenelastische Spannungen, In: Harries C.D. (eds) Wissenschaftliche Veröffentlichungenausdem Siemens – Konzern, Springer, Berlin, Heidelberg, pp 231-239.

1924, Palmgren, A. A., Durability of ball bearings. 2. Ver. dt. Ing., Volume 68, pp 339.

1930, Soderberg, C. R., Fatigue of safety and working stress, Transactions of the American Society of Mechanical Engineers, Volume 52 (Part APM-52-2), pp 13-28.

1933, Gough, H. J., Crystalline structure in relation to failure of metals - especially by fatigue, Edgar Marburg Lecture, Proceedings of the American Society for Testing and Materials, Volume 33, Issue II, pp3-114.

1934, Orowan, E. Z., ZurKristallplastizität. I, Tieftemperaturplastizität und Beckersche Formel, Zeitschriftfür Physik, Volume 89, Issue 9-10, pp605-613.

1938, Taylor, G. I., Plastic strain in metals, J. Institute of Metals, Volume 62,pp 307-324.

1940, Bragg, W. L., The structure of a cold worked metal, Proceedings of the Physical Society, Volume 52, Issue 1, pp105-109.

1940, Burger, J. M., Geometrical considerations concerning the structural irregularities to be assumed in a crystal, Proceedings of the Physical Society, 52, 1, 23-33.

1942, Gensamer, M., Pearsall, E. B., Pellini, W. S., Low, J. R. Jr., Trans. ASM, 30, 983.

1945, Miner, M. A., Cumulative damage in fatigue, J. appl. Mech., 67, Al59-164.

1946, Neuber, H., Theory of Notch Stresses: Principles for Exact Stress Calculations, J. W. Edwards, Ann Arbor, Michigan.

1948, Epremian, E., Nippes, E. F., Transactions of the American Society of Metals, Volume 40, pp 870-896.

1949, Read, W. T., Shockley, W., Quantitative Predictions from Dislocation Models of Crystal Grain Boundaries, Physical Review, Volume 75, Issue 4, pp 692.

1950, Read, W. T., Shockley, W., Dislocation models of grain boundaries, Physical Review, Volume 78, Issue 3, pp 275

1953, Horger, O. J., ASTM, Special technical publication, Volume 144, pp 44

1953, Manson, S.S., Behavior of materials under conditions of thermal stress, National Advisory Committee for Aeronautics, NACA TN-2933

1954, Coffin, L.F., A study of the effects of cyclic thermal stresses on a ductile metal. Transactions of American Society for Testing and Materials 76: 931-950.

1954, Polakowski, N. H., Palchoudhuri, A., Trans. Amer. Soc. Test. Mat., 54, p701.

1955, Wood, W. A., Bulletin of the Institute of Metals, Volume 3, pp 5-6.

1956, Prager, W., A New Method of Analyzing Stresses and Strains in Work Hardening Plastic Solids, Journal of Applied Mechanics, Volume 23, pp. 493-496.

1956, Allen, N. P., Forrest, P. G., Proceedings of the International Conference on the Fatigue of Metals, London, pp 327-340.

1957, Siebel, E., Gaier, M., The influence of surface roughness on the fatigue strength of steels and non-ferrous alloys, The Engineers' Digest, Volume 18, Issue 3, pp 109-112.

1958, Kachanov, L. M., The Theory of Creep. Kennedy A.J. (ed., English Translation), National Lending Library, Boston Spa.

1958, Besseling, J.F., A Theory of Elastic, Plastic and Creep Deformations of an Initially Isotropic Material. Journal of Applied Mechanics, Volume 25, pp 529-536.

1960, Hammond, R. A. F., Williams, C., *Metallurgical Reviews*, Volume 5, Issue 18, pp165.

1960, Li, J. C. M., Some elastic properties of an edge dislocation wall, Acta Metallurgica, Volume 8, Issue 8, pp563-574.

1961, Kuguel, R., A relation between theoretical stress concentration factor and fatigue notch factor deducted from the concept of highly stresses volume, ASTM STP Proc, 61, pp732–748.

1963, Li, J. C. M., Petch Relation and Grain Boundary Sources, Transactions of the Metallurgical Society of AIME, 227, 239-247.

1963, Almen, J. O., Black, P. H., Residual Stresses and Fatigue in Metals, McGraw-Hill Book Co., New York.

1963, Paris, P.C., Erdogan, F., A critical analysis of crack propagation laws, J. Basic. Eng. 85, p528.

1966, Armstrong, P.J., Frederick, C.O., A Mathematical Representation of the Multiaxial Bauschinger Effect. CEGB Report No. RD/B/N 731.

1967, Feltner, C. E., Laird, C., Cyclic stress-strain response of F.C.C. metals and alloys – I Phenomenological experiments, Acta Metallurgica, Volume 15, Issue 10, pp 1621-1632.

1967, Laird, C., The Influence of Metallurgical Structure on the Mechanisms of Fatigue Crack Propagation, STP415, ASTM, DOI: 10.1520/STP47230S.

1967, Mróz, Z., On the description of anisotropic work hardening, Journal of the Mechanics and Physics of Solids, volume 15, issue 3

1969, Plumbridge, W. J., Ryder, D. A., Metall. Rev., 14, p119.

1969, Ellison, E. G., Journal of Mechanical Engineering Sciences, Volume 11, pp 318-339.

1969, Neumann, P., Coarse slip model of fatigue, Acta Metall., Volume 17, Issue 9, pp 1219-1225.

1970, Kocks, U. F., On the temperature and stress dependence of the dislocation velocity stress exponent, Scripta Metallurgica, Volume 4, Issue 1, pp 29-31.

1970, Ashby, M. F., Philosophical Magazines, Volume 21, pp 399-424.

1971, Strang, G., The finite element method and approximation theory, SYNSPADE Proceedings, Academic Press, pp547-584.

1971, Thompson, A.W. Backofen, W.A., The Effect of Grain Size on Fatigue, Acta Metallurgica, Volume 19, pp 597.

1972, Grosskreutz, J. C., Shaw, G. G., Acta Met, 20, p523.

1972, Phillips, A., Tang, J. L., The Effect of Loading Paths on the Yield Surface at Elevated Temperatures, International Journal of Solids and Structures, Volume 8, Issue 4, pp 463-474.

1972, Walton and Ellison, Intern. Metal. Reviews, 17, p100-116.

1974a, Neumann, P., New experiments concerning the slip processes at propagating fatigue cracks – I, Acta Metallurgica, Volume 22, Issue 9, pp 1155-1165.

1974b, Neumann, P., The geometry of slip processes at a propagating fatigue crack – II, ActaMetallurgica, Volume 22, Issue 9, pp 1167-1178.

1974, Peterson, R.E., Stress Concentration Factors, Wiley, New York

1975, Dafalias, Y.F., Popov, E.P., A model of nonlinearly hardening materials for complex loading, ActaMechanica, volume 21, issue 3

1975, Mróz, Z., Lind, N.C., Simplified theories of cyclic plasticity, Acta Mech., volume 22, issue 1

1975, Krempl, E., On the interaction of rate and history dependence in structural metals, Acta Mechanica, volume 22, issue 1

1975, Lubliner, J., Non-smooth dissipation functions and yield criteria, Acta Mechanica, Volume 22, Issue 3

1975, Radhakrishnan, V. M., Baburamani, P. S., An investigation of the effect of pre-straining on fatigue crack growth, Materials Science and Engineering, Volume 17, Issue 2, pp 283-288.

1976, Bathe, K. J., Wilson, E.L., Numerical Methods in Finite Element Analysis, Prentice Hall, ISBN: 978-0-136-27190-1

1976, Dafalias, Y. F., Popov, E. P., Plastic Internal Variables Formalism of Cyclic Plasticity, Journal of Applied Mechanics, Volume 43, pp. 645-650.

1976, Miller, A., An inelastic constitutive model for monotonic, cyclic, and creep deformation - Part I: Equations development and analytical procedures, Journal of Engineering Materials and Technology, volume 98, issue 2, p97

1978, Zaverl Jr., F., Lee, D., Constitutive relations for nuclear reactor core materials, Journal of Nuclear Materials, volume 75, issue 1, p14

1979, Laird, C., Ramanathan, S., Journal of Microscopy, volume 116, Issue 1, Pages 123–140

1979, Ritchie, R. O., Near-threshold fatigue crack propagation in steels, International Metals Reviews, Volume 20, pp 205-230.

1979, McEvily, A. J., Staehle Eds., R. W., Corrosion Fatigue, National Association of Corrosion Engineers, Houston; Duquette, D. J., in Fatigue and Microstructure, 1978 ASM Materials Science Seminar, American Society for Metals, Metals Park, Ohio, pp 335-363.

1979, Phillips, A., Lee, C.W., Yield Surfaces and Loading Surfaces. Experiments and Recommendations, International Journal of Solids and Structures, Vol. 15, pp. 715-729.

1979, Chaboche, J.L., Dang Van, K., Cordier, G., Modelization of the strain memory effect on the cyclic hardening of 316 stainless steel, SMiRT-5, Berlin.

1979, Essmann, U., Mughrabi, H., Annihilation of dislocations during tensile and cyclic deformation and limits of dislocation densities, Philosophical Magazine A, Volume 40, Issue 6, pp731

1980, Kliman, V., Bílý, M., The influence of mode control, mean value and frequency of loading on the cyclic stress-strain curve, Material Science and Engineering, Volume 44, Issue 1, pp 73-79.

1980, Turner, A. P. L., Martin, T. J., Cyclic creep of type 304 stainless steel during unbalanced tension-compression loading at elevated temperature, Metallurgical and Materials Transactions A, Volume 11, Issue 3,pp 475-481.

1981, Drucker, D.C., Palgen, L., On stress-Strain Relations Suitable for Cyclic and Other Loadings, Journal of Applied Mechanics, Vol 48, pp. 479-485.

1981, Meckings, H., Kocks, U. F., kinetics of flow and strain-hardening, Acta Metallurgica, Volume 29, pp1865-1875.

1982, Nagtegaal, J. C., On the implementation of inelastic constitutive equations with special reference to large deformation problems, Computer Methods in Applied Mechanics and Engineering, 33, p469-484.

1983, Cameron, W. E., McCulloch, M. T., Walker, D. A., Boninitepetrogenesis: chemical and Nd–Sr isotopic constraints, Earth and Planetary Science Letters, Volume 65, pp75-89.

1983, Chaboche, J.L., Rousselier, G., On the Plastic and Viscoplastic Constitutive Equations, Part I - Rules Developed with Internal Variable Concept, Journal of Pressure Vessel Technology, Volume 105, Issue 2

1983, Chaboche, J.L., Rousselier, G., On the Plastic and Viscoplastic Constitutive Equations, Part II – Application, Journal of Pressure Vessel Technology, volume 105, issue 2

1983, Tseng, N.T., Lee, G.C., Simple Plasticity Model of the Two-Surface Type, ASCE Journal of Engineering Mechanics, Volume 109, pp. 795-810

1984, Cailletaud, G., Kaczmarek, H., Policella, H., Some elements on the multiaxial behaviour of 316l stainless steel at room temperature, Mechanics of Materials, volume 3, issue 4, p333

1984, Elline, F., Kujawaski, D., Plastic strain energy in fatigue failure, Journal of Engineering Materials and Technology Transactions, Volume 106, pp 342-347.

1984, Krempl, E., Lu, H., The hardening and rate-dependent behaviour of fully annealed Type 304 Stainless Steel under biaxial in-phase and out-of-phase strain cycling at room temperature, Journal of Engineering Materials and Technology, volume 106, p376

1984, Lorenzo, Fernando, Laird, Campbell,A new approach to predicting fatigue life behavior underthe action of mean stresses, Material Science and Engineering, Volume 62, Issue 2, pp205-210.

1985, Casey, J., Sullivan, T. D., Pressure dependency, strength-differential effect, and plastic volume expansion in metals, International Journal of Plasticity, Volume 1, Issue 1, pp 39-61.

1985, Franciosi, P., The concepts of latent hardening and strain hardening in metallic single crystals, ActaMetallurgica, Volume 33, Issue 9, pp 1601-1612.

1985, McDowell, D. L., A two surface model for transient nonproportional cyclic plasticity, Part I: Development of Appropriate Equations, Journal of Applied Mechanics, Volume 52, Issue 2, pp298-302.

1985, Ohashi,Y., Kawai, M., Kaito, T., Inelastic behavior of type 316 stainless steel under multiaxial nonproportional cyclic stressings at elevated temperature, Journal of Engineering Materials and Technology, Volume 107, Issue 2, pp 101-109.

1985, Putatunda, S. K., Rigsbee, J. M., Effect of specimen size on fatigue crack growth rate in AISI 4340 steel, Engineering Fracture Mechanics, Volume 22, Issue 2, PP335-345.

1985, Simo, J. C., Taylor, R.L., Consistent tangent operators for rate-independent elastoplasticity, Computer Methods in Applied Mechanics and Engineering, volume 48, pp101-118.

1985, Tanaka, E., Murakami, S., Ooka, M., Effects of strain path shapes on non-proportional cyclic plasticity, Journal of the Mechanics and Physics of Solids, volume 33, issue 6, p559

1986, Simo, J. C., Taylor, R.L., A return mapping algorithm for plane stress elastoplasticity, International Journal for Numerical Methods in Engineering, volume 22, pp649-670.

1986, Chaboche, J. L., Time-independent constitutive theories for cyclic plasticity, International Journal of Plasticity, volume 2, issue 2

1986, Dafalias, Y.F., Bounding Surface Plasticity-Part I: Mathematical Foundation and Hypoplasticity, Journal of Engineering Mechanics, volume 112, issue 9

1986, Dafalias, Y.F., Herrmann, L.R., Bounding Surface Plasticity, Part II - Application to Isotropic Cohesive Soils, Journal of Engineering Mechanics, volume 112,issue 12

1986, Dafalias, Y.F., Anandarajah, A., Bounding Surface Plasticity, part III - Application to Anisotropic Cohesive Soils, Journal of Engineering Mechanics, volume 112,issue 12

1986, Haupt, P., Tsakmakis, Ch., On kinematic hardening and large plastic deformations, International Journal of Plasticity, volume 2, issue 3

1986, Khan, A. S., Parikh, Y., Large deformation in polycrystalline copper under combined tension-torsion loading, unloading and reloading or reverse loading, International Journal of Plasticity, volume 2,issue 4, p379

1986, Tanaka, K., Kobayashi, S., Sato, Y., Thermomechanics of transformation pseudoelasticity and shape memory effect in alloys, International Journal of Plasticity, volume 2, issue 1

1987, Benallal, A., Marquis, D., Constitutive equation for nonproportional cyclic elasto-viscoplasticity, Journal of Engineering Materials and Technology, volume 109, p326

1987, Boller, Chr., Seeger, T., Materials Data for Cyclic Loading, Elsevier, ISBN: 978-0-444-42875-2.

1987, Eckert, Rainer, Laird, Campbell, Bassani,John, Mechanism of fracture produced by fatigue cycling with a positive mean stress in copper, Materials Science and Engineering, Volume 91, pp 81-88.

1987, Kim K. T., Carroll, M. M., Compaction equations for strain hardening porous materials, International Journal of Plasticity, Volume 3, Issue 1, pp63-73.

1987, Mughrabi, H., The long-range internal stress field in the dislocation wall structure of persistent slip bands, Physica Status Solidi (A), Volume 104, Issue 1, pp 107-120.

1988, Dieter, G. E., Mechanical Metallurgy, McGraw Hill, ISBN: 978-0-071-00406-8.

1988, Fatemi, A., Socie, D.F., A critical plane approach to multiaxial fatigue, Fatigue & Fracture of Engineering Materials & Structures, volume 11,issue 3

1988, Wang, Z., Laird, C., Relationship between loading process and Masing behavior in cyclic deformation, Materials Science and Engineering: A, Volume 101, Pages L1-L5.

1989, Sinha, A. K., Ferrous Physical Metallurgy, Butterworths, London.

1989, McDowell, D.L., Evaluation of intersection conditions for two-surface plasticity theory, International Journal of Plasticity, volume 5, p25

1989, Rauch, E.F., Schmitt, J.H., Dislocation substructures in mild steel deformed in simple shear Materials Science and Engineering A, volume 113, p 441

1989, Lukáš, P., Kunz, L., Effect of mean stress on cyclic stress–strain response and high cycle fatigue life, International Journal of Fatigue, Volume 11, Issue 1, pp 55-58.

1990, Doong, S. H., Socie D. F., Robertson, I. M., Dislocation Substructures and Nonproportional Hardening. ASME Journal of Engineering Materials and technology Vol. 112, No. 4, pp. 456–465.

1990, Forman, R. G., Mettu, S. R., Behavior of surface and corner cracks subjected to tensile and bending loads in Ti-6Al-4V alloy, NASA Technical Memorandum 102165.

1990, Yoshida,Fusahito, Uniaxial and biaxial creep-ratcheting behavior of SUS304 stainless steel at room temperature, International Journal of Pressure Vessels and Piping, Volume 44, Issue 2, pp 207-223.

1991, Chaboche, J. L., On some modifications of kinematic hardening to improve the description of ratchetting effects, International Journal of Plasticity, Volume 7, Issue 7, pp 661-678.

1991, Voyiadjis, G.Z., Sivakumar, S. M., A Robust Kinematic Hardening Rule for Cyclic Plasticity with Ratcheting Effects, Part I: Theoretical Formulation, ActaMechanica, Volume 90, pp105.

1992, Guionnet, C., Modeling of Ratcheting in Biaxial Experiments, Journal of Engineering Materials and Technology, Volume 114, pp 56-62.

1992, Zhang, S., Wu, C., Ferrous Materials, Metallurgical Industry Press, Beijing.

1992, Ross, R. B., Metallic Materials Specification Handbook, Fourth Ed., Chapman & Hall, London.

1992, Haupt, P., Kamlah, M., Tsakmakis, Ch.,Continuous representation of hardening properties in cyclic plasticity,International Journal of Plasticity, volume 8,pp803

1992, Guionnet, C.,Modeling of Ratcheting in Biaxial Experiments. Journal of Engineering Materialsand Technology, Volume 114, p56-62.

1993, Hartmann, S., Haupt, P., Stress computation and consistent tangent operator using non-linear kinematic hardening models, International Journal for Numerical Methods in Engineering, 36, p3801.

1993, Delobelle, P., Synthesis of the elastoviscoplasticbehavior and modelization of an austenitic stainless steel ..., Part 1: Behaviour,International Journal of Plasticity, Volume 9, Issue 1, pp65

1993, Delobelle, P., Synthesis of the elastoviscoplasticbehavior and modelization of an austenitic stainless steel ..., Part 2: Phenomenological Modelization, International Journal of Plasticity, volume 9, issue 1, p87

1993, Li, Y., Laird, C., Masing behavior observed in monocrystalline copper during cyclic deformation, Materials Science and Engineering: A, Volume 161, Issue 1, pp 23-29.

1993a, Ohno, N., Wang, J.D., Kinematic hardening rules with critical state of dynamic recovery, part I: Formulation, International Journal of Plasticity, Volume 9, Issue 3, pp 375-390.

1993b, Ohno, N., Wang, J.D., Kinematic hardening rules with critical state of dynamic recovery, part II: Application, International Journal of Plasticity, Volume 9, Issue 3, pp 391-403.

1994, Hassan, Tasnim, Kyriakides,Stelios, Ratcheting of cyclically hardening and softeningmaterials, I: uniaxial behaviour, International Journal of Plasticity, Volume 10, Issue 2, pp 149-184.

1994, Holste, C., Bretschneider, J., Hache T., in Proc. 10thInternational Conference on the Strength of Materials, Sendai, ed.H. Oikawa, K. Maruyama, S. Takeuchi and M.Yamaguchi. The Japan Institute of Metals, pp 477.

1994a, Jiang, Y., Sehitoglu, H., Cyclic ratchetting of 1070 steel under multiaxial stress states, International Journal of Plasticity, Volume 10, Issue 5, pp 579-608.

1994b, Jiang, Y., Sehitoglu, H., Multiaxial cyclic ratchetting under multiple step loading, International Journal of Plasticity, Volume 10, Issue 8, pp 849-870.

1994, Ohno, N., Wang, J. D., Kinematic hardening rules for simulation of ratchetting behaviour, European journal of mechanics: A. Solids, Volume 13, Issue 4, pp 519-531.

1994, Tanaka, E., A nonproportionality parameter and a cyclic viscoplastic constitutive model taking into account amplitude dependence and memory effects of isotropic hardening. European Journal of Mechanics, A/Solids 13, 155–173.

1994, Voyiadjis, G. Z., Sivakumar, S. M., Cyclic Plasticity and Ratchetting, Studies in Applied Mechanics, 35, 253-295.

1995, Ristinma, M., Cyclic plasticity model using one yield surface only, International Journal of Plasticity, volume 11,issue 2, p163

1995, Haupt, P., Kamlah, M., Representation of cyclic hardening and softening properties using continuous variables, International Journal of Plasticity, volume 11,issue 3, p267

1995, McDowell, D. L., Stress state dependence of cyclic ratcheting behavior of two rail steels, International Journal of Plasticity, volume 11, p397

1995, Jiang, Y., Kurath, P., Characteristics of Armstrong-Frederick type plasticity models, International Journal of Plasticity, volume 12, issue 3, p387

1995, Ypma, T. J., Historical development of Newton-Raphson method, Society for Industrial and Applied Mathematics, Volume 37, Issue 4, pp 531-551.

1996, Ellyin, F., Fatigue Damage, Crack Growth and Life Prediction, Springer Publication, ISBN:978-9-400-91509-1

1996, Corona,E., Hassan, T., Kyriakides, S., On the performance of kinematic hardening rules in predicting a class of biaxial ratcheting histories, International Journal of Plasticity, Volume 12, pp 117.

1996, Jiang, Y., Sehitoglu, H., Modeling of Cyclic Ratchetting Plasticity - Part I: Development of Constitutive Relations, ASME Journal of Applied Mechanics, volume 63,issue 3, p720

1996, Raman, S. G. S., Padmanabhan, K. A., Effect of prior cold work on the room-temperature low-cycle fatigue behavior of AISI 304LN stainless steel, International Journal of Fatigue, Volume 18, pp 71-79.

1997, Jiang, Y., Kurath, P., Nonproportional cyclic deformation: critical experiments and analytical modeling, International Journal of Plasticity, volume 13, p743.

1997, Mughrabi, Haël, Christ, Hans-Jürgen, Cyclic Deformation and Fatigue of Selected Ferritic and Austenitic Steels: Specific Aspects, ISIJ International, Volume 37, Issue 12, pp 1154-1169.

1998, Suresh, S., Fatigue of Materials (2nd Edition), Cambridge University Press, Cambridge, ISBN: 978-0-52-157847-9.

1998, Basuroychowdhury, I. N., Voyiadjis, G. Z., A multiaxial cyclic plasticity model for nonproportional loading cases, International Journal of Plasticity, volume 14, p855.

1998, Voyiadjis, G. Z., Basuroychowdhury, I. N., A Plasticity Model for Multiaxial Cyclic Loading and Ratcheting, ActaMechanica, Vol 126, pp. 19-35.

1998, Estrin, Y., Dislocation theory based constitutive modelling: foundations and applications, Journal of Materials Processing Technology, 80-81, pp33-39.

1999, Frost, N. E., Marsh, K. J., Pook, L. P., Metal Fatigue, Dover Publication, ISBN: 978-0-486-40927-9

1999, Makkonen, M., Size effect and notch size effect in metal fatigue. Thesis for the degree of Doctor of Science (Technology), Lappeenranta University of Technology. ActaUniversitatisLappeenrantaensis 83.

2000, Valiev, R. Z., Islamgaliev, R. K., Alexandrov, I. V., Bulk nanostructured materials from severe plastic deformation, Prog. Mater. Sci., 45, p103-189.

2000, Brown, L.M., Dislocation plasticity in persistent slip bands, Materials Science and Engineering A, Volume 285, pp35-42.

2000, Abdel-Karim, M., Ohno, N., Kinematic hardening model suitable for ratcheting with steady-state, International Journal of Plasticity, volume 16, p225.

2000, Bari, Shafiqul, Hassan, Tasnim, Anatomy of coupled constitutive models for ratcheting simulation, International Journal of Plasticity, Volume 16, Issues 3-4, pp 381-409.

2000, Ohno, N., Abdel-Karim, M., Uniaxial ratcheting of 316FR steel at room temperature - Part II: constitutive modeling and simulation, Journal of Engineering Materials and Technology, vol 122, p35

2000, Peeters, B., Kalidindi, S.R., van Houtte, P., Aernoudt, E., A crystal plasticity based work-hardening/softening model for B.C.C. metals under changing strain paths, ActaMaterialia, volume 48, p2123

2001, Jiang, Y., An experimental study of inhomogeneous cyclic plastic deformation, Journal of engineering materials and technology, Volume 123, Issue 3, pp 274-280.

2001, Plumtree, A., Abdel-Raouf, H. A., Cyclic stress–strain response and substructure, International Journal of Fatigue, Volume 23, pp 799-805.

2001a, Peeters, B., Seefeldt, M., Teodosiu, C., Kalidindi, S.R., van Houtte, P., Aernoudt, E., Work-hardening/softening of b.c.c. polycrystals during changing strain paths: I. An integrated model based on substructure and texture evolution, and its prediction of the stress–strain behavior of an IF steel during two-stage strain paths, ActaMaterialia, volume 49, p1607

2001b, Peeters, B., Seefeldt, M., Kalidindi, S.R., van Houtte, P., Aernoudt, E., The incorporation of dislocation sheets into a model for plastic deformation of b.c.c. polycrystals and its influence on *r*-values, Material Science and Engineering A, volume 319-321, p188

2002, Bari, Shafiqul, Hassan, Tasnim, An advancement in cyclic plasticity modelling for multiaxial ratcheting simulation, International Journal of Plasticity, volume 18, Issue 7, pp873-894.

2002, Kang, G., Gao, Q., Yang, X., Uniaxial cyclic ratcheting and plastic flow properties of SS304 stainless steel at room and elevated temperatures, Mechanics of Materials, Volume 34, pp 145.

2002, Kobayashi, M., Ohno, N., Implementation of cyclic plasticity models based on a general form of kinematic hardening, International Journal for Numerical Methods in Engineering, 53, p2217-2238.

2002, Sedláček, R., Blum, W., Kratochvíl, J., Forest, S., Subgrain Formation during Deformation - Physical Origin and Consequences, Metallurgical And Materials Transactions A, Volume 33A, pp 319-327.

2003, AubinVéronique, Quaegebeur Philippe, Degallaix Suzanne, Cyclic plasticity of a duplex stainless steel under non-proportional loading, Materials Science and Engineering: A, Volume 346, Issue 1-2, pp 208-215.

2003, Makkonen, M., Notch size effects in the fatigue limit of steel, International Journal of Fatigue, Volume 25, Issue 1, pp17-26.

2003, Shigley, J. E., Charles R. Mischke, Richard G. Budynas, Mechanical Engineering Design (7th ed.), McGraw Hill Higher Education. ISBN 978-0-072-52036-1.

2003, Hu, W., Wang, C.H., The implementation of a constitutive model with weighted dynamic recovery and its application, Computational Mechanics, volume 31, pp445

2003, Kassner, M. E., Kyle, K., Taylor hardening in five power law creep of metals and class M alloys, Nano and Microstructural Design of Advanced Materials, pp255-271.

2003, Kulkarni, S. C., Desai, Y. M., Kant, T., Reddy, G. R., Parulekar, Y., Vaze, K. K., Uniaxial and biaxial ratchetting study of SA333 Gr.6 steel at room temperature. International Journal of Pressure Vessels and Piping 80, pp179-185.

2003, Mecking, H., Kocks, U. F., Physics and phenomenology of strain hardening: the FCC case, Progress in Material Science, pp171-273.

2004, Tvergaard, V., On fatigue crack growth in ductile materials by crack-tip blunting, Journal of the Mechanics and Physics of Solids, volume 52, issue 9, pp2149-2166

2004, Mughrabi, H., On the current understanding of strain gradient plasticity, Materials Science and Engineering: A, volumes 387-389, pp209-213.

2004, Fan, Z., Jiang, J., Investigation of low cycle fatigue behavior of 16MnR steel at elevated temperature. Zhejiang DaxueXuebao (Gongxue Ban)/Journal of Zhejiang University (Engineering Science) 38, 1190-1195.

2004, Zhang, J., Jiang, Y., A study of inhomogeneous plastic deformation of 1045 steel. ASME J. Eng. Mater. Technol. 126, 164–171.

2005, Sauzay, M., brillet, H., Monnet, I., Mottot, M., Barcelo, F., Fournier, B., Pineau, A., Cyclically induced softening due to low-angle boundary annihilation in a martensitic steel, materials Science and Engineering: A, volumes 400-401, p241-244.

2005, Lee, Y., Pan, J., Hathaway, R.B., Barkey, M.E., Fatigue Testing and Analysis (Theory and Practice), Elsevier, ISBN 0-7506-7719-8

2005, Chia, K. H., Jung, K., Conrad, H., Dislocation density model for the effect of grain size on the flow stress of a Ti–15.2 at.% Mo β-alloy at 4.2–650 K, Mater. Sci. Eng. A, vol 409, p32

2005, Dunne, F., Petrinic, N. Introduction to Computational Plasticity. Oxford university press.

2005, Gupta, C., Chakravartty, J.K., Reddy, G.R., Banerjee, S. Uniaxial cyclic deformation behaviour of SA 333 Gr 6 piping steel at room temperature. International Journal of Pressure Vessels and Piping, volume 82, p459-469.

2005, Yang, X., Low cycle fatigue and cyclic stress ratcheting failure behavior of carbon steel 45 under uniaxial cyclic loading, International Journal of Fatigue, Volume 27, pp 1124–1132.

2005, Yaguchi, M., Takahashi, Y., Ratchetting of viscoplastic material with cyclic softening, part 1: experiments on modified 9Cr–1Mo steel, International Journal of Plasticity, Volume 21, pp 43-65.

2006, Manson, S. S., Halford G. R., Fatigue and Durability of Structural Materials, ASM International, ISBN: 978-0-871-70825-0.

2006, Rahaman, S. M., Finite Element Analysis and Related Numerical Schemes for Ratcheting Simulation, Ph.D. thesis submitted in North Carolina State University, USA.

2006, Maier, H. J., Gabor, P., Gupta, N., Karaman, I., Haouaoui, M., Cyclic stress–strain response of ultrafine grained copper, International Journal of Fatigue, Volume 28, pp 243-250.

2006, Bouvier, S., Haddadi, H., Levée, P., Teodosiu, C., Simple shear tests: experimental techniques and characterization of the plastic anisotropy of rolled sheets at large strains, Journal of Materials Processing Technology, volume 172, p96

2006, Bouvier, S., Gardey, B., Haddadi, H., Teodosiu, C., Characterization of the strain-induced plastic anisotropy of rolled sheets by using sequences of simple shear and uniaxial tensile tests, Journal of Materials Processing Technology, volume 174, p115

2006, Zhan, Z.L., Tong, J., A study of cyclic plasticity and viscoplasticity in a new nickel-based super alloy using unified constitutive equations - Part I and II, Mechanics of Materials, volume 39, p64

2006, Sinclair, C.W., Poole, W.J., Bréchet, Y., A model for the grain size dependent work hardening of copper, ScriptaMaterialia, Volume 55, Issue 8, p739

2007, Totten, G. E., Steel Heat Treatment - Metallurgy and Technologies, Second Ed., CRC Press, Taylor and Francis Group, Boca Raton.

2007, Tao, Gang, Xia, Zihui, Ratcheting behavior of an epoxy polymer and its effect on fatigue life, Polymer Testing, Volume 26, Issue 4, pp 451-460.

2007, Maalekian, Mehran, The Effects of Alloying Elements on Steels (I), Christian Doppler Laboratory for Early Stages of Precipitation, InstitutfürWerkstoffkunde, Schweißtechnik und SpanloseFormgebungsverfahren, TechnischeUniversität Graz.

2007, Khan, A. S., Chen, X., Abdel-Karim, M., Cyclic multiaxial and shear finite deformation response of OFHC: Part I, experimental results. International Journal of Plasticity 23, 1285–1306.

2007, Jiang, Y., Zhang, J., Benchmark experiments and characteristic cyclic plasticity deformation, International Journal of Plasticity, volume 24, p1481

2007, Borodii, V. M., Shukaev, M. S., Additional cyclic strain hardening and its relation to material structure, mechanical characteristics, and lifetime. International Journal of Fatigue 29, 1184–1191.

2007, Pook, L. P., Metal Fatigue - What It Is, Why It Matters, Springer, ISBN: 978-1-402-05596-6.

2007, Rauch, E.F., Gracio, J.J., Barlat, F., Work-hardening model for polycrystalline metals under strain reversal at large strains, ActaMaterialia, Volume 55, pp2939-2948.

2008, EA de Souza Neto, D Peric, DRJ Owen, Computational Methods For Plasticity - Theory And Applications, John Wiley and Sons, Ltd. Publication, ISBN 978-0-470-69452-7

2008, Kubin, L., Devincre, B., Hoc, T., Modeling dislocation storage rates and mean free paths in face-centered cubic crystals, ActaMaterialia, Volume 56, Issue 20, pp 6040-6049.

2008, Date, Shingo, Ishikawa, Hiroshi, Otani, Tomomi, Takahashi, Yukio, Effect of ratcheting deformation on fatigue and creep-fatigue life of 316FR stainless steel, Nuclear Engineering and Design, Volume 238, Issue 2, pp 336-346.

2008, Jiang, Y., Zhang, J., Constitutive modeling of cyclic plasticity deformation of a pure polycrystalline copper, International Journal of Plasticity, Volume 24, pp 1890-1915.

2009, Arcari, Attilio, De Vita, Raffaella, Dowling,Norman, E., Mean stress relaxation during cyclic straining of high strength aluminum alloys, International Journal of Fatigue, Volume 31, Issues 11–12, pp 1742-1750.

2009, Li, X., Almazouzi, A., Deformation and microstructure of neutron irradiated stainless steels with different stacking fault energy, Journal of Nuclear Materials, Volume 385 (2), Issue 31, pp 329-333.

2009, Gao, Z., Zhao, T., Wang, X., Jiang, Y., Multiaxial fatigue of 16MnR steel. ASME Journal of Pressure Vessel Technology 131.

2009, Lu, K., Lu, L., Suresh, S., Strengthening Materials by Engineering Coherent Internal Boundaries at the Nanoscale, Science, Volume 324, Issue 5925, pp 349-352.

2010, Mughrabi, Hael, Fatigue, an everlasting materials problem - still en vogue, Proceedia Engineering, Volume 2, Issue 1, pp 3-26.

2010, Sivaprasad, S., Paul, Surajit Kumar, Das, Arpan, Narasaiah, N., Tarafder, S., Cyclic plastic behaviour of primary heat transport piping materials: Influence of loading schemes on hysteresis loop, Materials Science and Engineering: A, Volume 527, Issue 26, pp 6858-6869.

2010, Shamsaei,N., Fatemi, A., Socie, D. F., Multiaxial cyclic deformation and non-proportional hardening employing discriminating load paths, International Journal of Plasticity, Volume 26, Issue 12, pp 1680-1701.

2010, Shamsaei, Nima, Fatemi, Ali, Effect of microstructure and hardness on non-proportional cyclic hardening coefficient and predictions, Materials Science and Engineering: A, Volume 527, Issue 12, pp 3015-3024.

2010, Paul, Surajit Kumar, Sivaprasad, S., Dhar, S., Tarafder S., Ratcheting and low cycle fatigue behavior of SA333 steel and their life prediction, Journal of Nuclear Materials, Volume 401, Issue 1-3, pp 17-24.

2010, Bergstrom, Y., Granbom, Y., Sterkenburg, D., A dislocation-based theory for the deformation hardening behaviour of DP Steels: impact of martensite content and ferrite grain size, Journal of Metallurgy, volume 2010

2011, Fournier, B., Sauzay, M., Pineau, A., Micromechanical model of the high temperature cyclic behavior of 9-12%Cr martensitic steels, International Journal of Plasticity, Volume 27, Issue 11, pp 1803-1816.

2011, Rauch, E.F., Gracio, J.J., Barlat, F., Vincze, G., Modelling the plastic behavior of metals under complex loading conditions, Modelling and Simulation in Materials Science and Eng. A, vol19, p1

2011a, Paul, Surajit Kumar, Sivaprasad, S., Dhar, S., Tarafder, S., Cyclic plastic deformation behaviour in SA333 Gr.6 C-Mn steel, Material Science and Engineering: A, Volume 528, Issue 24, pp 7341-7349.

2011b, Paul, Surajit Kumar, Sivaprasad, S., Dhar, S., Tarafder, S., Key issues in cyclic plastic deformation: experimentation, Mechanics of Materials, Volume 43, Issue 11, pp 705-720.

2011c, Paul, Surajit Kumar, Experimentation and material modelling for cyclic plastic deformation behaviour in primary heat transport piping (PHT) materials, Ph.D. Thesis, Jadavpur University, India.

2013, Khutia, N.,Dey, P. P., Paul, Surajit Kumar, Tarafder, S., Development of Non Masing Characteristic Model for LCF and Ratcheting Fatigue Simulation of SA333 C-Mn Steel, Mechanics of Materials, Volume 65, pp 88-102.

2013, Barlat, F., Ha, J., Gracio, J. J., Lee, M., Rauch, E. F., Vincze, G., Extension of homogeneous anisotropic hardening model to cross-loading with latent effects, International Journal of Plasticity, volume 46, p130-142.

2013, Carvalho-Resende, T., Bouvier, S., Abed-Meraim, F., Balan, T., Sablin, S.-S., Dislocation-based model for the prediction of the behavior of b.c.c. materials – Grain size and strain path effects, International Journal of Plasticity, Volume 47, p29

2013, Estrin, Y., Vinogradov, A., Extreme grain refinement by severeplastic deformation: A wealth of challenging science, ActaMaterialla, volume 61, issue 3, p782-817

2013, Watanabe, E., Asao, T., Toda, M., Yoshida, M., Horibe, S., Relationship between Masing behavior and dislocation structure of AISI 1025 under different stress ratios in cyclic deformation, Materials Science and Engineering: A, Volume 582, pp 55-62.

2014, Dong, Y., Kang, G., Yu, C., Dislocation-based cyclic polycrystalline visco-plastic constitutive model for ratchetting of metals with face-centered cubic crystal structure, Computational Material Science, Volume 91, p75

2014, Pan, Q. S., Lu, L., Strain-controlled cyclic stability and properties of Cu with highly oriented nanoscale twins, ActaMaterialia, Volume 81, pp 248-257.

2014, Sivaprasad, S., Bar, H. N., Gupta, Suneel Kumar, Arora, Punit, Bhasin, V., Tarafder, S., A comparative assessment of cyclic deformation behaviour in SA333 Gr.6 steel using solid, hollow specimens under axial and shear strain paths, International Journal of Fatigue, Volume 61, pp 76-86.

2015, Schayes, C., Vogt, J.B., Bouquerel, J., Palleschi, F., Zaefferer, S., Cyclic plasticity mechanism of M330-35A steel, International Journal of Fatigue, volume 82, Part 3, p530

2016, Mughrabi, Hael, The α-factor in the Taylor flow-stress law in monotonic, cyclic and quasi-stationary deformations: Dependence on slip mode, dislocation arrangement and density, Current Opinion in Solid State and Materials Science, volume 20, issue 6, p411.

Blank Page

Chapter 2

SYMMETRIC UNIAXIAL LOADING

In this chapter, uniaxial cyclic plastic behaviour of SA333 steel is studied for symmetric loading condition. Modelling for the experimentally observed material behaviours is attempted based on micro-mechanics and dislocation density. The material behaviours are simulated in finite element platform using the model.

Content **Page**

Blank Page

2.1 Introduction

It is already discussed that, the field of application of the material SA333 Grade-6 C-Mn steel has critical safety issues against earthquake loading and cyclic plastic deformation of the material may occur even for small amplitude loadings. Therefore, a comprehensive understanding of its cyclic plastic behaviour is necessary. The material behaviour, when subjected to uniaxial and symmetric loading, is discussed in this chapter. In comparison to the complex real life loading condition of the material, the uniaxial and symmetric loading condition may sound idealistic. But, for modelling complex behaviour it is important to start from the basic loading situation.

2.2 Experiment and Observation

According to ASTM E606M, uniaxial (tension-compression) low cycle fatigue tests were conducted on the material, by Bhabha Atomic Research Centre, India, for various strain amplitudes ranging from ±0.35% to ±1.00% at room temperature and quasi-static condition, in the standard environment. Schematic representation of the specimen and actual experimental arrangement are shown in figure 2.1a and figure 2.1b respectively.

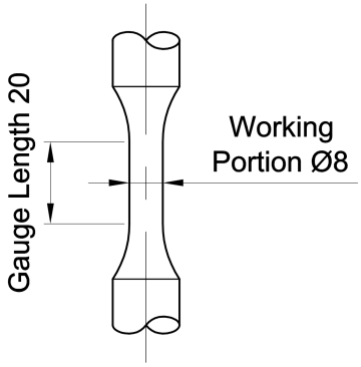

Fig. 2.1a: *Schematic diagram of uniaxial LCF specimen.*

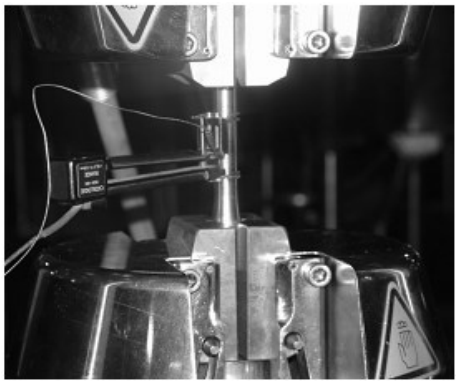

Fig. 2.1b: *Uniaxial testing system.*

In the experimental results, Bauschinger effect (Bauschinger, 1881 and 1886), cyclic softening (Chai and Laird, 1987; Paul et al., 2011) non-Masing initially and later Masing behaviour (Masing, 1923) at saturation cycles are predominantly observed. The typical experimental results are shown in figure 2.2a, figure 2.2b and figure 2.2c, figure 2.2d respectively.

2.3 Material Modelling – General plasticity framework

The material is considered as homogeneous and isotropic, and linearly elastic. The plasticity analysis of the material is introduced by a suitable yield criterion $\sigma_{eq} = \sigma_0$. Here, σ_{eq} is the equivalent stress and $\sigma_0$is the initial yield stress. Mathematically, $\sigma_{eq} - \sigma_0 = 0$ repeats the same condition with a function on the left hand side, known as the yield function ϕ.

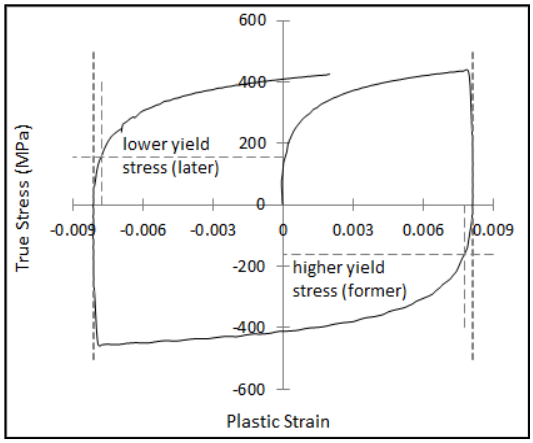

Fig. 2.2a: *Typical experimental Result showing Bauschinger effect.*

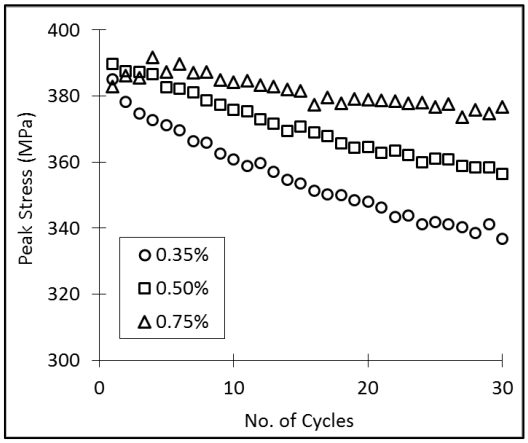

Fig. 2.2b: *Experimental results showing cyclic softening.*

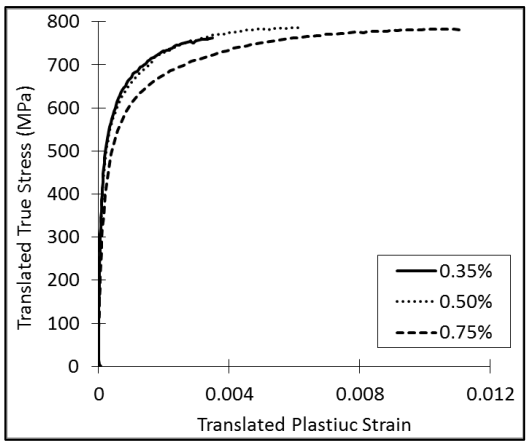

Fig. 2.2c: *Experimental results showing non-Masing behaviour at initial cycle.*

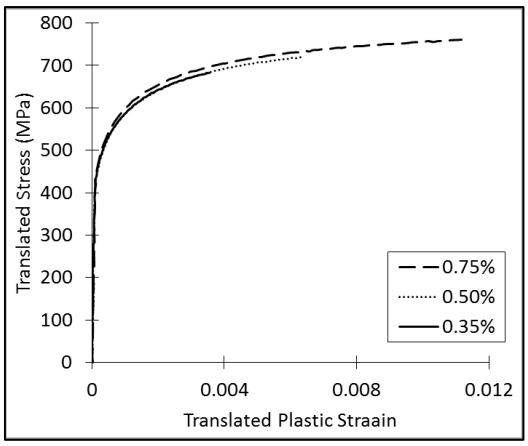

Fig. 2.2d: *Experimental results showing Masing behaviour up to 0.75% strain amplitude at 30th cycle.*

Beyond the elastic limit, where small displacement and small strain analysis is applicable, the incremental total strain can be additively decomposed into elastic and plastic strain components $\left(d\varepsilon_{ij} = d\varepsilon_{ij}^{e} + d\varepsilon_{ij}^{p}\right)$. Even when large rigid body rotations are involved with small strains, this simple algebraic decomposition of strains does not yield accurate results.

The large displacement analysis strongly recommends the estimation of the accurate (true) strain components with their energy conjugate stress by calculating deformation gradient. The kinematics of the thin-walled bodies are mostly characterized by large displacement but small strain. But for the present study, both the solid cylindrical and the thin tubular specimen (for multiaxial case) are free from rigid body rotation and also, the angle of twist and axial displacement are small (equivalent strain amplitude is less than 1.0%) and thereby the additive decomposition of strain is adopted considering small displacement and small strain philosophy.

The present material (metal) is analysed based on continuum plasticity theories i.e. the material is incompressible $\left(\varepsilon_{ij}^{p}\delta_{ij} = 0\right)$ in the plastic regime, or in other words, plastic deformation takes place without changing the volume of the material. Therefore, plastic strain components are purely deviatoric. Incompressible plasticity comprises five

independent plastic strain components, one of the direct plastic strain component is dependent on the other two.

Incompressibility hypothesis endorse no effects of the hydrostatic stress component on yielding and the plastic deformation. Hence, the distortion energy criterion is considered suitable in this case. In its simplest form in case of perfectly plastic (no hardening) incompressible material, the von-Mises yield function is read as: $\phi = \sigma_{eq} - \sigma_0 = \left[\frac{3}{2} S_{ij} S_{ij}\right]^{1/2} - \sigma_0$, where, S_{ij} are the deviatoric stress components or reduced state of stress. The yield function is represented by an open cylinder of radius σ_0, on π-plane* in the deviatoric stress space. For metals (isotropic and incompressible), the von-Mises equivalent/effective stress is a function of the total plastic work as developed from the distortion energy principle (von Mises, 1913). This is why the von-Mises yield function, for most of the metallic material, is considered as the plastic potential surface.

In the plastic regime, the constitutive stress-plastic strain relation for elastic – perfectly plastic material were first proposed by Prandtl (1924) as an extension of Levy (1870) – von Mises (1913) equations for plain strain deformation. The general form of the equations were given by Reuss (1930) as $d\varepsilon_{ij}^{p} = S_{ij} d\lambda$. The total strain increment at any moment, according to Prandtl-Reuss equation is $d\varepsilon_{ij} = \left[\frac{dS_{ij}}{2G} + \frac{(1-2\nu)}{E}\delta_{ij}\, d\sigma_m\right] + \left[S_{ij} d\lambda\right]$.

Lode (1926) conducted multiaxial tests on metals with axial load and internal pressure, and later, Taylor and Quinney (1931) experimented by imposing tension-torsion multiaxial loading, and, they both corroborated the applicability of von-Mises yield criteria and Prandtl-Reuss flow rule are the most realistic description of the isotropic plastic behaviour of metallic materials (Chakrabarty, 2006). Extensive experimentations also by Hohenemser (1931), Morrison and Shepherd (1950) and others, in this regard, have also established conformity with their predecessors.

For the work hardening material (metals), the complete quantification of the plastic strain is dependent on the hardening characteristics of the material. Hill (1950) assumed that the resistance to the distortion is measured by the isotropic expansion of yield surface during plastic flow retaining its shape and position with respect to the hydrostatic state of stress. On the other hand, Prager (1955, 1956) proposed a different hardening rule which considers the yield surface can move in the stress space in any direction of strain increment retaining its shape and size. Considering both the hardening mechanisms, the von-Mises yield function becomes:

$$\phi = \left[\frac{3}{2}\left(S_{ij} - \alpha_{ij}\right)\left(S_{ij} - \alpha_{ij}\right)\right]^{1/2} - \sigma_c = 0 \qquad (2.1)$$

here, α_{ij} are deviatoric back stress components respectively. Current yield stress σ_c is additively decomposed into initial yield stress (σ_0) and isotropic hardening/softening (R).

---

* *Also known as the deviatoric plane, it is a plane in the deviatoric stress space equally inclined to the three principal axes and perpendicular to the hydrostatic axis.*

The hardening rules specifically describe the evolutions of isotropic hardening stress and/or back stress (kinematic hardening) components. For work-hardening materials, Hill (1950) developed the complete stress-strain equation in a more general manner as: $d\varepsilon_{ij} = \left[\frac{dS_{ij}}{2G} + \frac{(1-2\nu)}{E}\delta_{ij}\, d\sigma_m\right] + \left[\frac{3}{2}S_{ij}\frac{d\varepsilon^p_{eq}}{\sigma_{eq}}\right]$.

Contemporarily, for plastic deformation of the perfectly plastic (neutrally stable) or strain hardening (stable) material, Drucker (1950, 1951, 1959) proposed a stability postulate, which is represented as: $d\sigma_{ij}d\varepsilon^p_{ij} \geq 0$. The postulate practically restricts the possibility of material softening and hence instability. Drucker's postulate is broader than the statement summarizes. It confirms the convexity of yield surface and suggests the maximum plastic dissipation (von-Mises, 1928; Taylor, 1947; and Hill, 1948). Consequences of the maximum plastic dissipation postulate are of the highest importance in the plasticity theory. The normality of the plastic flow direction to the potential surface can be directed from the principle of maximum plastic dissipation.

The possibility and direction of plastic strain increment (plastic flow) for strain-hardening material is generally directed by the flow rule. The possibility and quantification of the plastic flow is ascertained by a non-negative scalar ($d\lambda$) similarly as in Prandtl-Reuss equation. It can be shown that the plastic multiplier is actually the equivalent plastic strain increment. Though, the complete quantification of the plastic strain magnitudes are dependent on the specific hardening rules and consistency condition. From the normality rule, the direction of the plastic flow, called the flow vector (n_{ij}) in plasticity analysis, is determined by the gradient of the potential surface in the stress direction. For von-Mises plasticity for metals, the flow rule is called the associative or associated flow rule when the yield surface is identical to the potential surface. The equation of the associated plastic flow is finally written as:

$$d\varepsilon^p_{ij} = d\lambda\frac{\partial\phi}{\partial S_{ij}} \tag{2.2}$$

The consistency condition implies that the plastic deformation occurs for the state of stress is to be in such a way that their equivalent always lies on the revised yield surface. The hypothesis enable the quantification of the plastic multiplier ($d\lambda$) for associated flow.

The condition is mathematically presented as: $\phi + d\phi = 0$, in yielded condition, $\phi = 0$, therefore, $d\phi = 0$ and expressed as:

$$d\phi = \frac{\partial\phi}{\partial S_{ij}}dS_{ij} + \frac{\partial\phi}{\partial\alpha_{ij}}d\alpha_{ij} + \frac{\partial\phi}{\partial\sigma_c}d\sigma_c = 0 \tag{2.3}$$

The plastic modulus is of great importance when the equivalent plastic strain increment $\left(d\varepsilon^p_{eq}\right)$ is computed using Newton iterative method in numerical simulations.

The plastic modulus is formulated from the consistency condition ($d\phi = 0$) conforming associative flow rule $\left(d\varepsilon_{ij}^{p} = d\lambda \frac{\partial \phi}{\partial S_{ij}}\right)$ and incorporating the specific hardening laws as:

$$h = n_{ij} \frac{dS_{ij}}{d\varepsilon_{eq}^{p}} = n_{ij} \frac{d\alpha_{ij}}{d\varepsilon_{eq}^{p}} + \frac{d\sigma_c}{d\varepsilon_{eq}^{p}} \tag{2.4}$$

where, $n_{ij} = \frac{\partial \phi}{\partial S_{ij}} = \frac{3}{2}\frac{S_{ij}}{\sigma_{eq}}$ and, $d\varepsilon_{eq}^{p} = \left[\frac{2}{3} d\varepsilon_{ij}^{p} d\varepsilon_{ij}^{p}\right]^{1/2}$. In the subsequent material modelling sections, in this chapter and later, the specific hardening laws suitable for the material, their quantification and proposed modifications are discussed.

2.3.1 Elastic parameters

Elastic parameters, Young's modulus = 210 GPa, Poisson's ratio = 0.3, are extracted from the uniaxial tensile tests following standard procedures. The cyclic yield stress is extracted from the saturated stress-plastic strain data in Low Cycle Fatigue tests, as all the strain amplitudes showing Masing behaviour at saturated condition (50th cycle).The value of initial cyclic yield stress is found to be 196 MPa in such a condition for all strain amplitudes.

2.4 Modelling for saturated cycles - the kinematic hardening rule

Accurate estimation of $d\varepsilon_{eq}^{p}$ requires incorporation of correctly characterised hardening laws. When the modelling of the cyclic plastic behaviour is concerned, the major role is played by the Kinematic Hardening (KH) rule. The mathematical application of KH rule is devised to generate stress-strain hysteresis loops and simulate the Bauschinger effect.

Inspired by Besseling (1958) type multi-segment formation and conforming non-linear Armstrong-Frederick (1966) phenomenology for each segments, Ohno and Wang (1993a,b) developed a multi-segmented non-linear kinematic hardening rule. The first terms of each segment offers the hardening due to dislocation pile-up and the seconds, gives the recovered energy due to annihilation of mobile dislocations at certain state of plastic deformation. The recovery activities of each segment can be controlled by a fitting parameter and are limited by the back stress thresholds.

The Ohno-Wang (OW) multi-segmented kinematic Hardening rule simulates uniaxial and biaxial stress-strain hysteresis loops well for symmetric and proportional loading conditions, but for asymmetric cases, over-predictions observed.

In this work, observing the critical stress-strain hysteresis curvature of the material, six-segmented non-linear Ohno-Wang KH rule is employed to simulate basic stress-strain hysteresis loops with Bauschinger effect. According to the model architecture, the total deviatoric back stress is:

$$\alpha_{ij} = \sum_{k=1}^{m} \alpha_{ij}^{k} \tag{2.5}$$

Here, α_{ij}^k is the k[th] segment of the deviatoric back stress tensor. For each segment, back stress evolution law is given as:

$$d\alpha_{ij}^k = C^k r^k \left[n_{ij} - \left(\frac{\left\| \alpha_{ij}^k \right\|}{r^k} \right)^{\chi^k + 1} l_{ij}^k \right] d\varepsilon_{eq}^p \tag{2.6}$$

C^k, r^k and χ^k are the material parameters for KH law where, C^k are the dimensionless hardening coefficients and r^k are the saturation values of α_{ij}^k for k[th] segment, which controls the bounds of the contributions of each recovery terms. χ^k is the parameter that controls the degree of nonlinearity by modifying the contribution of the dynamic recovery part. In the above expression, l_{ij}^k is the direction vector to the corresponding segment of deviatoric back stress, and $l_{ij}^k = \frac{3}{2} \frac{\alpha_{ij}^k}{\left\| \alpha_{ij}^k \right\|}$ where, $\left\| \alpha_{ij}^k \right\| = \left[\frac{3}{2} \alpha_{ij}^k \alpha_{ij}^k \right]^{\frac{1}{2}}$.

The KH parameters are calculated from the stress-strain data of the saturated loop at highest strain amplitude (0.75 %). The saturated loops for all the strain amplitudes are 'Masing' in the plastic regime as observed in the experimental results (figure 2.2d).

2.4.1 The hardening modulus for kinematic hardening only

For the simulation of saturated stress-strain hysteresis loops, the material model consists of only kinematic hardening rule with constant cyclic yield stress. The hardening modulus, for this case, is deduced to be:

$$h = \sum_{k=1}^{m} C^k r^k \left[\frac{3}{2} - \left(\frac{\left\| \alpha_{ij}^k \right\|}{r^k} \right)^{\chi^k + 1} l_{ij}^k \, n_{ij} \right] \tag{2.7}$$

2.4.2 Kinematic hardening parameters

For Ohno-Wang KH law, the parameters (C^k and r^k) are determined from saturated (30[th] cycle) fully reversed loading branch of highest strain amplitude (0.75 %) experimental. A single set of KH parameters is sufficient to evaluate the KH behaviour of the material due to the Masing nature of the plastic curves at saturation. The procedure is outlined by Jiang and Sehitoglu (1996).

Under fully reversed uniaxial loading the values of C^k and r^k regulates the curvature of the loading and unloading branch of the hysteresis loop. Figure 8 schematically shows such a loading branch. Here $\Delta\varepsilon^p$ indicates plastic strain range i.e. twice the plastic strain amplitude and $\Delta\sigma$ represents the stress range, also twice the stress amplitude. The above curve can be described by the following four parameter equation: $\Delta\varepsilon^p = a \left(\frac{\Delta\sigma - \Delta\sigma_0}{\Delta\sigma_u - \Delta\sigma} \right)^m$ where, a and m are power law coefficient and exponent respectively. $\Delta\sigma_0$ and $\Delta\sigma_u$ are the cyclic yield stress range and ultimate stress range respectively. The objective of the fitting function is to get extrapolated data at high strain amplitude to cover maximum range in LCF tests.

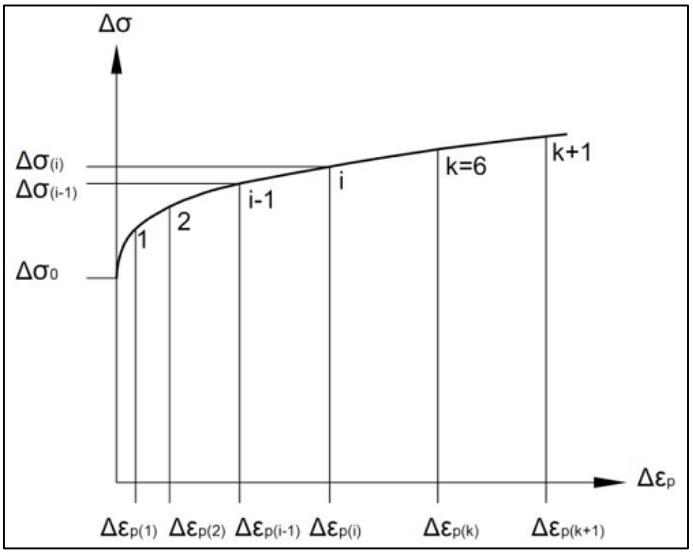

Fig. 2.3: *Stress vs. plastic strain curve of the loading branch of the saturated cycle.*

From the above equation, a set of seven pre-defined data points $\Delta\varepsilon_k^p$, and $\Delta\sigma_k$ are selected (figure 8) and the values of C^k and r^k are determined correspondingly. $C^k = \sqrt{\frac{2}{3}}\frac{2}{\Delta\varepsilon_k^p}$, where, k = 1, 2 … 6. For calculating six r^k it is necessary to calculate H^k first. The formula adopted for calculating H^k and r^k are respectively, $H^k = \frac{\Delta\sigma_k - \Delta\sigma_{k-1}}{\Delta\varepsilon_k^p - \Delta\varepsilon_{k-1}^p}$ and $r^k = \frac{2}{3}\frac{H^k - H^{k+1}}{C^k}$. The values of KH Parameters C^k and r^k are obtained by following the outlined procedure, is presented in table 2.1.

Table 2.1: *C^k and r^k values.*

$\mathbf{C^1}$ = 16323	$\mathbf{C^2}$ = 4082.5	$\mathbf{C^3}$ = 1633	$\mathbf{C^4}$ = 816.5	$\mathbf{C^5}$ = 363	$\mathbf{C^6}$ = 163
$\mathbf{r^1}$ =13.8MPa	$\mathbf{r^2}$ =16.6MPa	$\mathbf{r^3}$ =19.8MPa	$\mathbf{r^4}$ =24.6MPa	$\mathbf{r^5}$ =32.5MPa	$\mathbf{r^6}$ =43.4MPa

The mathematical fitting parameter χ^k (Eq. 2.6), which regulates the dynamic recovery contribution, is set to zero for balanced loading where fully active dynamic recovery is enabled. But, for unbalanced or asymmetric loading, the non-zero value of χ^k allows partial recovery.

2.4.3 Simulation of saturated stress-strain hysteresis loops

Uniaxial cyclic plastic deformations are simulated in ABAQUS CAE (v6.8) commercial finite element platform. Only the working (gauge length) portion of the actual specimens are modelled. Specimens are discretised adopting structural meshing with total 847 nodes. To maintain a radially oriented structure, 144 linear wedge (6-noded) elements are used at the central zone and for rest of the body, 576 linear hexahedral (8-noded) elements are used. Both the elements with linear shape functions are allowed for full integration. Maintaining the symmetry, displacement boundary conditions are imposed according to the strain amplitudes using balanced triangular amplitude function. The material model along with the properties, are incorporated through user material subroutine (UMAT). The iterative

solver for the equivalent plastic strain increment and the overall integration schemes, as discussed in the previous chapter, are chosen carefully.

2.4.4 Outcome of the simulations with OW kinematic hardening model

The simulations of the saturated stress-strain hysteresis loops for all strain amplitude are compared with the respective experimental results as shown in figure 2.4a, 2.4b and 2.4c.

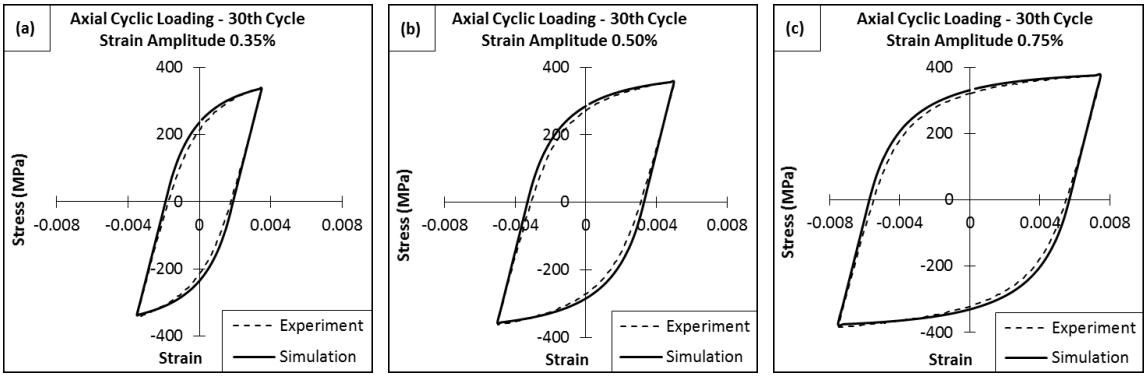

Fig. 2.4: *Comparison of (uniaxial) experimental and simulated stress-strain hysteresis loops for strain amplitude* ***(a)*** *0.35%,* ***(b)*** *0.50% and* ***(c)*** *0.75% at saturated (30^{th}) cycle.*

2.4.5 Discussion

When comparing with the experimental hysteresis loops, the simulations show excellent matching (figure 2.4a, 2.4b and2.4c) of the cyclic stress-strain behaviour of the material after saturation (30^{th} cycle). It is one of the advantages of the segmented non-linear KH rules over conventional Armstrong-Frederick KH model.

Considering the good agreement between experimental and simulated results at various strain amplitudes, the KH rule along with all the material parameters extracted from the experimental results are found to be acceptable. Also, the KH parameters are observed to be strain amplitude independent.

The initial transient cycles, before saturation, are not simulated well by the material model. It is reported in the literature that, cyclic hardening or softening is inevitably observed in the initial transient cycles (in the present study, 1-30 cycles) of cyclic plasticity experimentations. An additional hardening rule or certain modification to the existing KH rule may be incorporated in the material model to simulate the same.

2.5 Phenomenological modelling for cyclic softening

There are other material responses observed for cyclic loading, in which cyclic hardening or, softening behaviour is largely observable in the experimental results. The rate of cyclic softening is observed to be reducing with cycles and gets saturated within first ~~a~~ few cycles. Again, total magnitude of softening is observed to be decreasing as strain amplitude increases.

The modelling of hardening or softening of cyclic peak stresses can be done by incorporating suitable isotropic hardening or softening rule respectively. For simplicity in modelling, it is sometimes assumed that the cyclic hardening and softening are isotropic in

nature (Hill, 1950). An exponential evolution of isotropic hardening was proposed by Zaverl and Lee (1978), which is mainly phenomenological mathematical fitting function. Conserving the directional behaviour of the loaded slip systems, another popular way of modelling of the cyclic hardening or softening is by modifying the dynamic recovery term of the KH rule. Researchers like Marquis (1979), Haupt et al. (1992), etc. have proposed such modifications to calibrate hardening or softening effects. Their philosophies were same – to modify of the dynamic recovery contribution of KH rule, but they proposed different evolution equations. Haupt and his co-workers suggested a history dependent equation where, Marquis's approach was rather simple and instantaneous.

The non-Masing behaviour of the material has incisive impact on the modelling scheme. For non-Masing behaviour of the material, irregular strain hardening character may be observed. For simulations of such behaviour, different KH parameters may be used for different strain amplitudes. It may sometimes be observed in the experimental results that there is insignificant difference in the plastic curvature and the dissimilar elastic portion is responsible for non-Masing behaviour. In those cases, one set of KH parameters are used for every strain-amplitudes and modification is made to the cyclic yield stresses.

Current yield stress σ_c is not considered constant, and can be additively decomposed into constant cyclic yield and isotropic softening stress. Initially non-Masing behaviour is observed in the experimental results for the present material, SA333 mainly in the elastic region and therefore, different cyclic yield stresses are used for different strain amplitudes.

The experimental results show that the cyclic hardening/softening has no directional influence in forward and reverse loading and therefore, considered isotropic in nature. In view of the fact, the proposition by Marquis is used to modify the cyclic yield stress with the idea that the generation of dislocations due to plastic deformation can enable more dynamic recovery (Marquis, 1979; Haupt et al., 1995) at the present state, or, it can contribute immediately after as isotropic softening. Therefore, the current yield stress evolves with 'Marquis' type function as:

$$\sigma_c = \sigma_0 + R\left(\varepsilon_{eq}^p\right) = K\left[1 + \lambda e^{-\omega\varepsilon_{eq}^p}\right] \tag{2.8}$$

Where, K is a constant, such that $K = \frac{\sigma_0}{1+\lambda}$. Parameter λ and ω control the softening.

2.5.1 The hardening modulus for combined hardening

For the combined isotropic and kinematic hardening plasticity, the plastic modulus is recast into the following form:

$$h = \sum_{k=1}^{m} C^k r^k \left[\frac{3}{2} - \left(\frac{\left\|\alpha_{ij}^k\right\|}{r^k}\right)^{\chi^k+1} l_{ij}^k \, n_{ij}\right] - K\left(\lambda\omega e^{-\omega\varepsilon_{eq}^p}\right) \tag{2.9}$$

2.5.2 Softening parameters (Marquis Modification)

The initial cycles are non-Masing mainly in the elastic regime (figure 2.2c) and is clearly reflected in the cyclic yield stress values calculated from the initial cycles. The plastic curvature of the loading branches of the initial cycles are observed not so misaligned with the Masing saturated curves and therefore, same kinematic hardening parameters can be used. The difference in cyclic yield stresses, calculated from initial cycles and 30th cycle is identical to the softening magnitude. The softening is equally observed in tension as well as in compression, hence considered isotropic in nature. The suitable values of initial cyclic yield stresses are presented in table 2.2.

Table 2.2: *Initial cyclic yield stresses.*

Strain Amplitude	Initial Cyclic yield Stress (MPa)
0.35%	248
0.50%	234
0.75%	222

Table 2.3: *Softening parameters.*

	Strain Amplitude		
	0.35%	0.50%	0.75%
λ	1.6	0.5	0.16
ω	-2.2	-1.9	-1.8

λ and ω are calibrated from the softening characteristics of respective strain amplitudes and adjusted by trial and error method during simulations. The values are presented in table 2.3.

2.5.3 Outcome of the phenomenological model

The simulated peak stress softening curves show good agreement with the actual softening behaviour when compared with the experimental results at various strain amplitudes as observed in the figure 2.5a, 2.5b, and 2.5c respectively for different strain amplitudes.

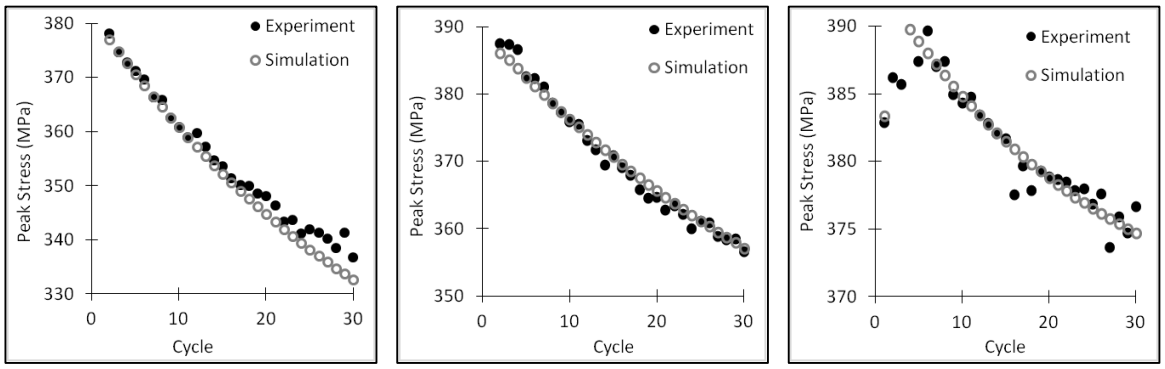

Fig. 2.5: *Peak Stress vs. Cycle, for (uniaxial) strain amplitudes:* ***(a)*** *0.35%,* ***(b)*** *0.50%, and* ***(c)*** *0.75%.*

2.5.4 Discussion

The original approach of Marquis i.e. modification of dynamic recovery is physically justifiable and reduction of the size of yield surface in deviatoric stress space without any damage mechanism is an unrealistic idea. Yet, the present work adopted such an idea for following reasons:

1) The reduction of yield value is the manifestation of the increased recovery (dislocation annihilations) at higher plastic deformation. It is not to be treated as damage induced softening as per the conventional concept.

2) In a segmented KH law, dynamic recovery is a cumulative influence bounded by several thresholds. The Marquis approach can be incorporated in segmented law also, but not in the simplest form. The calibration of parameter would involve a meticulous procedure with no such improvements in the results than present model.

The non-Masing behaviour of the material is captured with a variation of initial yield stresses with strain amplitude. The values are extracted from experimentally observed initial cycles and finalised by trial and error.

The overall contribution of the 'Marquis' function for softening worked nicely. Cyclic softening is simulated with good agreements by the function when applied on cyclic yield stress. Though, the approach is based on an idea of possible physical phenomena, it fails to distinguish the cyclic hardening and normal strain hardening observed during monotonic loading. Or it can be said more specifically that, the model neither identifies nor quantifies the class of dislocations and their dynamics, indulged in the particular action of cyclic hardening or softening. Therefore, a deep in-sight in the dislocation aspect is required.

2.6 Investigation by Tunnelling Electron Microscopy

To understand the behaviour of the material, Transmission Electron Microscopy is done by Philips CM200 operated at 200 kV. It is observed from the TEM micrograph is that, at the onset of plastic deformation, the possibility of dislocation pile-ups are high. Similar reason can cause higher softening rate after stress reversal due to reorientation of dislocation structure making favourable conditions, which is clearly manifested in experimental results. Low strain amplitudes show more hardened loops with larger softening rate than high strain amplitudes and non-Masing behaviour is believed to be the manifestation.

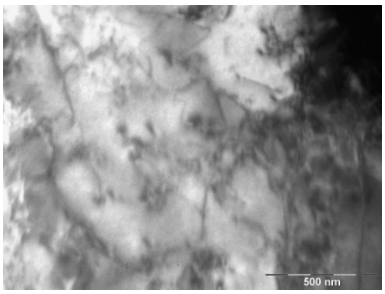

Fig. 2.6a: *TEM micrograph at 'as received' condition.*

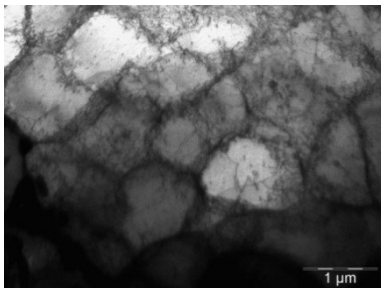

Fig. 2.6b: *TEM micrograph after 10 cycles (1% strain amplitude).*

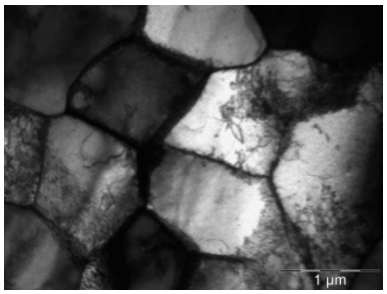

Fig. 2.6c: *TEM micrograph after failure (500 cycles, 1% strn ampl).*

Though the TEM micrographs show no definitive dislocation structure for the material in 'as received' condition (figure 2.6a), there are traces (memory?) of obscure formations, shaped during previous plastic deformation like rolling. TEM micrograph after 20 load reversals in figure 2.6b shows prominent sub-cellular structures with rough tangles of dislocations. Therefore, it can be considered that, at the onset (may be within a few cycles) of plastic deformation, the dislocation substructures are adequately formed. This assumption endorses the model's simplicity to promote a consistent cyclic softening mechanism activated right from the beginning. When the sub-grains are formed,

annihilations of the entrapped dislocations at sub grain boundary create a recovery of stored energy, manifested as isotropic softening stress and algebraically added to the cyclic yield stress. TEM micrograph after failure in figure 2.6c, shows larger sub-cellular structures with dense wall made of dislocation tangles and practically clean interior.

2.7 Understanding of the micro-mechanism

The modelling of hardening or softening of cyclic peak stresses can be done by incorporating suitable isotropic hardening or softening rule respectively. For simplicity in modelling, it is sometimes assumed that the cyclic hardening and softening are isotropic in nature (Zaverl and Lee, 1978). Conserving the directional behaviour of the loaded slip systems, another popular way of modelling of the cyclic hardening or softening is by modifying the dynamic recovery term of the KH rule. Researchers like Marquis (1979), Haupt et al. (1992), etc. have proposed such modifications to calibrate hardening or softening effects. For better understanding of the actual phenomenology, a rigorous metallurgical investigation through decades reveals that pile-up and annihilation of the dislocations with different kinetics may result in different macroscopic hardening and softening manifestation.

During plastic deformation of a metallic material, continuous generation and annihilation of dislocations occur. The remaining dislocations at any instance, try to align themselves such as to reduce their individual contribution to the stored energy. The rearrangements of dislocations are resulting from the dissimilar rotations of the neighbouring lattices (Read and Shockley, 1950). These reorientations of the dislocations continue to occur to a certain extent of plastic deformation while, the stable dislocation substructures are fully developed (Sedláček et al., 2002). The substructures are cellular and surrounded by walls consist of rough tangles of dislocations and the interiors of the cells have a correspondingly much lower dislocation density. The sub-cells are often disoriented for small plastic deformation. The simplest case of ‘misorientation’ can be tilted sub-grains forming low angle tilt boundary with an array of edge dislocations. The low angle sub-grain boundary commonly has misorientation angle less than 15° (Shockley and Read, 1949; Shockley, 1950). The formations of adequate number of sub-structures depend on loading conditions and many other factors like, material microstructure, previous loading history, undergone heat treatment, etc.

A moving dislocation, in the vicinity of sub-structure, takes part either by pilling-up at sub-grain walls reinforcing the wall entanglements or, by getting annihilated with its compatible pair, undermining the wall and relieving some stored energy. The relieved energy makes free passage for the remaining dislocations resulting the macroscopic softening. Though the overall manifestation of the annihilation is softening, the dissimilar kinetics of the dislocations involved, have different impacts on the microstructure and the stress response of the material. The effect of annihilated mobile dislocations is generally included in the ‘dynamic recovery’ of the kinematic hardening (KH) rule (Mecking and Kocks, 1981; Kocks and Mecking, 2003) with the directional behaviour. Annihilation of the stationary dislocations entrapped in the sub-cell wall, can undermine the sub-granular structure

(Sauzay et al., 2005; Fournier et al., 2011). The reductions of boundary dislocations primarily resolve the boundary misorientation and eventually cause the dissolution of the boundary as observed for large strain applications. Thus, the effect of annihilations of boundary dislocations can be a reasonable phenomenon to justify cyclic softening in low cycle fatigue (LCF) loadings. There are reasons to believe that, if the adequate number of sub-granular structures form considering all favourable conditions during early stages of deformation, then only, the possibility of having monotonic cyclic softening is devisable from the early cycles.

Lattice reorientation facilitates accumulation of dislocations at favourable locations and gradually piled-up to form the boundary for 'misoriented' sub-grains. Simultaneously occurring annihilations of dislocations from the locality undermine the formation and eventually disband the boundary (grain growth). With increasing plastic deformation, the reorganisation of the crystal lattices gradually optimizes and the misorientation of the sub-grains reduces. The reduction of the misorientation is directly related to the saturation of cyclic softening.

2.7.1 Dislocation Based Modelling

A moving dislocation, in the vicinity of its compatible pair (opposite Burger's vector) gets annihilated, relieving some stored energy. The relieved energy is used to make free passage for the remaining dislocations resulting the macroscopic softening. The effect of annihilated mobile dislocations is generally included in the 'dynamic recovery' of the kinematic hardening (KH) rule (Kocks and Mecking, 2003), which is essential to the cyclic plastic simulations for generating stress-strain hysteresis loops. Therefore, by modifying the dynamic recovery term, cyclic softening can be modelled in cyclic plastic loadings (Marquis, 1979; Haupt et al., 1992). Marquis (1979) proposed an evolution of the dimensionless parameter, which amplifies the dynamic recovery contribution in KH rule, through an exponential decay function of accumulated plastic strain.

During plastic deformation of material, continuous generations, entanglements and annihilations of dislocations simultaneously occur. Entanglements and annihilations are two phenomena of contrasting philosophy, causing hardening and softening respectively. With increasing plastic deformation, probability of both entanglements and annihilations simultaneously increased. There are reasons to believe that, the two opposite phenomena become stable, gradually after a certain amount of plastic deformation, when the dislocation kinetics and lattice reorientation optimizes the energy usage (Read and Shockley, 1950). The condition of such equilibrium can be observed physically as the saturation of cyclic softening.

Mobile dislocations in specific slip systems when interact with the sub-grain boundary, may result in annihilation of both mobile dislocations and the stationary dislocations entrapped in the sub-cell wall. The annihilation of mobile dislocations is incorporated in dynamic recovery of kinematic hardening whereas, annihilation of entrapped dislocations is modelled for the cyclic softening. The annihilations of stationary dislocations entrapped in the sub-cell wall reduce the dislocation density in the boundary wall and offers free

passage for other dislocations of any slip system passing through. Therefore, irrespective of direction of the slip, the annihilations of boundary dislocations result in macroscopic softening which may be considered isotropic in nature.

The scheme of the present model is to calculate the softening stress σ_1 (negative) and add algebraically to get the current yield stress,

$$\sigma_c = \sigma_0 + \sigma_1 \tag{2.10}$$

A mobile dislocation of opposite sign to the boundary dislocation within a closure proximity, called 'critical annihilation distance' (y) (Essmann and Mughrabi, 1979; Sauzay etal., 2005), makes the annihilation possible. At any instant Δt, if the velocity of mobile dislocations is v and for a half cycle mobile dislocation density ρ (m^{-2}) be reduced by annihilation when interacting with the entrapped dislocations $(density = \Lambda\, m^{-1})$ at one side of the sub-cell wall. The reduction of entrapped dislocation density in the sub-cell wall (Sauzay et al., 2005; Fournier et al., 2011) is:

$$\Delta\Lambda = -2y(v\Delta t)\frac{\rho}{2}\Lambda \tag{2.11}$$

Here, the negative sign signifies the reduction of entrapped dislocation density. Figure 2.7 schematically represents of the possible scenario of annihilation of boundary dislocations when mobile dislocations passes non-parallel to the low angle sub-grain boundary.

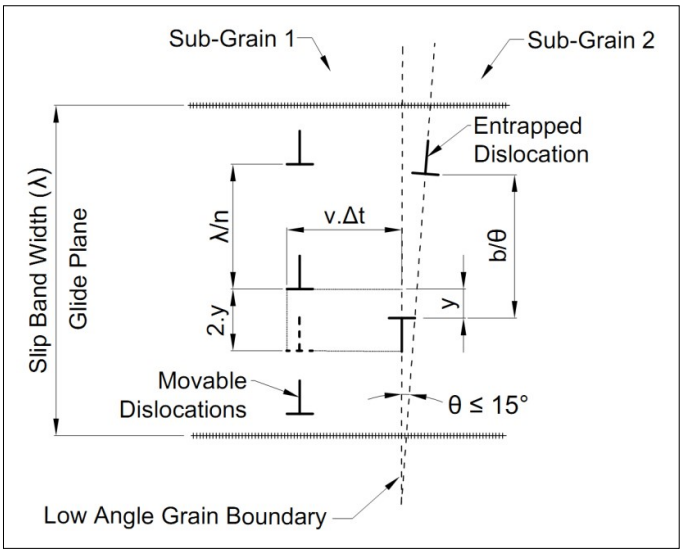

Fig. 2.7: *Schematic representation of annihilation of dislocations at low angle grain boundary.*

Following the Orowan equation of slip, for infinitesimal time $\Delta t \to 0$, the total slip rate is:

$$\dot{\gamma} = \rho\frac{\Delta L}{\Delta t}b = \rho v b \tag{2.12}$$

Where, L is the bowing out distance and b is the magnitude of the Burger's vector. As for polycrystals, total shear strain is the sum of incremental shear components from different (S_n slip systems are active) slip system (Kocks and Mecking, 2003):

$$\sum_{n=1}^{S_n} \dot{\gamma} \qquad (2.13)$$

$\dot{\gamma}^p$ is calculated assuming that an average slip is occurring at every slip system. Combining Eq. 2.12 and Eq. 2.13 and substituting in Eq. 2.11 gives:

$$\dot{} \qquad S_n \quad -\frac{}{b} \Lambda \qquad (2.14)$$

For n dislocations stopping at the boundary of the sub-grain of size D, then back stress generated (Sinclair et al., 2006) would be:

$$\sigma_1 = \frac{\alpha M G b}{D} n \qquad (2.15)$$

α is the strength of interaction, a geometric fitting parameter of typical values from 0.3 to 0.4 for steel polycrystals (Mugrabhi, 2016), in this work, $\alpha = 0.30$ is taken. M is known as average Taylor factor. For BCC polycrystalline ferrite, $M = 2.99$ is appropriate (Estrin, 1998; Kassner et al., 2003).

If n is the possible annihilation sites within a slip band of width λ, then $n = \Lambda\lambda$. Therefore, softening stress increment per slip system gives:

$$\Delta\sigma_1 = -\frac{\alpha M^2 G b}{S_n} \frac{\Lambda}{D} \lambda \frac{y}{b} \Delta\varepsilon_{eq}^p \qquad (2.16)$$

Maximum distance qualified as critical annihilation distance in a slip band (figure 2.7) is:

$$y = \frac{\lambda}{2n} \qquad (2.17)$$

Where, y is a combination critical annihilation distance of pure edge dislocation ($y_{edge} \approx 1.6\,nm$) and pure screw dislocation ($y_{screw} \approx 50\,nm$). There are total 48 slip systems possible in a single BCC crystal as shown in the table 2.4, but slip systems on {123} plane, are not easily activated. Therefore it is taken that, 24 active slip systems possible in a single BCC crystal.

Table 2.4: *BCC Slip Systems.*

Slip Plane	Slip Direction	No. of Slip Systems
{110}	<111>	12
{112}	<111>	12
{123}	<111>	24

Taylor model assumes that plastic strain components are homogeneous in each grain in the material and at least five slip systems are generally activated independently in each grain to accommodate the macroscopic plastic strain as per von-Mises plasticity is concerned. Therefore, the possible combinations of 5 slip systems within the 24 would be ${}^{24}C_5$. Where low angle grain boundary of edge type dislocations is formed, the adjacent sub-grain consists of only 1 slip system with dislocations parallel to the boundary dislocations (Read and Shockley, 1950). In this context, possible combination of 5 slip systems with none having the dislocations parallel to the adjacent grain boundary within the 24 possible slip systems would be ${}^{24-1}C_5$. Therefore, the probability (Sauzay, 2009) of total annihilation (p) would be:

$$p = 1 - \frac{{}^{24-1}C_5}{{}^{24}C_5} \approx 0.21 \tag{2.18}$$

Considering the probability p, the total softening stress increment would be:

$$\Delta\sigma_1 = -\frac{\alpha M^2 Gbp}{S_n}\frac{\Lambda}{D}\frac{\lambda}{b}\frac{\lambda}{2n}\Delta\varepsilon_{eq}^{p} \tag{2.19}$$

Thus, annihilations at the low angle grain boundary decrease the entrapped dislocation density and macroscopic softening is observed. To obtain the evolution of the entrapped dislocations density (Λ), Integrating Eq. 2.14 and putting condition $\Lambda = \Lambda_0$ at $\gamma^p = 0$, results:

$$\Lambda = \Lambda_0 \exp\left(-\frac{y}{b}\gamma^p\right) \tag{2.20}$$

Consequently, the reduction in entrapped wall dislocation density relieves the misorientation (Read and Shockley, 1950). At any instant, $\theta = b\Lambda$, the evolution of the misorientation angle is:

$$\dot{\theta} \qquad \dot{} \tag{2.21}$$
$$b$$

2.7.2 Hardening Modulus

Now, when the hardening functions are completely defined, the plastic modulus (Eq. 2.4) for the combined kinematic and isotropic hardening plasticity is represented in the exact form:

$$h = \sum_{k=1}^{m} C^k r^k \left[\frac{3}{2} - \left(\frac{\left\|\alpha_{ij}^k\right\|}{r^k}\right)^{\chi^k+1} l_{ij}^k n_{ij}\right] - \frac{\alpha M^2 Gbp}{S_n}\frac{\Lambda}{D}\frac{\lambda}{b}\frac{\lambda}{2n} \tag{2.22}$$

Here, in Eq. 2.22 the first term represents the hardening contribution of the kinematic hardening rule adopted and the latter is the softening contribution.

2.7.3 Material parameters for annihilation model

The softening model assumes certain uncoupled hypothesis of interaction between two different families of dislocations, one is moving and another is entrapped in the sub-grain wall. The mechanism is activated when these two families are adequately developed and assumed unhindered by other's influences. Required softening parameters for the cyclic softening mechanism are mainly realised from TEM observations, by trial and error and from literature, and suitably calibrated. Table 2.5 provides the estimated values of the required parameters:

Table 2.5: *Material parameter for dislocation annihilation at low angle sub-grain boundary.*

Parameter		**α**	**M**	**G**	**b**	**D**	**λ**	**Λ_0**	**n**	**S_n**
Unit				**MPa**	**nm**	**µm**	**nm**	**m^{-1}**	**per λ**	
Strain Amplitudes	**0.35%**	0.30	2.99	80769	0.25	1.2	60	3.5×10^8	12	5
	0.50%							2.8×10^8	24	
	0.75%							1.4×10^8	32	

The average sub-grain size as observed in TEM micrographs (figure 2.6b) is $1.2\ \mu m$. Considering the small range of application, the slip bandwidth is assumed constant throughout the range. The slip bandwidth is taken as $60\ nm$ (for DP steel, Carvalho-Resende et al., 2013).

The represented values of the dislocation densities at the sub-cell boundary (Λ_0) in table 2.5 are to be considered as the quantification of the misorientations associated with the boundary initially. With the plastic deformation prior to the adequate formation of the sub-grains, the misorientation may resolve if ample scope of reorganisation is provided to the unit crystal lattices adjacent to the boundary. For higher strain amplitudes, the lattices get greater opportunity to reorient them as larger plastic deformations are absorbed. The misorientation of sub-grains is therefore depends on pre-staining and obviously previous heat treatment cycles. Without sufficient knowledge, the values of Λ_0 are chosen accordingly as gradually decreasing, and calibrated for all strain amplitudes. The choices of Λ_0 give an initial misorientation angles 5°, 4° and 2° for 0.35%, 0.50% and 0.75% strain amplitudes respectively. The smaller misorientations also get saturated faster while undergoing larger plastic deformations. The misorientation does not absolutely disappear, and thus value of Λ also asymptotically saturates to a minimum non-zero value. Though before that, disbanding of sub-grain boundary and formation of larger sub-grains (grain growth) may eventually occur.

It is considered that the mobile dislocation density increases with increasing plastic strain and accordingly, the possible annihilation sites (n) also increase. The values of n are chosen by trial and error and critical annihilation distances (y) are calculated accordingly. The y values are contributed by both edge and screw dislocations and can be calibrated for

a mixed population of mobile dislocations and/or for entrapped dislocations at sub grain boundaries, if the proportion of edge and screw dislocations are known.

According to the standard practice in continuum mechanics, five active slip systems are considered, though in reality, there are rarely more than three active slip systems involved, in each particular grains. However, a rigorous and case specific investigation may be used.

2.7.4 Outcome of the physically based modelling

The material modelling is based on uniaxial LCF behaviour of SA333 C-Mn steel. Figure 2.8 – 2.10 show the comparison of experimental and simulated stress-strain hysteresis loops at 30th cycle, and peak stress softening with cycle for tension-compression cyclic loading subjected to the strain amplitudes from 0.35%, 0.50% and 0.75% respectively for the material SA333 Gr.6 C-Mn steel. Comparisons of the results of uniaxial FE Simulations of LCF with experiments are shown below:

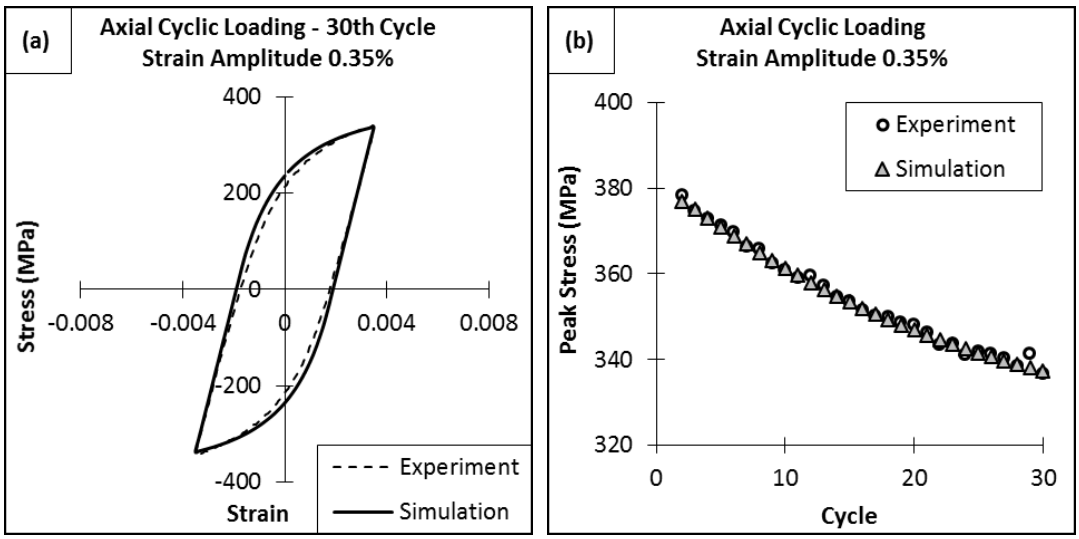

Fig. 2.8: *Comparison of uniaxial experimental and simulated results for 0.35% strain amplitude,* ***(a)*** *stress-strain hysteresis loops at 30th cycle,* ***(b)*** *peak stress vs. number of cycles.*

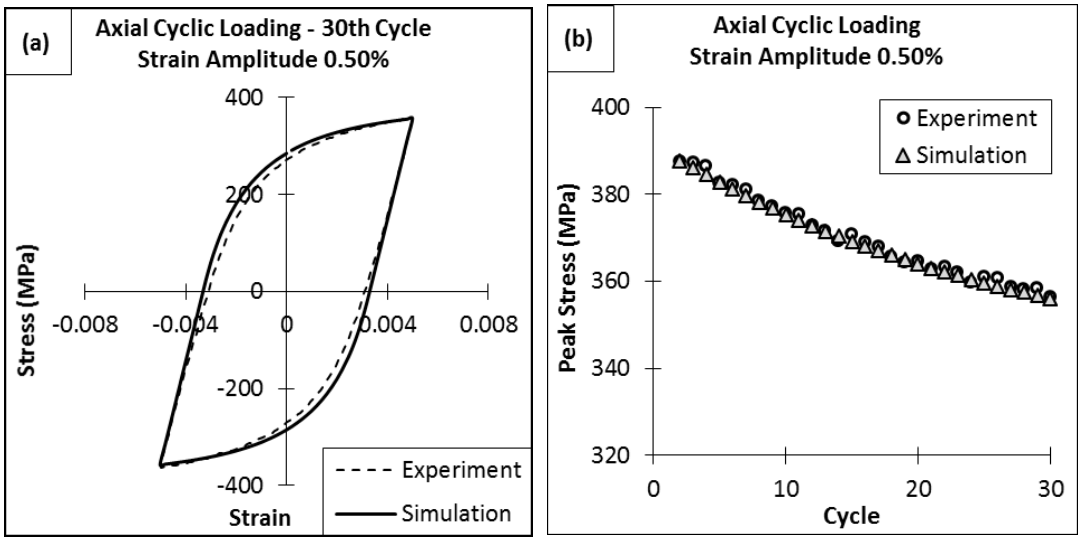

Fig. 2.9: *Comparison of uniaxial experimental and simulated results for 0.50% strain amplitude,* ***(a)*** *stress-strain hysteresis loops at 30th cycle,* ***(b)*** *peak stress vs. number of cycles.*

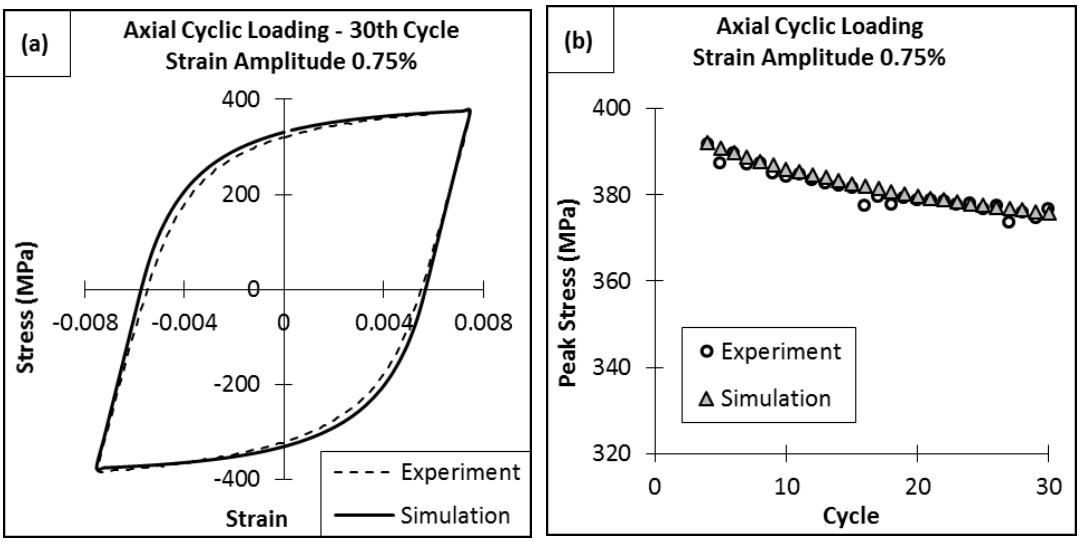

Fig. 2.10: *Comparison of uniaxial experimental and simulated results for 0.75% strain amplitude,* ***(a)*** *stress-strain hysteresis loops at 30th cycle,* ***(b)*** *peak stress vs. number of cycles.*

The reduction of low angle boundary dislocation density can be manifested as the decrement of misorientation angle (Sauzay et al., 2005; Fournier et al., 2011). The cyclic softening model based on dislocation annihilations has also simulated the exponential decrement of the boundary misorientation angle as observed in figure 2.11.

2.7.5 Discussion

When comparing with the experimental hysteresis loops, the simulations show a good agreement with the cyclic behaviour of the material. From the results, it is observed that the Ohno-Wang KH rule is well suited for the material. The peak stress softening curves show good match to the actual softening behaviour. The phenomenon of dislocation annihilation based softening mechanism not only qualitatively, but also quantitatively recognised the cyclic softening of the material.

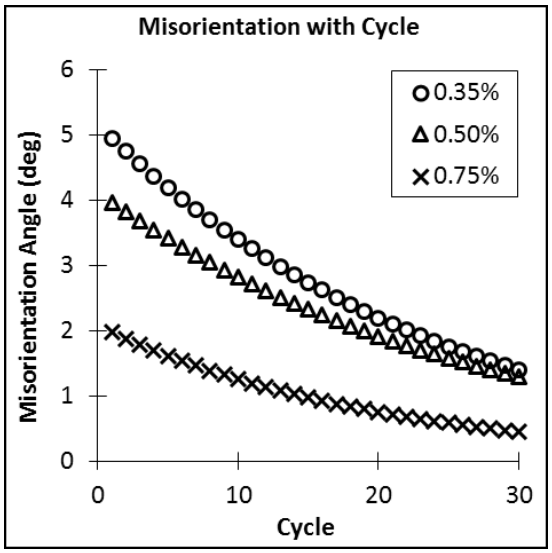

Fig. 2.11: *Gradual disappearance of boundary misorientation with cycle, for all strain amplitudes.*

The initial misorientation angle is high in low strain amplitude as the generated dislocation density is less and lattices are not reorganised. The misorientation angle never actually vanishes but saturates asymptotically. The simulated curves (figure 2.11) followed the same pattern.

2.8 Conclusion

The present work deals with three cyclic plastic phenomena namely: i) hysteresis loop and Bauschinger effect, ii) the Masing behaviour and, iii) cyclic softening in initial transient cycles. The hysteresis loop and Bauschinger effect is well taken by Ohno-Wang kinematic hardening law. The parameters of Ohno-Wang law have been calculated from uniaxial LCF data. One set of KH parameter is sufficient as the material shows Masing behaviour. Cyclic softening is qualitatively and quantitatively simulated using dislocation annihilation model at low angle sub-grain boundary (Sauzay, 2009). The model parameters are taken from literature, determined from TEM Microstructure and also evolved by trial and error method during simulations. The set of parameters, thus evolved for the material SA333 Gr-6 C-Mn steel can simulate the uniaxial and in-phase biaxial (tension-torsion) cyclic plastic behaviour of the material.

Though there are a few adjustable parameters involved in the model, proper investigation and case specific precise measurement can yield accurate values for them. The overall contribution of the idea of softening at low angle grain boundary is validated and found transferable for different loading arrangements.

2.9 Acknowledgements

The authors acknowledge Bhabha Atomic Research Centre, Mumbai for financial assistance through collaborative project and National Metallurgical Laboratory, Jamshedpur for experimental support. The authors also acknowledge Dr. Surajit Kumar Paul, NML, Jamshedpur for TEM micrographs.

2.10 References

ASTM E606M

3DS SIMULIA ABAQUS CAE (v6.8), User's Manual.

1870, Levy, M., Comptes Rendus, Académie des Sciences, Volume 70, pp 1323-1325.

1881, Bauschinger, J., Über die Veranderung der Elasticitatsgrenze und elastcitatsmodulverschiedener, Metal Civiling N.F., Volume 27, pp 289-348.

1913, von Mises, R., Mechanik der festenKörperimplastisch-deformablen Zustand. Nachrichten von der Gesellschaft der Wissenschaftenzu Göttingen, Mathematisch-Physikalische Klasse, Volume 4, pp 582-593.

1923, Masing, G., ZurHeyn'schen Theorie der Verfestigung der Metalledurchverborgenelastische Spannungen. In: Harries C.D. (eds.) Wissenschaftliche Veröffentlichungenausdem Siemens-Konzern. Springer, Berlin, Heidelberg, pp 231-239.

1924, Prnadtl, L., Proceedings of the First International Congress of Applied Mechanics, Delft, 43.

1926, Lode, W., Versuche über den Einfluss der mittleren Hauptspannung auf das Fliessen der Metalle Eisen, Kupfer und Nickel, Zeitschriftfür Physik, Volume 36, Issue 11-12, pp 913-939.

1928, von Mises, R., Mechanik der plastischen Formänderung von Kristallen, Zeitschriftfür Angewandte Mathematik und Mechanik (ZAMM - Journal of Applied Mathematics and Mechanics), Volume 8, Issue 3, pp 161-185.

1930, Reuss, A., Berücksichtigung der elastischen Formänderung in der Plastizitätstheorie, Zeitschriftfür Angewandte Mathematik und Mechanik (ZAMM - Journal of Applied Mathematics and Mechanics), Volume 10, Issue 3, pp 266-274.

1931, Hohenemser, K., Fließversuche an Rohrenaus Stahl beikombinierter Zug- und Torsionsbeanspruchung, Zeitschriftfür Angewandte Mathematik und Mechanik (ZAMM - Journal of Applied Mathematics and Mechanics), Volume 11, Issue 1, pp 15-19.

1931, Taylor, G. I., Quinney, H., The Plastic Distortion of Metals, Philosophical Transactions of the Royal Society A, Volume 230, pp 681-693.

1947, Taylor, G. I., A Connexion between the criteria of Yield and the Strain Ratio Relationship in Plastic Solids, proceedings of the Royal Society A, Volume 191, Issue 1027, pp 441-446.

1948, Hill, R., A theory of the yielding and plastic flow of anisotropic metals, Proceedings of the Royal Society A, Volume 193, Issue 1033, pp 281-297.

1949, Shockley, W., Read, W. T., Quantitative Predictions from Dislocation Models of Crystal Grain Boundaries, Physical Review, Volume 75, Issue 4, pp 692.

1950, Drucker, D. C., Stress-strain Relations in the Plastic Range – a Survey of Theory and Experiment, O.N.R. Report, NR-041-032.

1950, Hill, R., Mathematical Theory of Plasticity, Oxford University Press, ISBN: 978-0-198-50367-5.

1950, Morrison, J. L. M., Shepherd, W. M., An Experimental Investigation of Plastic Stress-Strain Relations, Proceedings of the Institution of Mechanical Engineers, Volume 163, Issue 1, pp 1-17.

1950, Read, W.T., Shockley, W., Dislocation models of crystal grain boundaries, Physical Review, Volume 78, Issue 3, pp 275-289.

1951, Drucker, D. C., A more fundamental approach to plastic stress-strain relations, Proceedings of the First US National Congress of Applied Mechanics, ASME, pp 487-491.

1955, Prager, W., The Theory of Plasticity: A Survey of Recent Achievements, Proceedings of the Institution of Mechanical Engineers, Volume 169, Issue 1, pp 41-57.

1956, Prager, W., A New Method of Analyzing Stresses and Strains in Work Hardening Plastic Solids, Journal of Applied Mechanics, Volume 23, pp. 493-496.

1958, Besseling, J. F., A Theory of Elastic, Plastic and Creep Deformations of an Initially Isotropic Material. Journal of Applied Mechanics, Volume 25, pp 529-536.

1959, Drucker, D. C., A definition of stable inelastic material, Journal of Applied Mechanics, Volume 26, pp 101-106.

1966, Armstrong, P.J., Frederick, C. O., A Mathematical Representation of the Multiaxial Bauschinger Effect. CEGB Report No. RD/B/N 731.

1978, Zaverl Jr., F., Lee, D., Constitutive relations for nuclear reactor core materials, Journal of Nuclear Materials, Volume 75, Issue 1, pp 14-19.

1979, Chaboche, J. L., Dang Van, K., Cordier, G., Modelization of the strain memory effect on the cyclic hardening of 316 stainless steel, SMiRT-5, Berlin

1979, Essmann, U., Mughrabi, H., Annihilation of dislocations during tensile and cyclic deformation and limits of dislocation densities, Philosophical Magazine A, Volume 40, Issue 6, pp 731-756.

1979, Marquis, D., Modelisation et Identification de I'Ecrouisage Anisotropic des Metaux, These Paris VI.

1981, Meckings, H., Kocks, U. F., kinetics of flow and strain-hardening, Acta Metallurgica, Volume 29, pp 1865-1875.

1985, McDowell, D.L., A two surface model for transient nonproportional cyclic plasticity: part 1 – development of appropriate equations, Journal of Applied Mechanics, Volume 52, pp 298-302.

1987, Chai, Hui-Fen, Laird, Campbell, Mechanisms of cyclic softening and cyclic creep in low carbon steel, Materials Science and Engineering, Volume 93, pp 159-174.

1992, Haupt, P., Kamlah, M., Tsakmakis, Ch., Continuous representation of hardening Properties in cyclic plasticity, International Journal of Plasticity, Volume 8, pp 803-817.

1993, Ohno, N., Wang, J.D., Kinematic hardening rules with critical state of dynamic recovery, part I: Formulation, International Journal of Plasticity, Volume 9, Issue 3, pp 375-390.

1993, Ohno, N., Wang, J.D., Kinematic hardening rules with critical state of dynamic recovery, part II: Application, International Journal of Plasticity, Volume 9, Issue 3, pp 391-403.

1995, Haupt, P., Kamlah, M., Representation of cyclic hardening and softening properties using continuous variables, International Journal of Plasticity, Volume 11, Issue 3, pp 267-291.

1996, Jiang, Y., Sehitoglu, H., Modelling of cyclic ratchetting plasticity, part I: development of constitutive relations, Journal of Applied Mechanics, Volume 63, Issue 3, pp 720-725.

1998, Estrin, Y., Dislocation theory based constitutive modelling: foundations and applications, Journal of Materials Processing Technology, Volume 80-81, pp 33-39.

2002, Sedláček, R., Blum, W., Kratochvíl, J., Forest, S., Subgrain Formation during Deformation - Physical Origin and Consequences, Metallurgical And Materials Transactions A, Volume 33A, pp 319-327.

2003, Kassner, M. E., Kyle, K., Taylor hardening in five power law creep of metals and class M alloys, Nano and Microstructural Design of Advanced Materials, pp 255-271.

2003, Kocks, U. F., Mecking, H., Physics and phenomenology of strain hardening: the FCC case, Progress in Material Science, pp 171-273.

2005, Sauzay, M., brillet, H., Monnet, I., Mottot, M., Barcelo, F., Fournier, B., Pineau, A., Cyclically induced softening due to low-angle boundary annihilation in a martensitic steel, materials Science and Engineering: A, Volumes 400-401, pp 241-244.

2006, Chakrabarty, J., Theory of Plasticity, Elsevier Butterworth-Heinemann, ISBN: 978-0-750-66638-2.

2006, Sinclair, C.W., Poole, W.J., Bréchet, Y., A model for the grain size dependent work hardening of copper, Scripta Materialia, Volume 55, Issue 8, pp 739-742.

2009, Saujay, M., Modelling of the evolution of micro-grain misorientations during creep of tempered martensite ferritic steels, Materials Science and Engineering: A, Volumes 510-511, pp 74-80.

2011, Fournier, B., Sauzay, M., Pineau, A., Micromechanical model of the high temperature cyclic behavior of 9-12%Cr martensitic steels, International Journal of Plasticity, Volume 27, Issue 11, pp 1803-1816.

2011, Paul, Surajit Kumar, Sivaprasad, S., Dhar, S., Tarafder, S., Key issues in cyclic plastic deformation: Experimentation, Mechanics of Materials, Volume 43, Issue 11, pp 705-720.

2013, Carvalho-Resende, T., Bouvier, S., Abed-Meraim, F., Balan, T., Sablin, S.-S., Dislocation-based model for the prediction of the behavior of b.c.c. materials – Grain size and strain path effects, International Journal of Plasticity, Volume 47, pp 29-48.

2016, Mughrabi, Hael, The α-factor in the Taylor flow-stress law in monotonic, cyclic and quasi-stationary deformations: Dependence on slip mode, dislocation arrangement and density, Current Opinion in Solid State and Materials Science, Volume 20, Issue 6, pp 411-420.

Chapter 3

SYMMETRIC MULTIAXIAL LOADING

In this chapter, biaxial (both in-phase and 90° out-of-phase) cyclic plastic behaviour of SA333 steel is studied for symmetric loading condition. Modelling for the experimentally observed material behaviours is attempted based on dislocation interactions and density. The material behaviours are simulated in finite element platform using the modified material model.

Content **Page**

Blank Page

3.1 Introduction

The present material under study, SA333 Grade-6 C-Mn steel is commonly used in primary heat transport (PHT) pipes in nuclear power plants, where it is subjected to multiaxial loading conditions.

A tension-torsion test is a biaxial test. A biaxial state of stress at any point can be represented, more generally, as: $\sigma_{kl} = \begin{bmatrix} 0 & 0 & 0 \\ 0 & 0 & \tau_{\theta z} \\ 0 & \tau_{z\theta} & \sigma_{zz} \end{bmatrix}$ in the cylindrical coordinate system, as shown in figure 3.1.

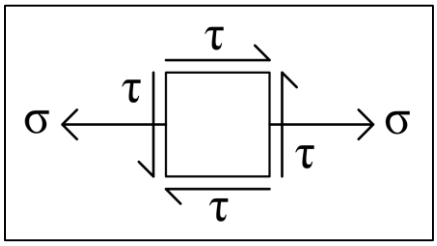

Fig. 3.1: *Biaxial state of stress*

In analysing torsional loading, care should be taken for the calculation of shear stress when subjected to elastic-plastic deformation. Generally, the shear stress is calculated on the outer surface of the specimen from the torque, using the relation valid for elastic deformations. Thus calculated shear stress shows a linear distribution along the radial direction with maximum at the outer surface. But, it is not truly applicable when elastic-plastic deformation is occurring. It is noticeable that, for a given strain in the elastic-plastic region, the elastically predicted (calculated) shear stress must overestimate the actual elastic-plastic shear stress response. However, this discrepancy can be minimized using a thin walled specimen. A

A more general case is the multiaxial loading where, the stress along the thickness direction is also realised. For multiaxial state of stress, the thick walled cylindrical specimen subjected to axial tension, torsion and internal pressure is experimented.

The multiaxial loadings can have phase differences with each other. If there is no phase difference, the loading is known as in-phase or proportional loading condition (Jiang and Kurath, 1997). The stress response in the ideally in-phase multiaxial loading is similar to that of uniaxial case. The primary slip system, in proportional loading, remains unchanged just like uniaxial cases, though in a different orientation. If the equivalent stress-rate vector is not normal to the yield surface, the loading is known as the out-of-phase or, non-proportional loading (Jiang and Kurath, 1997). In case of non-proportional loading, the maximum shear plane rotates, activating several crystallographic slip systems due to which, additional hardening responses may be observed which is known as non-proportional hardening (Benallal and Marquis, 1987).

In this present study, the micro-mechanism of the non-proportional hardenings are investigated and suitable modelling of the same is attempted. The finite element simulated

results for the non-proportional loading are compared with experimental results to validate the model.

3.2 Experimental observations

Symmetric proportional (in-phase) and non-proportional (90° out-of-phase) tension-torsion low cycle fatigue tests were conducted by Bhabha Atomic Research Centre, India, at various strain amplitudes for the material SA333 Grade-6 C-Mn steel in quasi-static condition at room temperature and at standard environmental condition. All the experiments were conducted according to ASTM E2207 in strain-controlled mode maintaining axial strain to engineering shear strain ratio is $\frac{1}{\sqrt{3}}$. Proportional tests are conducted for ±0.50%, ±0.75% and ±1.00% equivalent strain amplitudes with triangular loading pulse. Non-proportional (90° out-of-phase) tests are conducted for ±0.35%, ±0.53% and ±0.70% strain amplitudes with sinusoidal torsional loading followed by 90° out-of-phase sinusoidal axial loading. Sinusoidal pulse and strain ratio is maintained to ensure circular loading path for maximum non-proportional hardening response.

Tubular specimens with gauge length of $30\ mm$, inside diameter of $22\ mm$ and wall thickness $1.7\ mm$ are used for experiments. The thin tubular specimen is used to ensure the biaxial (plane stress) condition. Schematic diagrams of the specimens are presented in figure 3.2 below.

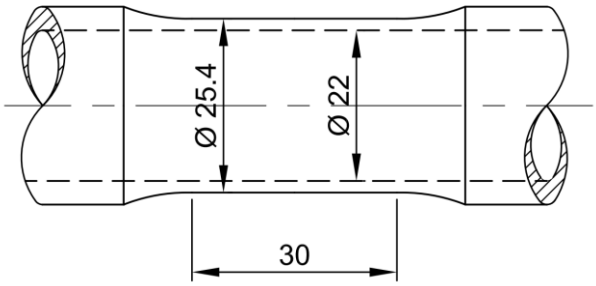

Fig. 3.2: *Schematic diagram of biaxial specimen.*

A biaxial extensometer (figure 3.3a) is used on the outer surface of the specimen to measure the axial extension and angle of twist while axial load and the torque are measured with load cells (figure 3.3b). All the tests were conducted in a servo-hydraulic universal testing machine with automated data acquisition system.

The material SA333, characterised in the chapter-2 for the symmetric uniaxial cyclic plastic loading. In this chapter, the material responses for the symmetric biaxial proportional and non-proportional loadings are discussed for the interested strain range. In proportional loading, the material shows similar responses (figure 3.4a) as uniaxial cases.

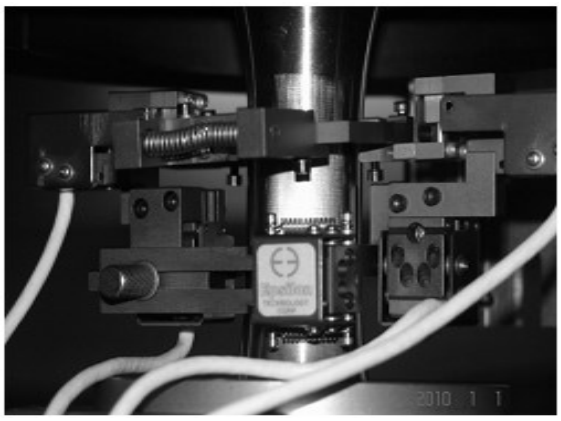

Fig. 3.3a: *Biaxial extensometer.*

Fig. 3.3b: *Biaxial testing system.*

In non-proportional loading, there are additional hardenings observed which can be manifested besides predominant cyclic softening, reducing the net softening magnitude (figure 3.4b). It is observed again that, the intensity of softening gradually decreases and gets saturated within first 30-50 cycles.

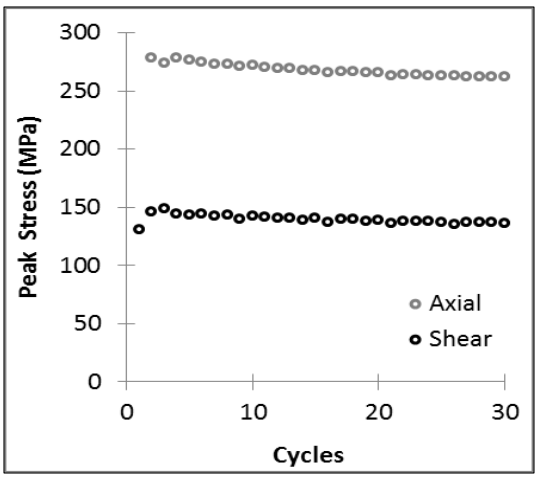

Fig. 3.4a: *Typical experimental results showing cyclic softening in proportional loading condition (axial strain amplitude 0.35%, shear strain amplitude 0.61%).*

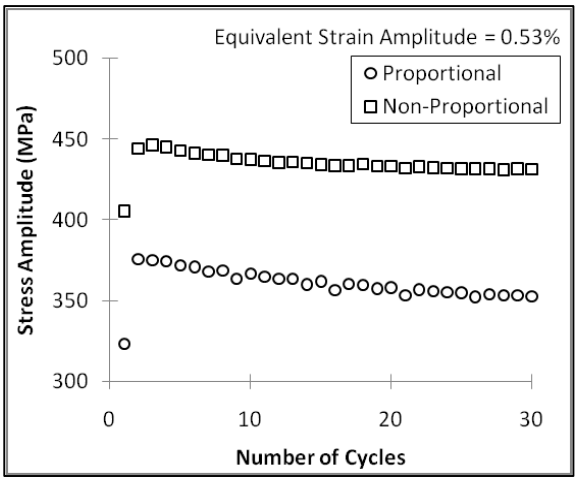

Fig. 3.4b: *Experimental Results showing cyclic softening in axial stress response for proportional and non-proportional loading condition, indicating cross hardening and non-proportional hardenings.*

The non-proportionality of loading condition gave rise to two types of additional hardening responses by the material, namely: non-proportional hardening and cross hardening (figure 3.4b).

3.3 Finite Element modelling

Multiaxial low cycle fatigue tests are simulated in ABAQUS CAE (v6.8) commercial finite element platform. Only the relevant (gauge length) portion of the actual specimens i.e. tubular specimen geometry is modelled as per the dimensions shown in figure 3.2. The part geometry is discretised adopting structural meshing with linear hexahedral (8-noded) elements. The total number of elements for the tubular specimen are 984 with 1722 nodes.

Displacement boundary conditions are imposed according to the strain amplitudes using balanced sinusoidal amplitude function at reference points, which are connected to the body through kinematic coupling. The axial displacement and angular twist are applied on the reference point set on the axis of the cylindrical specimen. The boundary conditions are employed in cylindrical coordinate system, as the geometries are axisymmetric. Figure 3.5 below shows such a model created in ABAQUS FE platform.

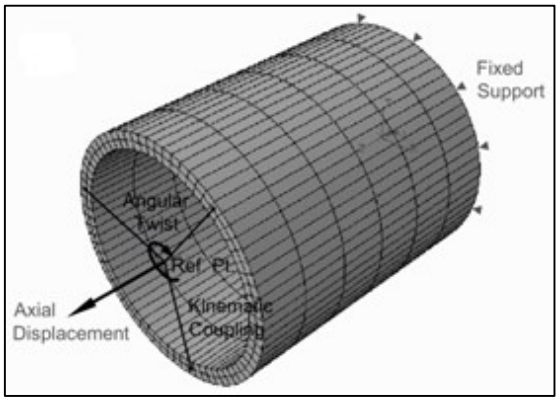

Fig. 3.5: *Discretised tubular specimen with kinematic coupling and loading arrangements.*

The material behaviour is incorporated in FE analysis through user material subroutine (UMAT). The in-phase or proportional loading condition shows alike material response as uniaxial case and does not require any modification in the material model. The same FE model can be used in case of non-proportional loading simulation, which only needs appropriate material mode.

3.4 Simulation of proportional loading

The material model used for uniaxial loading as discussed in the previous chapter, has been used to simulate in-phase Biaxial (tension-torsion) cyclic loading condition. The shear components (stress/strain) are calculated at the outer surface of the tubular specimen, consistent with the measurements in the experiments. Experimental axial and shear stress-strain loops for saturated cycles are compared with corresponding simulated results. Experimental and simulated results for cyclic softening in initial transition cycles are also compared in figure 3.6a-d, 3.7a-d and 3.8a-d for respective strain amplitudes.

For 0.50% equivalent strain amplitude (figure 3.6d), the simulated shear loops are about 14% over-predicted. Similar over-prediction in shear peak stress is also observed in stress path shown in figure 3.9b. The mismatch is also observable in other strain amplitudes as well, may be in the different axis but following the same tendency.

The shear peak stresses for 0.75% and 1.00% equivalent strain amplitudes are matching well, whereas, a 6% under-prediction is observed in the corresponding axial peak stresses (figure 3.7 and 3.8). This over-prediction is due to the inconsistency maintaining the strain ratio during experiments, which is clearly seen in the stress-path at peak loads (fig. 3.9b).

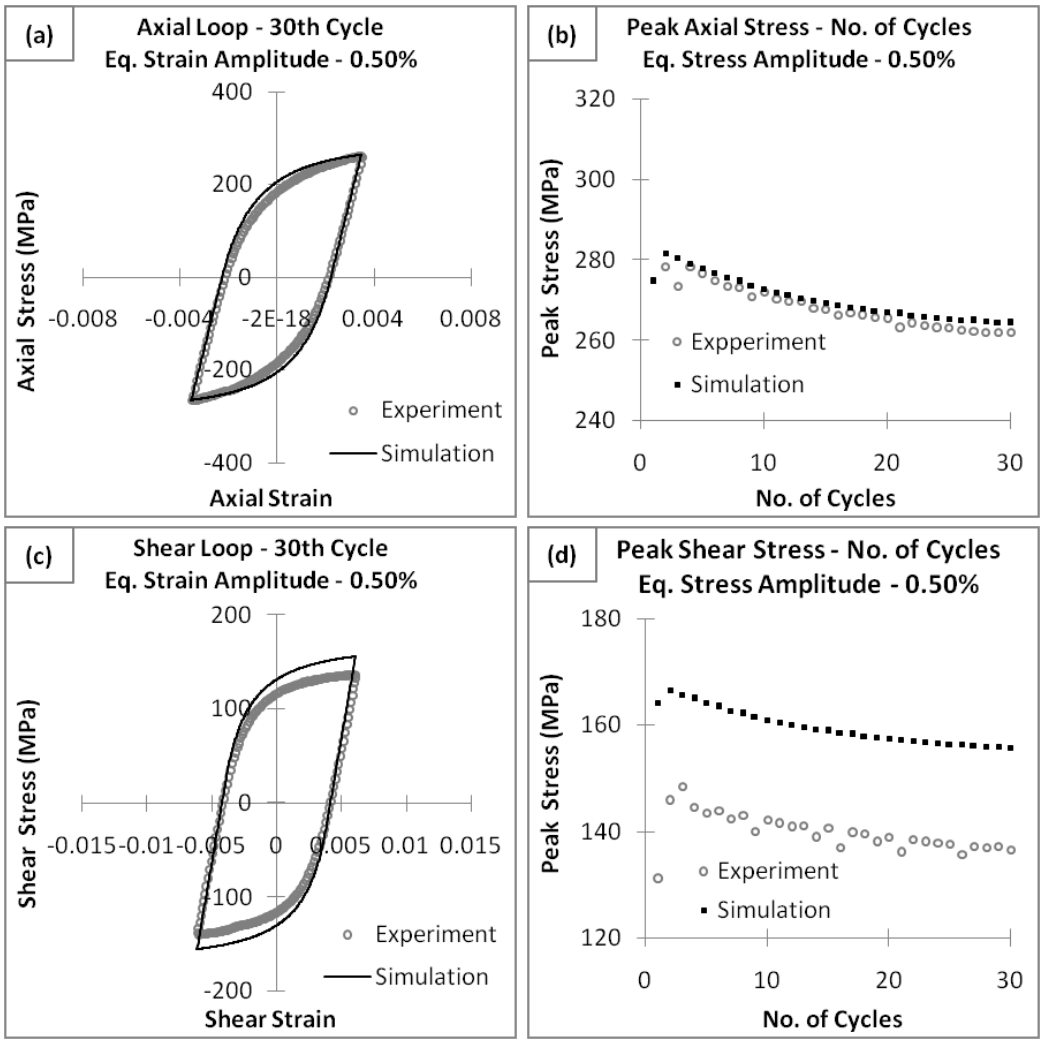

Fig. 3.6: *Comparison of in-phase tension-torsion experimental and simulated results for 0.50% equivalent strain amplitude,* ***(a)*** *axial stress-strain hysteresis loops at 30th cycle,* ***(b)*** *peak axial stress vs. cycles,* ***(c)*** *shear stress-strain hysteresis loops at 30th cycle,* ***(d)*** *peak shear stress vs. cycles.*

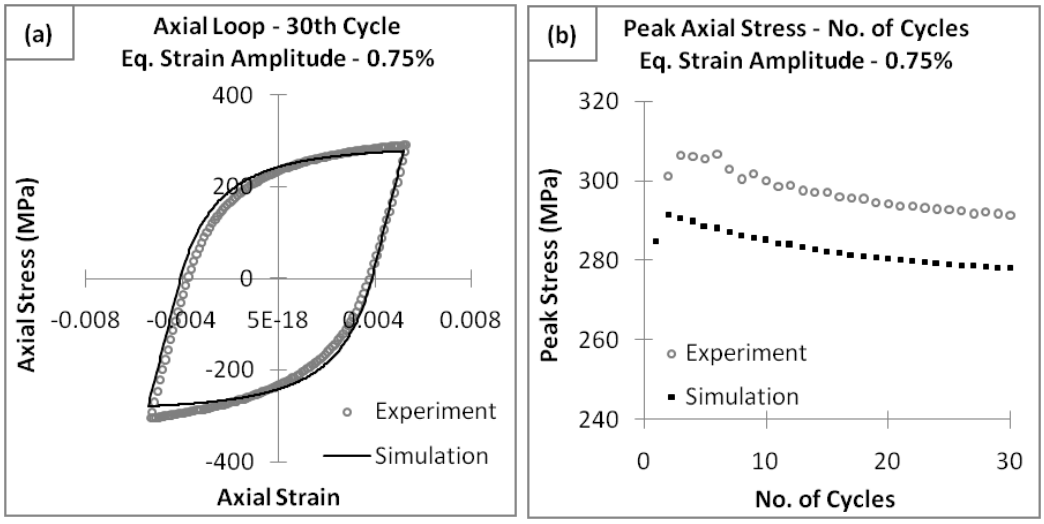

Fig. 3.7: *Comparison of in-phase tension-torsion experimental and simulated results for 0.75% equivalent strain amplitude,* ***(a)*** *axial stress-strain hysteresis loops at 30th cycle,* ***(b)*** *peak axial stress vs. cycles.*

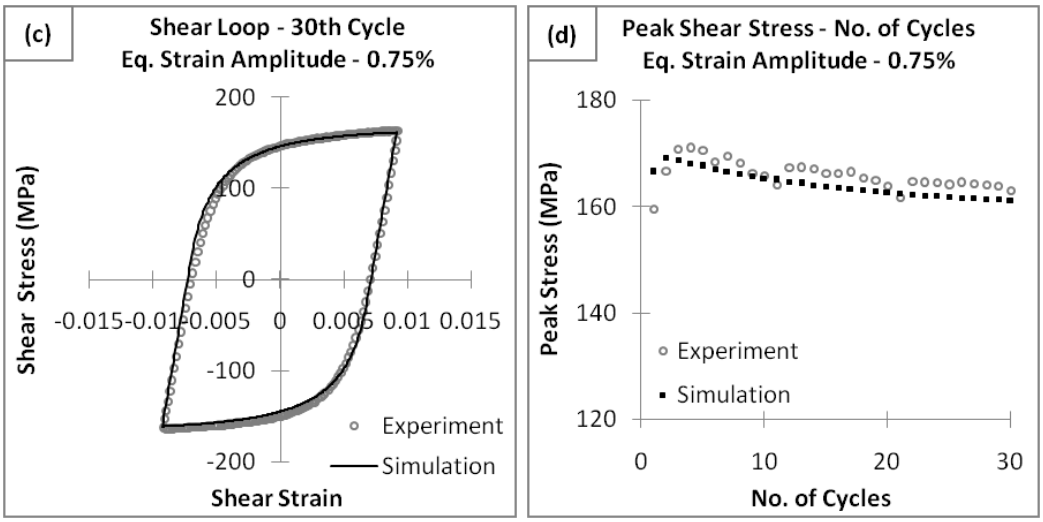

Fig. 3.7: *Comparison of in-phase tension-torsion experimental and simulated results for 0.75% equivalent strain amplitude,* ***(c)*** *shear stress-strain hysteresis loops at 30th cycle,* ***(d)*** *peak shear stress vs. cycles.*

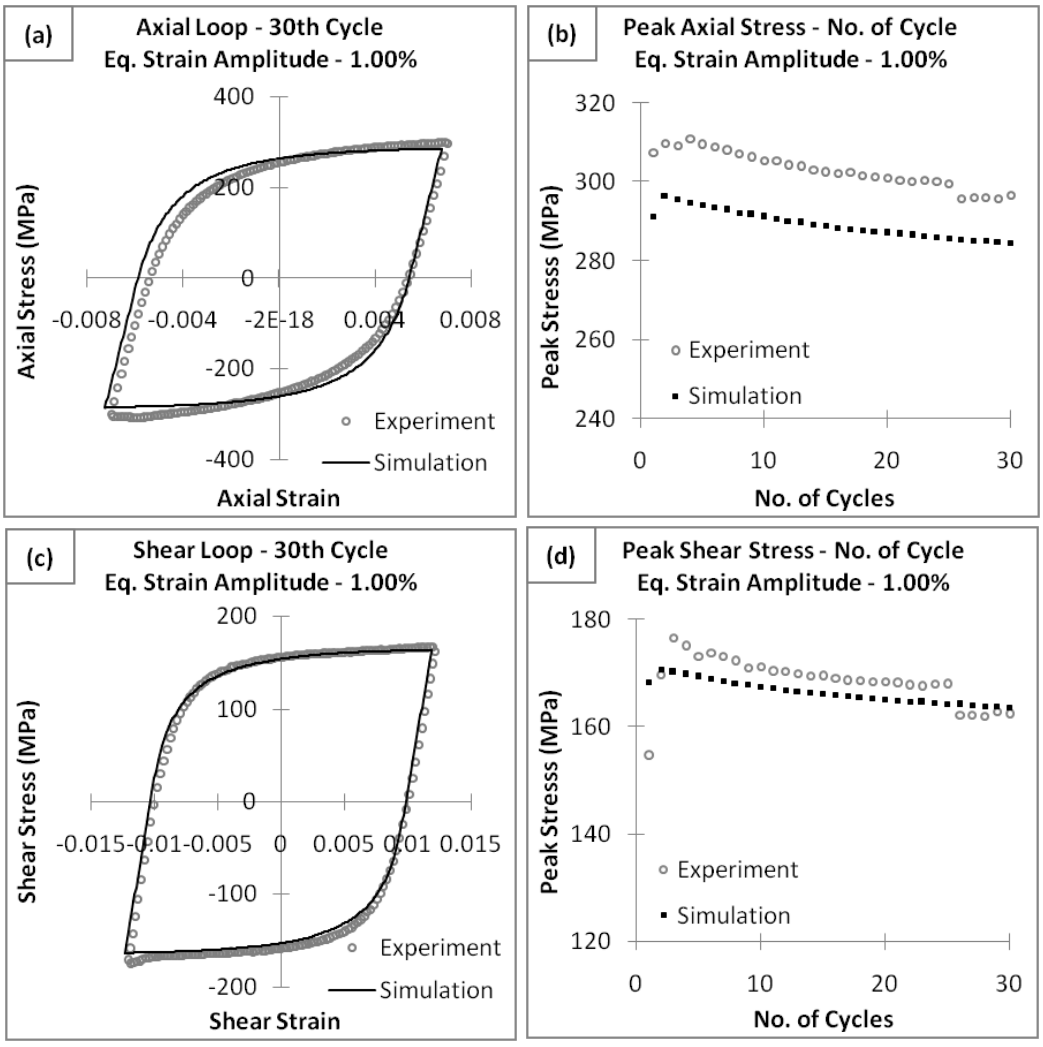

Fig. 3.8: *Comparison of in-phase tension-torsion experimental and simulated results for 1.00% equivalent strain amplitude,* ***(a)*** *axial stress-strain hysteresis loops at 30th cycle,* ***(b)*** *peak axial stress vs. cycles,* ***(c)*** *shear stress-strain hysteresis loops at 30th cycle,* ***(d)*** *peak shear stress vs. cycles.*

The strain-path and stress (response) path for both experimental and simulated proportional loading conditions are represented in figure 3.9a-b. The response (stress) path is a hysteresis curve instead of being linear. Which gives a clear indication of the development of non-proportionality in the material behaviour. The micro-mechanism behind such material behaviour are required to be researched for the sake of a better understanding of the complex non-proportion multiaxial behaviour of the material.

Despite the quantitative disparity, qualitative estimation of the cyclic softening and hysteresis loop curvature confirms the transferability of the model and material parameters derived from the uniaxial LCF tests in the in-phase biaxial loading condition.

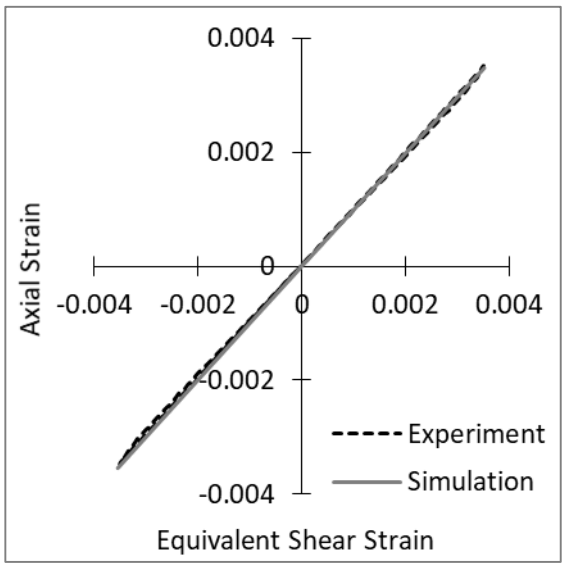

Fig. 3.9a: *Strain path for in-phase loading (equivalent strain amplitude 0.50%, 30th cycle).*

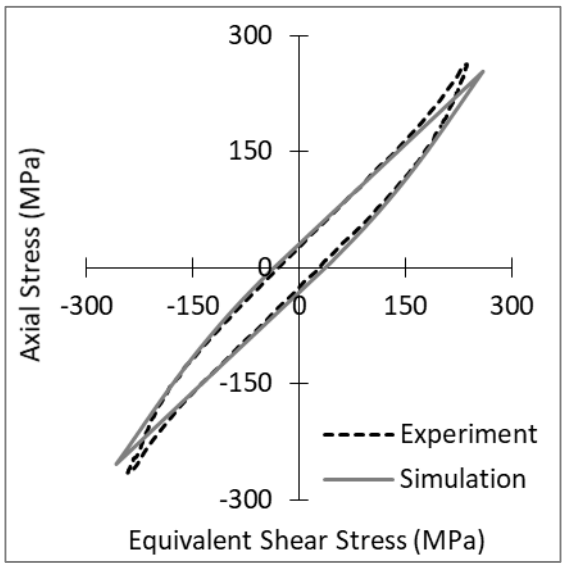

Fig. 3.9b: *Stress (response) path for in-phase loading (equivalent strain amplitude 0.50%, 30th cycle).*

3.5 Dislocation based explanation for the non-proportional hardening

In this work it is attempted to explain the material behaviour observed in experimental results for both the in-phase and out-of-phase loading with a dislocation based framework.

The magnitude of this non-proportional hardening is strongly dependent on loading amplitude and history. It is evidently reported by Tanaka et al. (1985a,b) that non-proportional hardening is dependent on the strain path, among which the circular strain path (sinusoidal pulse) gives predominantly higher hardening response. It is also reported (Kanazawa, 1979) that the magnitude of non-proportional hardening is dependent on phase difference of loadings, and the maximum hardening effect is observed for 90° out-of-phase loading conditions.

In addition, the work of Lamba (1977), Kanazawa et al. (1979), Nouailhas et al. (1983) and Benallal and Marquis (1987) reported that a different and sudden hardening effect may be observed in out-of-phase loading when loading upto a certain extent in a particular direction is followed by loading in a different direction occurs. This kind of hardening is known as

the cross hardening effect and saturates as soon as it reaches its magnitude. It is observed that the magnitude of cross hardening is dependent on the loading amplitude.

For physical based modelling of the non-proportional hardening behaviour, a good understanding of the dislocation dynamics in out-of-phase loading is indispensable. Any hardening response is developed due to the restriction to the free glide of mobile dislocations. These restrictions are evolved due to many reasons, among which, interaction of two dislocations shows versatile behaviour including softening. Interacting dislocations can have different kinetics and can lie in different slip systems (combination of slip plane and directions). In the work of Kubin et al. (2008), the possible interactions of dislocations are classified in six kinds, three of them are accounted for forest interactions between non-coplanar slip systems, resulting in the formation of junctions or locks, namely the Lomer–Cottrell lock, the Hirth lock and the glissile junction. There are two non-contact interactions for dislocations gliding in parallel slip planes with same or different Burger's vectors, known as the self-interaction and the coplanar interaction. And the last interaction is the collinear interaction, produces annihilations. In BCC and FCC crystals, there are twelve such slip systems exist, which can be activated easily. The total possible interactions between mobile dislocations in a BCC crystal can be captured by a matrix of 144 (12×12) interaction coefficients (Franciosi, 1985). This interaction matrix actually designates the generalised hardening character of the material. It is reported by Kubin and his co-workers (2008) that, there exists six independent coefficients to represent the matrix considering symmetry assumptions, which are associated with six different types of dislocation interactions.

Effect of these six interactions are incorporated in the simplified mathematical model broadly generalised by three families of dislocations namely forward, reverse and latent dislocations depending on their origins. In cyclic plastic loading, changes in strain-path occur due to load reversal or due to non-proportional loading. Strain-path change can activate different slip systems. The built-up dislocation structure in the first deformation path becomes unstable when a sudden and abrupt strain-path change occurs (Barlat et al., 2003; 2011), though, a stable phase is achieved after some plastic deformation and the obvious sub-structure formation cannot be hindered for a long time.

It can be speculated that, a huge number of dislocations get transferred immediately from existing slip systems to the newly active slip systems when non-proportionality is triggered (Rauch et al., 2007, 2011). The phenomena can cause the latent hardening (Franciosi, 1985; Barlat et al., 2003; 2011; Rauch et al., 2011). The transferred dislocations are usually piled-up initially to deliver a sudden rise in flow stress as cross hardening and gradually get streamlined, mobile and naturally evolving. While the dislocations remain tangled, all the mobile dislocations in every active slip systems experience constriction and overall manifestation is isotropic non-proportional hardening. Latent hardening can therefore be recognised as the micro-mechanism behind sudden cross hardening and gradually influencing non-proportional hardening as observed in the non-proportional experiments, most effectively in case of orthogonal strain-path changes.

Fundamentally, the interactions of forward dislocations in the primary slip systems are incorporated in the KH rule as the hardening term. The interactions of reverse dislocation population is captured by the dynamic recovery mechanism (Kocks and Mecking, 1979). But, the KH rule remains insensitive to the interaction of the latent dislocations developed by the non-parallel strain-path changes.

To activate latent effect in the mathematical model, a non-proportionality trigger is required. The non-proportionality caused by non-parallel changes in the strain-path, can be defined by many ways (Schmitt et al., 1985; Benallel and Marquis, 1987; Tanaka, 1994). One of the efficient way is by the angle made by deviatoric stress rate vector and plastic strain rate vector (Jiang and Kurath, 1997). The degree of non-proportionality is scaled from zero to one for 0° to ±90° and introduced in numerical modelling as proposed by Benallal and Marquis (1987). This numerical parameter, if detects any differences in loading phases, triggers the latent hardening mechanisms and amplifies the non-proportional hardening effects according to the degree of non-proportionality.

3.6 Modelling for non-proportional loading

The material is considered homogeneous and isotropic in the elastic regime and continuum incompressible plasticity framework is followed. The basic formulation is described previously in the chapter-2. The modification due to the latent effect is proposed in the cyclic yield stress as it is additively decomposed into initial cyclic yield stress (σ_0), softening stress (σ_1) and non-proportional hardening stress (σ_2), as:

$$\sigma_c = \sigma_0 + \sigma_1 + \sigma_2 \tag{3.1}$$

Where σ_1 arises due to annihilation of dislocations at sub-grain boundaries, assuming already formed stable dislocation structures and σ_2 is evolved from the latent hardening due to strain-path changes. Both the softening and hardening mechanisms are isotropic as observed in the experimental results and realised from micromechanics.

3.6.1 Softening Model (Isotropic)

The cyclic softening stress σ_1 is evolved from the annihilations of the dislocations forming the sub-grain walls (Sauzay et al., 2005; Sinclair et al., 2006) at the low angle sub-grain boundaries. The starting of sub-cell formation, in case of non-proportional loading, can be delayed until a few initial cycles until the strain-path change events to become stable. Ignoring that short delay, the softening model is implemented right from the beginning as it was in case of uniaxial loading (Bhattacharjee et al., 2018). The mechanism is discussed in the previous chapter. The quantification of initial dislocation densities (Λ_0) at the sub-grain boundary, is accordingly calibrated as per the plastic deformations engrossed before the sub-cell formation. The softening stress is calculated in an incremental form as:

$$\Delta\sigma_1 = -\frac{\alpha M^2 G b}{S_n}\frac{\Lambda}{D}\lambda\frac{y}{b}\Delta\varepsilon^p \tag{3.2}$$

Where, α is the interaction strength, M is Taylor factor, G is the shear modulus, b is the magnitude of Burger's vector, Λ is the dislocation density of edge dislocation at the sub grain boundary per unit length, D is the average sub-grain size, λ is the slip band width, S_n is the number of independent slip systems taken to be five to accommodate von-Mises plasticity, y is the critical annihilation distance.

If n is the number of annihilation site per slip band interacting with low angle sub-grain boundaries then $y = \lambda/2n$. If p is the probability of annihilation of dislocations of opposite sign, the softening stress increment takes the form:

$$\Delta\sigma_1 = -\frac{\alpha M^2 Gbp}{S_n}\frac{\Lambda}{D}\frac{\lambda^2}{2nb}\Delta\varepsilon^p \tag{3.3}$$

3.6.2 Latent Hardening Model (isotropic)

The mechanical behaviour of metals is frequently related to the average mobile dislocation density ρ through the fundamental equation $\tau = \tau_0 + \tau_{Taylor} = \tau_0 + \alpha Gb\sqrt{\rho}$, where τ_0 is the Peierls stress related to lattice friction and solute contents, G is shear modulus, b is the magnitude of the Burger's vector and α is a factor that weights the dislocation interactions. The equation is generally known as the Taylor pile-up model for forest dislocation (Taylor, 1934; Davoudi, 2014).

The Taylor equation is quite effective as long as monotonic modes of deformation are considered where the detail physical processes occurring on each slip system are not influential, the averages are sufficient. However, for complex loading conditions, different dislocation interactions in different slip systems may have diverse manifestation in the macroscopic material behaviour. To account for such distinction, the averaged interaction coefficient α becomes interaction matrix α_{ij} with respective dislocation densities ρ_j in jth slip system.

For a more exhaustive account of the dislocation interactions, the critical resolved shear stress (τ_{CRSS}) on a specific slip system j, should depend on the dislocation densities ρ_j associated with each slip systems j, may be expressed (Kocks, 1966) as:

$$\tau_{CRSS} = \tau_0 + Gb\sqrt{\sum_j \alpha_{ij}\rho_j} \tag{3.4}$$

α_{ij} is the dislocation interaction matrix, represents the magnitude of interactions for the pairs of dislocation of ith and jth slip systems.

For BCC material, 12 slip systems can be easily activated on {110} plane <111> direction (table 2.4, chapter-2) and the interactions of dislocations in every two slip systems lead to a 12x12 matrix. Kubin et al. (2008) pointed out that due to the diagonal symmetry and occurrence of four <111> axis with ternary symmetry reduces the matrix with six independent coefficients. These coefficients are associated with six specific types for interactions. The matrix α_{ij} is defined with only two coefficients $\alpha_1 = 1$ (for coplanar

systems) and $\alpha_2 = 1.1$ (for non-coplanar systems) in the case of steel (Lipinski and Berveiller, 1989) considering only self and latent hardening (Franciosi, 1985) for the present purpose. When τ_{CRSS} represents the CRSS, the average interaction coefficient is:

$$\tau_{CRSS} = \tau_0 + Gb\sqrt{\sum_j \alpha_{ij}\rho_j} = \tau_0 + Gb\sqrt{\rho\sum_j \alpha_{ij}\frac{\rho_j}{\rho}} = \tau_0 + \alpha Gb\sqrt{\rho} \quad (3.5)$$

Where, α is the square root of the average value of α_{ij} weighted by the ratios ρ_j/ρ (with $\rho = \sum\rho_j$ is the total dislocation density in the grain). In the case of monotonic deformation, the lattice orientations and activities on the slip systems evolve slowly and the averaging of this equation remains similar until the end of the deformation. Consequently, the evolution of the parameter α remains limited and the average value over all the grains of the polycrystals will appear constant. A similar expression may be used for the polycrystalline flow stress (σ) as:

$$\sigma = M\tau \quad (3.6)$$

Here, M is the average Taylor factor that relates CRSS of polycrystals and the overall flow stress. The relationship comes from the kinetics of deformation. Incorporating the directions of slip and slip plane normal and considering upper bound (Taylor assumption) double averaging (over grain and slip systems) method for uniaxial tension the average Taylor factor for polycrystals is determined (Estrin, 1998; Kassner et al., 2003). The flow stress σ can be additively decomposed into two parts like CRSS:

$$\sigma = \sigma_0 + \sigma_{Taylor} = M\left(\tau_0 + \tau_{Taylor}\right) \quad (3.7)$$

Where, σ_0 is taken as initial yield stress of the material coming from the lattice friction and σ_{Taylor} represents further hardening stress due to pile-up of dislocations with average density ρ. The evolution of average dislocation density is governed by the following equation (Tabourot, 1997; Dong et al., 2014) proposed by Mecking and Kocks (1981):

$$d\rho = \frac{1}{bL}\frac{M\,dq}{S_n} - \frac{2y}{b}\rho M\,dq \quad (3.8)$$

The first term is an athermal storage rate that is essentially sensitive to the mean-free-path L for the mobile dislocations and the second term indicates the dynamic recovery of dislocation density, dependent on temperature and strain rate (Estrin and Mecking, 1984; Rauch et al., 2011). The dislocation density is evolved depending on the increment of the size of the plastic strain memory surface. Chaboche and his co-workers (1979) theorised plastic strain memory surface to respect the fact that, the effective plastic deformation incorporating activation of slip plane in the microscopic level. The definition of the memory surface in the plastic strain space is:

$$F = \frac{2}{3}\left(\varepsilon_{ij}^p - \beta_{ij}\right)\left(\varepsilon_{ij}^p - \beta_{ij}\right) - q^2 \le 0 \quad (3.9)$$

Here, β_{ij} is the centre of the memory surface and q is the radius. For strain controlled LCF, $\beta_{ij} = 0$ and q is a constant equal to the plastic strain amplitude. Therefore, dq is zero. For ratcheting, the plastic strain centre shifts due to the ratcheting strain according to:

$$d\beta_{ij} = (1-\eta)\, H(F) \left\langle n_{ij}\, n_{ij}^{*} \right\rangle n_{ij}^{*}\, d\varepsilon_{eq}^{p} \tag{3.10}$$

Where, η is a tuning parameter and controls the shift. $H(F)$ stands for a Heaviside function, and defined as: $H(F) = 1, for\ F \geq 0$ and $H(F) = 0\ for\ F < 0$. n_{ij} is the flow vector, and n_{ij}^{*} is the normal to the plastic strain memory surface, and is given as:

$$n_{ij}^{*} = \frac{2}{3}\frac{\varepsilon_{ij}^{p} - \beta_{ij}}{q} \tag{3.11}$$

Chaboche et al. introduced an expression to account for the increase in the size of the plastic strain memory surface, and later McDowell (1985) modified the expression adding a threshold term, defined as:

$$dq = \left[\eta H(F) - \xi q\left(1 - H(F)\right)\right] \left\langle n_{ij}\, n_{ij}^{*} \right\rangle d\varepsilon_{eq}^{p} \tag{3.12}$$

Where, ξ is another tuning parameter, describes the expansion of the memory surface.

The mean free path (L) in Eq. 3.8, for mobile dislocation, is a function of current dislocation density. Mean free path is also dependent on geometric features like grain (or sub-grain) size, distance between large particles etc. The evolution equation for the mean free path is proposed by Estrin and Mecking (1984). If ρ_j is the dislocation density of slip system j, then:

$$\frac{1}{L} = \frac{1}{L_0} + \frac{\sqrt{\sum_j a_{ij}\rho_j}}{K} \tag{3.13}$$

Where, L_0 is the initial value of mean free path, it can be taken same as the sub-grain size ($1.2\ \mu m$) as it is assumed, the dislocation sub-structures are already formed. The interaction constant K is defined by Rauch et al. (2007) as 'the number of forest dislocations, a moving dislocation is able to cross before being trapped by obstacles'. Considering the average dislocation density (ρ) and average weighted interaction coefficient (α), the evolution equation for the mean free path is:

$$\frac{1}{L} = \frac{1}{L_0} + \frac{\alpha\sqrt{\rho}}{K} \tag{3.14}$$

A reasonable refinement of Eq. 3.8 would consist in splitting the second (recovery) term into two separate contributions in order to isolate self-annihilation (collinear) from indirect annihilation. Indeed, dislocations are expected to interact strongly with dislocations moving on the same slip plane but in the reverse direction, while the rearrangement promoted by

the motion of other dislocations in different planes is probably less effective. This will add considerable complexity in the model, making it physically justified. For non-proportional loading condition, strain path changes after considerable monotonic prestraining (plastic). A model containing a single parameter (e.g. the dislocation density) is unable to provide a good description of the transient hardening observed after an abrupt change in strain path. In addition, a full tensorial treatment with six independent interaction coefficients, considering a minimum of twelve slip systems in each grain for a cubic structure and as many dislocation densities, would rapidly become too complex for a systematic identification of all the relevant parameters with dedicated mechanical tests.

For simplicity, Rauch and his co-workers (2011) considered the idea that different loading conditions including forward loading, reverse loading and loading in any arbitrary direction, may result in three distinct 'families' of dislocations. These families are sufficient to produce the essential mechanical features observed for prestrained samples. Therefore, the average dislocation density can be additively decomposed into three families, $\rho = \rho_f + \rho_r + \rho_l$ respectively associated with the forward, reverse and latent interactions.

For monotonic loading, the net dislocation density available at any instance can be regarded as the forward dislocation density (ρ_f). This mainly contributes to the hardening by forest pile-up according to the Taylor model. The standard kinematic hardening rules of Armstrong-Frederick (1966) format include the changes of forward dislocation densities through its hardening (first) term. The dislocation density evolves through Eq. 3.8.

In-process Change in strain-path, may activate new slip systems in the crystals lattice and the total or a part of the available dislocations (density ρ_f) stored in the primarily activated slip systems before the strain-path change occurs, are transferred into the newly activated slip systems. This transfer causes a sudden dislocation crowd most likely to entangle in the newly active slip systems. The resistance because of the pile-up thus produces a hardening effect in those slip systems.

Any dislocations with opposite Berger's vector originate the reverse dislocation family even during the monotonic forward loading. In addition, when the strain-path is reversed (180°), a part of the available (previously stored) dislocation density, sensitive to the polarity of the stress, fortifies the reverse family and disappears gradually (Rauch et al., 2007) due to strong collinear interactions. The disappearance of the polarized fraction of the dislocation density (ρ_r) is manifested as the Bauschinger effect. The dynamic recovery terms of any standard kinematic hardening rules in Armstrong-Frederick format, is designed to reproduce the reverse dislocations interactions in mathematical material models.

For typical dislocation based modelling, without using kinematic hardening, the disappearance of the reverse dislocation density can be captured by an evolutionary law (Rauch et al., 2007):

$$d\rho_r = -\frac{1}{bL}\frac{\rho_r}{\rho_f}\frac{M\,dq}{S_n} \qquad (3.15)$$

The changes in direction of strain-path between 0° to 180° is classified as non-proportional loading. The part of the dislocation density to be transferred is related on the degree of non-proportionality and causes the latent hardening effect. The latent dislocation density transferred to the new slip system is:

$$\rho_l = A\,\rho_f \tag{3.16}$$

here, A is the non-proportionality parameter, described by Benallel and Marquis (1987) as:

$$A = 1 - \cos^2\theta \tag{3.17}$$

For proportional loading $A = 0$ whereas, for non-proportional loading $0 < A \leq 1$.The phase angle (θ) between deviatoric stress rate vector and the plastic strain rate vector is found as:

$$\cos\theta = \frac{d\varepsilon_{ij}^{p}\, dS_{ij}}{\left(d\varepsilon_{ij}^{p}\, d\varepsilon_{ij}^{p}\right)^{1/2}\left(dS_{ij}\, dS_{ij}\right)^{1/2}} \tag{3.18}$$

The remaining fraction of the forward population remains in the previous slip system and evolve according to Eq. 3.8 simultaneously. The population, after delivering to the reverse and latent families, is incorporated in the KH rule for hardening contribution.

The kinematic hardening rules do not incorporate the latent hardening due to non-proportional strain-path change. Just after the first strain-path change occurs, the sudden increase in the flow stress is observed due to the entanglement of suddenly transferred dislocations into the latent slip system, which globally affect and manifested as the cross hardening effect. Not only that, a decreased softening rate is also observed in the material response, which is caused by the non-proportional hardening developed from the evolution of the remaining dislocations after the evolution of latent dislocation family. From the Taylor equation applied on the latent dislocation family (Rauch, 2011), the extra hardening due to non-proportionality (σ_2) is:

$$\sigma_2 = \alpha MGb\sqrt{\rho_{\cdot} \cdot K \rho_l} \tag{3.19}$$

Where, K_l is the latent hardening coefficient, comes from the ratio of the coefficients of interaction matrix as, α_{ij}/α_{ii}. The initial dislocation density in that latent slip plane just after its activation was ρ_l. This initial dislocation density in the latent system evolves in two possible ways. It is considered that, the latent entanglement is gradually reduced when the dislocations are allowed to reorganise over time because of strong collinear interactions and aided by plastic deformation. If no further non-parallel strain-path change occurs, the latent dislocation density will decrease as (Rauch et al., 2011):

$$d\rho_l = -2y\rho_l \frac{M\, dq}{S_n} \tag{3.20}$$

Simultaneously, excited by the plastic deformation, the remaining dislocations in the latent system generally evolves following Eq. 3.8 and represented by $\rho_{\tilde{f}}$. The calculation of non-proportional hardening considers both of them. In the present model, the plastic modulus is formulated as follows:

$$h=\sum_{k=1}^{m} C^k r^k \left[\frac{3}{2}-\left(\frac{\left|\alpha_{ij}^k\right|}{r^k}\right)^{\chi^k+1} l_{ij}^k n_{ij}\right]-\frac{\alpha M^2 Gbp}{S_n}\frac{\Lambda}{D}\frac{\lambda}{2n}\frac{\lambda}{b}+\frac{\alpha M^2 Gb}{S_n} 2y\sqrt{\rho_{\tilde{f}}^{K}\rho_l} \tag{3.21}$$

The additional (third) term in the expression (Eq. 3.21) incorporates the latent hardening.

3.7 Determination of Material Parameters

The material SA333 was studied in the chapter-2 for uniaxial cyclic plastic loading. The elastic properties, cyclic yield stress and KH parameters are available from there.

Till the steady state condition of strain-path change events to occur, the sub-structure formation is hindered. After the quarter cycle when non-proportionality is triggered, any previously build dislocation based formations become unstable (Barlat et al., 2003; 2011). And thereafter it takes considerable plastic deformation (may be 3-5 initial cycles, where no cyclic softening is observed), to reconstruct the stable dislocation structures. The amount of plastic deformation is quantified and corresponding misorientation angels at low angle sub-grain boundaries and initial boundary dislocation densities (Λ_0) are calculated. The correlation can be obtained from the uniaxial cases.

Table 3.1: *Initial dislocation densities at low angle sub-grain boundary.*

Equivalent strain amplitude	**Effective plastic deformation (q) till stable sub-structures form, after quarter cycle**	**Initial boundary dislocation density (Λ_0) in m^{-1}**
0.35%	0.10%	3.8×10^8
0.53%	0.15%	3.6×10^8
0.70%	0.18%	3.5×10^8

Other required parameters for the softening mechanism, remain unaltered as in the uniaxial case. The model do not consider the initial 3-5 cycles, where hardening predominates and implement active softening from the beginning.

The present model requires some additional parameters like the value of the initial dislocation density which is taken as $10^8\ m^{-2}$ as per conventional theory. The value of initial mean free path (L_0) is taken as the average sub-grain size of $1.2\ \mu m$. For FCC crystals, parameter K is calculated to be 180 by Kubin et al. (2008) for 1 MPa stress and large mean free path of $1.8\ mm$. In the present study, for BCC material, for 1.2 μm mean free path $K = 100$ is taken by trial and error. The average value of latent hardening coefficient $K_l = 1.6$ gives good results in the FE simulations (Rauch et al., 2011).

3.8 Simulation of non-proportional loading

Similar FE model is used for non-proportional loading as it was in case of proportional biaxial loading simulation. Only the material model is modified to account for the non-proportional hardening and the sinusoidal loading amplitude is used in spite of triangular.

The stress-strain hysteresis loops for strain controlled non-proportional cyclic plastic (tension-torsion) experiments are simulated and compared with experimental results separately for both axial and shear components in figure 3.10a-d, 3.11a-d and 3.12a-d. Both axial and shear hysteresis loops are simulated well in engineering sense. From the comparison of peak stress vs. cycle, shown above for both axial and shear case, it is clearly seen that, the softening rate is in tolerable agreement for both axial and shear components.

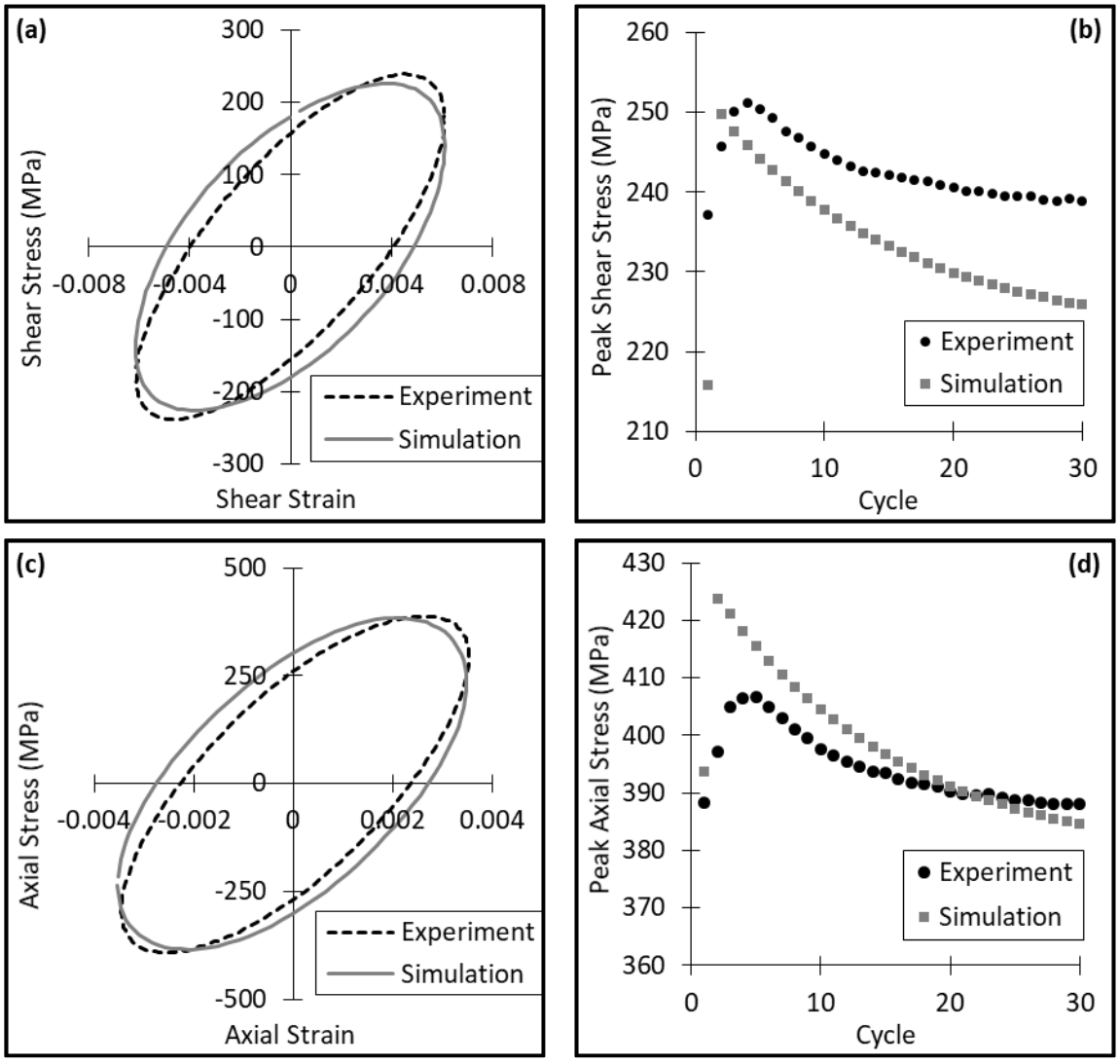

Fig. 3.10: *Comparison of 90° out-of-phase biaxial tension-torsion experimental and simulated results for 0.35% equivalent strain amplitude,* ***(a)*** *shear stress-strain hysteresis loops at 30th cycle,* ***(b)*** *Peak shear stress vs. cycles,* ***(c)*** *axial stress-strain hysteresis loops at 30th cycle,* ***(d)*** *peak axial stress vs. cycles.*

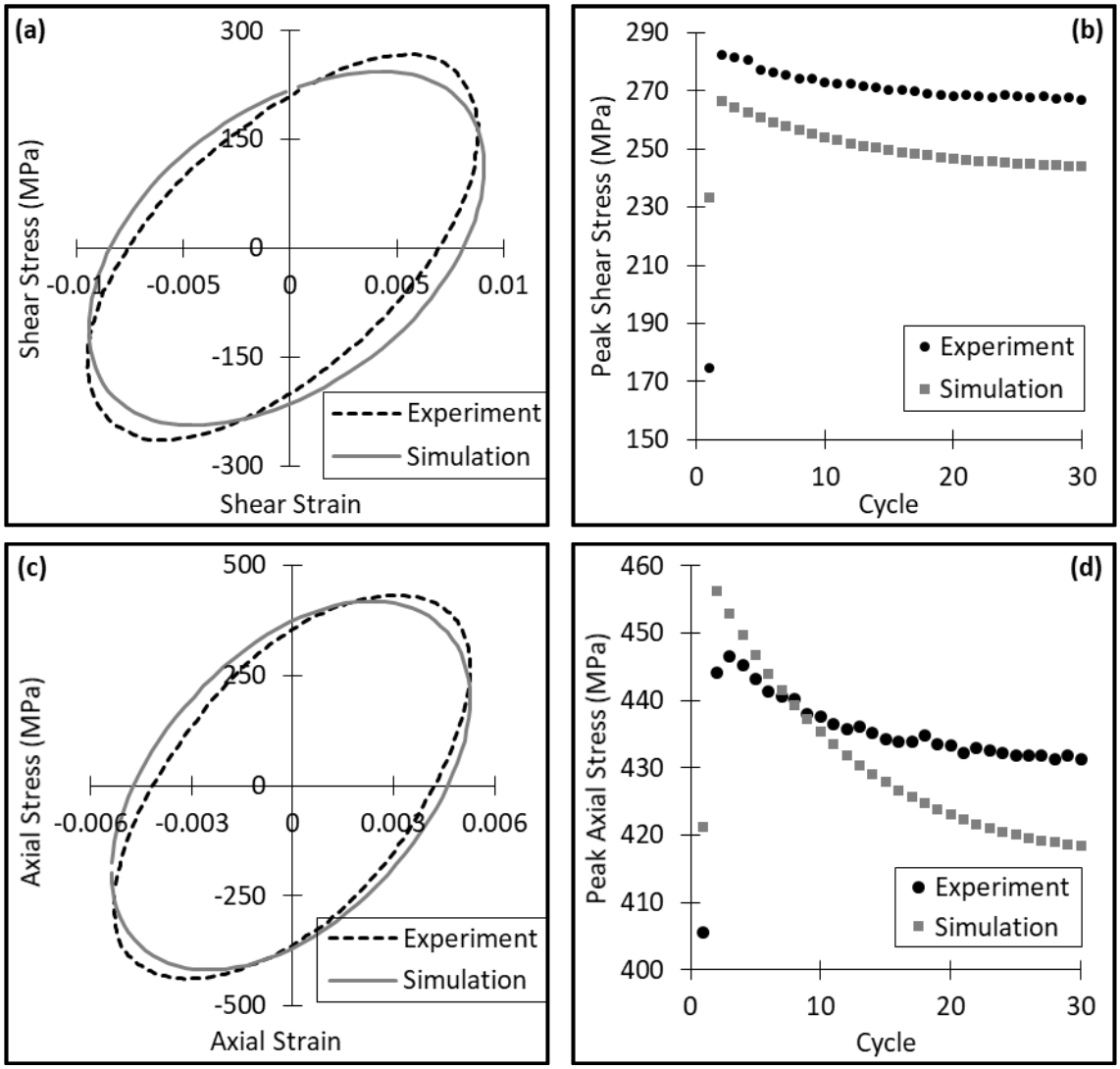

Fig. 3.11: *Comparison of 90° out-of-phase biaxial tension-torsion experimental and simulated results for 0.53% equivalent strain amplitude,* ***(a)*** *shear stress-strain hysteresis loops at 30th cycle,* ***(b)*** *peak shear stress vs. cycles,* ***(c)*** *axial stress-strain hysteresis loops at 30th cycle,* ***(d)*** *peak axial stress vs. cycles.*

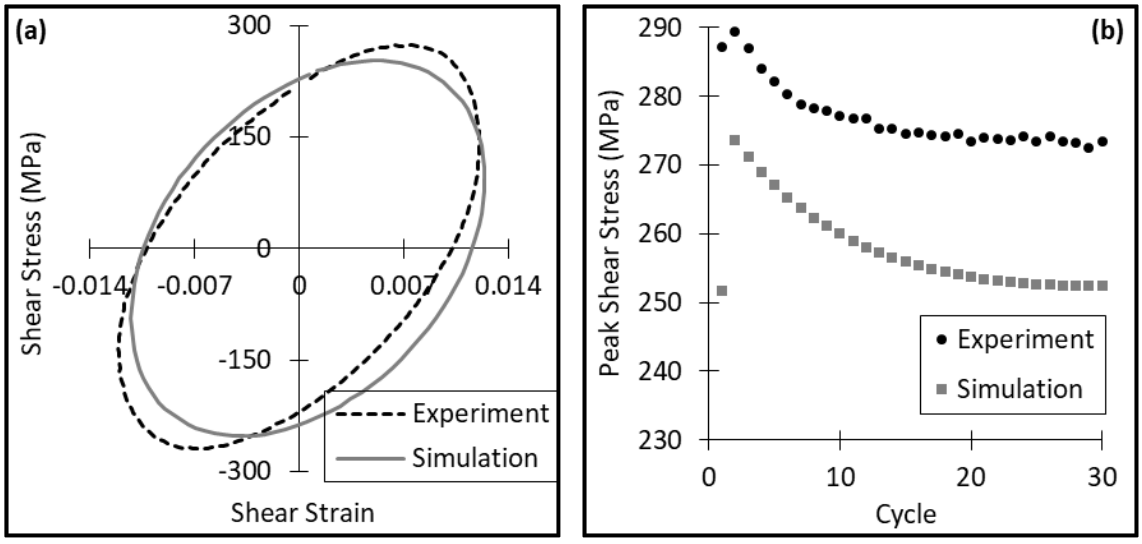

Fig. 3.12: *Comparison of 90° out-of-phase biaxial tension-torsion experimental and simulated results for 0.70% equivalent strain amplitude,* ***(a)*** *shear stress-strain hysteresis loops at 30th cycle,* ***(b)*** *peak shear stress vs. cycles.*

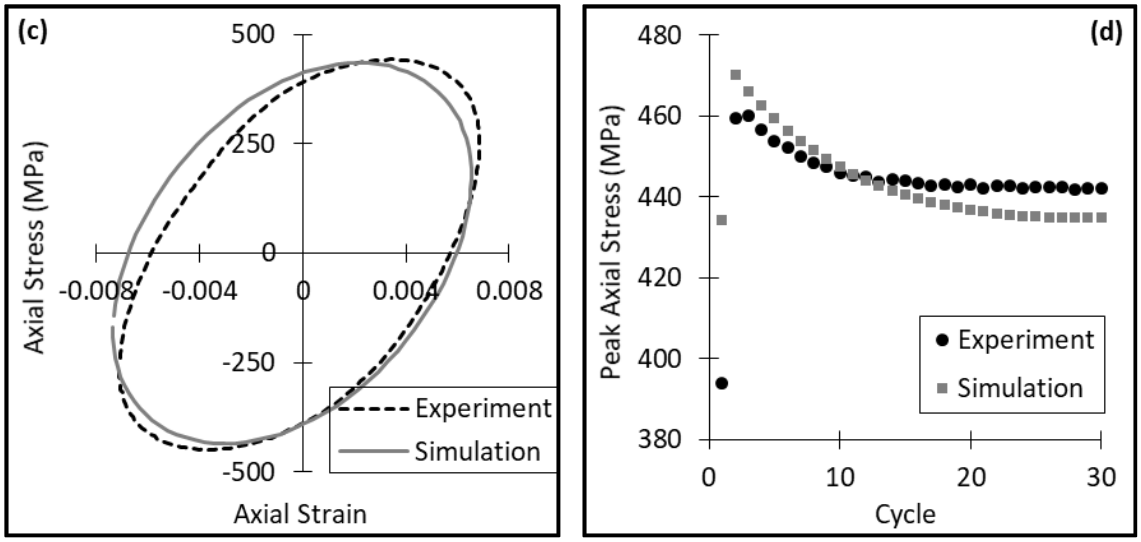

Fig. 3.12: *Comparison of 90° out-of-phase biaxial tension-torsion experimental and simulated results for 0.70% equivalent strain amplitude,* ***(c)*** *axial stress-strain hysteresis loops at 30th cycle,* ***(d)*** *peak axial stress vs. cycles.*

The experimental stress-path clearly shows the mismatch in figure 3.13d. The stress-path also shows that, with the loading cycles, the circular stress-path could not be achieved in the experiments (figure 3.13b and 3.13d). Though, the strain-path has retained its shape (figure 3.13a and 3.13c). May be deformation induced anisotropy is supposed to be affecting the shear stress.

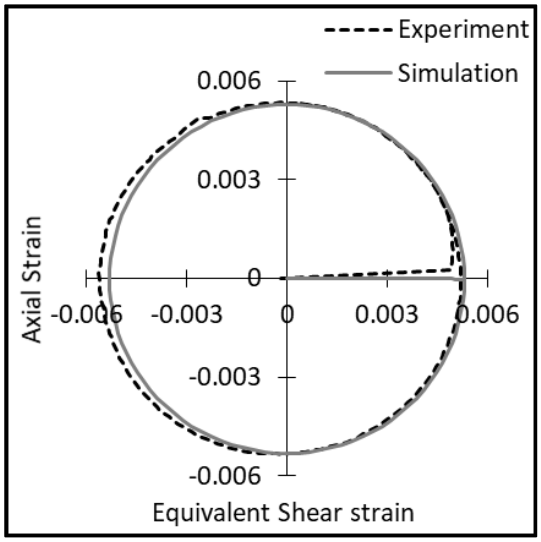

Fig. 3.13a: *Strain (controlled) path for 90° out-of-phase loading at 1st cycle (equivalent strain amplitude 0.50%).*

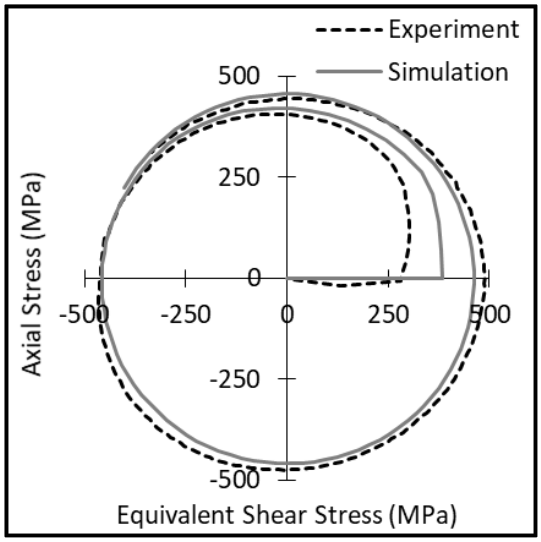

Fig. 3.13b: *Stress (response) path for 90° out-of-phase loading at 1st cycle (equivalent strain amplitude 0.50%).*

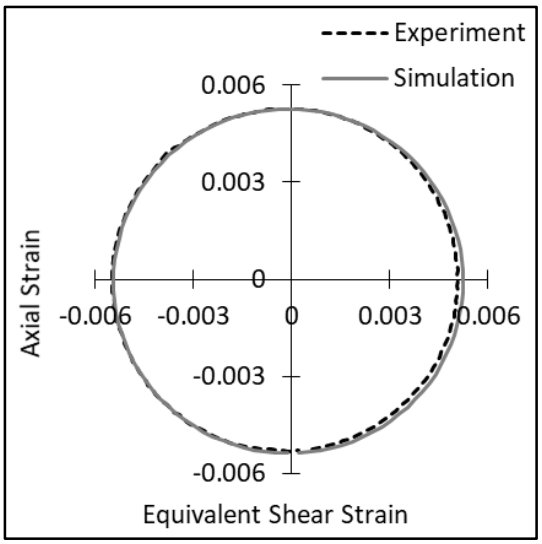

Fig. 3.13c: *Strain (controlled) path for 90° out-of-phase loading at 30th cycle (equivalent strain amplitude 0.50%).*

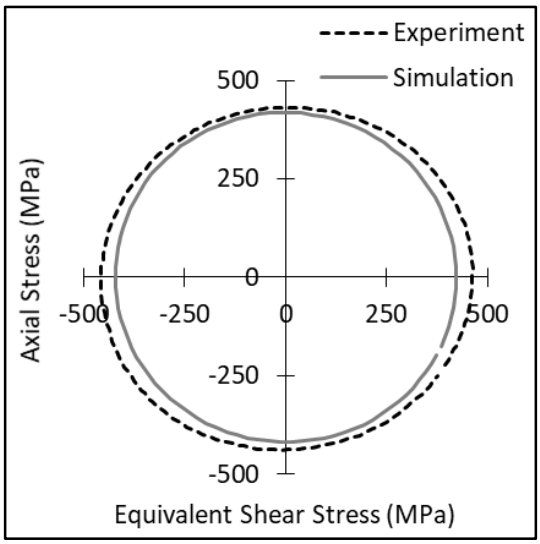

Fig. 3.13d: *Stress (response) path for 90° out-of-phase loading 30th cycle (equivalent strain amplitude 0.50%).*

3.9 Conclusion

In the present work, the elastic-plastic shear stresses are computed in the finite element analyses whereas the experimental shear stresses are elastically predicted. Their comparisons show the obvious differences. The hardening/softening rates are affected too by the shear stress intensity. The calculations of the axial stress, on the other hand, is pretty straight forward and do not get influenced by the elastic assumptions.

The softening model discussed in the previous chapter is supposed to simulate in-phase biaxial loading because ideally no non-parallel strain-path changes occur. But the experimental results show that the ratio of axial to equivalent shear stress response (proportionality ratio) is not maintained. There is a change in biaxial response in loading and unloading path and formation of hysteresis is observed. There are small (within 10%) deviations of the simulated peak stresses (axial or shear) from the experimental results are observed.

The latent hardening model captured the cross hardening and non-proportional hardening effect qualitatively and the deviation is 5% - 10%. The non-proportional hardenings may be better characterised considering more exhaustive estimation of dislocation densities and the interaction coefficients in different slip systems. In addition, anisotropic material response may be incorporated to obtain better compliance.

Finally, it can be concluded that modified Ohno-Wang Kinematic hardening rule and KH parameters calibrated from the uniaxial LCF tests are suitable to simulate hysteresis loops in multiaxial loading conditions. The cyclic softening model by dislocation annihilation in low angle sub-grain boundary is effective and in agreement with the latent hardening model which is considered as a suitable micro-mechanism to explain the non-proportional hardening behaviour of the material.

3.10 Acknowledgement

The authors acknowledge Bhabha Atomic Research Centre, Mumbai for financial assistance through collaborative project and National Metallurgical Laboratory, Jamshedpur for experimental support.

3.11 References

ASTM E2207

3DS SIMULIA ABAQUS CAE(v6.8), User's Manual.

1934, Taylor, G. I., The mechanism of plastic deformation of crystals, part 1 – theoretical, Proceeding of the Royal Society of London, Series A, Volume 145, Issue 855,pp 362-387.

1966, Armstrong, P. J., Frederick, C. O., A Mathematical Representation of the Multiaxial Bauschinger Effect. CEGB Report No. RD/B/N 731.

1966, Kocks, U. F., A statistical theory of flow stress and work hardening, Philosophical Magazine, Volume 13, Issue 123, pp 541-566.

1977, Lamba, H. S., Non-proportional cyclic plasticity, Ph.D. Thesis, Department of Theoretical and Applied Mechanics, University of Illinois, Report No. 413.

1979, Chaboche, J. L., Dang Van, K., Cordier, G., Modelization of the strain memory effect on the cyclic hardening of 316 stainless steel, SMiRT-5, Berlin

1979, Kocks, U. F., Mecking, H., in Strength of Metals and Alloys, (Edited by: P. Haasen, V. Gerald and G. Kostorz), Pergamon Press, Volume 1, pp 345.

1979, Kanazawa, K., Miller, K. J., Brown, M. W., Cyclic Deformation of 1% Cr-Mo-V Steel under Out-of-Phase Loads, Fatigue of Engineering Materials and Structures, Volume 2, pp. 217-228.

1981, Meckings, H., Kocks, U. F., kinetics of flow and strain-hardening, Acta Metallurgica, Volume 29, pp 1865-1875.

1983, Nouailhas, D., Policella, H., Kaczmarek, H., On the Description of Cyclic Hardening Under Complex Loading Histories, Constitutive Laws for Engineering Materials - Theory and Application, Proceedings of the International Conference (ed. by Desai, C. S., and Gallagher, R. H.), pp. 45-49.

1984, Estrin, Y., Mecking, H., A unified phenomenological description of work hardening and creep based on one-parameter models, Acta Metallurgica, Volume 32, Issue 1, pp 57-70.

1985, Franciosi, P., The concepts of latent hardening and strain hardening in metallic single crystals, Acta Metallurgica, Volume 33, Issue 9, pp 1601-1612.

1985, McDowell, D.L., A two surface model for transient nonproportional cyclic plasticity, Journal of Applied Mechanics, volume 52, p298

1985, Schmitt, J. H., Aernould, E., Baudelet, B., Yield loci for polycrystalline metals without texture, Material Science and Engineering, Volume 75, pp 13-20.

1985a, Tanaka, E., Murakami, S., Ooka, M., Effects of strain path shapes on non-proportional cyclic plasticity, Journal of Mechanics and Physics of Solids, Volume 33, Issue 6, pp 559-575.

1985b, Tanaka, E., Murakami, S., Ooka, M., Effects of plastic strain amplitude on non-proportional cyclic plasticity, Acta Mechanica, Volume 57, pp 167-182.

1987, Benallal, A., Marquis, D., Constitutive equation for nonproportional cyclic elasto-viscoplasticity, Journal of Engineering Materials and Technology, Volume 109, pp 326-336.

1989, Lipinski, P., Berveiller, M., Elastoplasticity of micro-inhomogeneous metals at large strains, International Journal of Plasticity, Volume 5, Issue 2, pp 149-172.

1994, Tanaka, E., A nonproportionality parameter and a cyclic viscoplastic constitutive model taking into account amplitude dependence and memory effects of isotropic hardening, European Journal of Mechanics - A/Solids, Volume 13, Issue 2, pp 155-173.

1997, Jiang, Y., Kurath, P., Nonproportional cyclic deformation: critical experiments and analytical modeling, International Journal of Plasticity, Volume 13, Issue 8-9, pp 743-763.

1997, Tabourot, L., Fivel, M., Rauch, E., Generalised constitutive laws for f.c.c. single crystals, Materials Science and Engineering: A, Volume 234 and 236, pp 639-642.

1998, Estrin, Y., Dislocation theory based constitutive modelling: foundations and applications, Journal of Materials Processing Technology, Volume 80-81, pp 33-39.

2003, Barlat, F., Ferreira Duarte, J. M., Gracio, J. J., Lopes, A. B., Rauch, E. F., Plastic flow for non-monotonic loading conditions of an aluminum alloy sheet sample, International Journal of Plasticity, Volume 19, pp 1215-1244.

2003, Kassner, M. E., Kyle, K., Taylor hardening in five power law creep of metals and class M alloys, Nano and Microstructural Design of Advanced Materials, pp 255-271.

2005, Sauzay, M., brillet, H., Monnet, I., Mottot, M., Barcelo, F., Fournier, B., Pineau, A., Cyclically induced softening due to low-angle boundary annihilation in a martensitic steel, materials Science and Engineering: A, volumes 400-401, pp 241-244.

2006, Sinclair, C.W., Poole, W.J., Bréchet, Y., A model for the grain size dependent work hardening of copper, Scripta Materialia, Volume 55, Issue 8, pp 739-742.

2007, Rauch, E.F., Gracio, J.J., Barlat. F., Work-hardening model for polycrystalline metals under strain reversal at large strains, Acta Materialia, volume 55, pp 2939-2948.

2008, Kubin, L., Devincre, B., Hoc, T., Modeling dislocation storage rates and mean free paths in face-centered cubic crystals, Acta Materialia, Volume 56, Issue 20, pp 6040-6049.

2011, Barlat, Frederic, Gracio, Jose J., Lee, Myoung-Gyu, Rauch, Edgar F., Vincze, Gabriela, An alternative to kinematic hardening in classical plasticity, International Journal of Plasticity, 27, pp 1309-1327.

2011, Rauch, E. F., Gracio, J. J., Barlat, F., Vincze, G., Modelling the plastic behavior of metals under complex loading conditions, Modelling and Simulation in Materials Science and Engineering, Volume 19, 035009.

2014, Davoudi, K. M., Vlassak, J. J., Dislocation Evolution During Plastic Deformation: Equations vs. Discrete Dislocation Simulations, arXiv preprint arXiv:1408.6609.

2014, Dong, Yawei, Kang, Guozheng, Yu, Chao, A dislocation-based cyclic polycrystalline visco-plastic constitutive model for ratcheting of metals with face-centered cubic crystal structure, Computational Material Science, Volume 91, pp 75-82.

2018, Bhattacharjee, S., Dhar, S., Acharyya, S. K., Gupta, S. K., Cyclic softening based on dislocation annihilation at sub-cell boundary for SA333 Grade-6 C-Mn steel, Modelling and Simulation in Materials Science and Engineering, Volume 26, 015001.

Chapter 4

ASYMMETRIC LOADING

In this chapter, both uniaxial and biaxial ratcheting behaviour of SA333 steel is studied for asymmetric loading condition. Modelling for the experimentally observed ratcheting behaviour of the material is attempted based on dislocation density. The ratcheting behaviour is simulated in the finite element platform using the modified material model.

Content **Page**

Blank Page

4.1 Introduction

Asymmetric cyclic loading results in either ratcheting or mean stress relaxation (Arcari et al., 2009) depending on the stress or strain control respectively. Both the asymmetric cyclic plastic phenomena leads to accelerated fatigue damage. The fatigue life evolution in low cycle fatigue (involving cyclic plasticity) considers plastic strain and therefore, the following discussion considers ratcheting, since it is the phenomena of progressive and directional accumulation of plastic strain during asymmetric stress cycling (Hassan and Kyriakides, 1992; Jiang and Sehitoglu, 1994). Another reason for focusing on the ratcheting is that, accurately defined material model can capture both the phenomena in FE simulation with respective control mode of loading.

In piping materials, such as SA333 Grade-6 C-Mn steel, used for pressurized heavy water reactors (PHWR) of nuclear power plants, ratcheting may be manifested due to cyclic loading arising for different reasons. Sometime ratcheting contributes unacceptable amount of permanent deformation in the piping component like, ovalization of T-joints and elbows under cyclic bending, thinning out the cross-sectional area and local bulging of pressurized pipes under cyclic loading etc. (Thomas, 1989; Li and Berton, 1993). Therefore, it is important to study the asymmetric cyclic plastic behaviour of the material under uniaxial and multiaxial loading conditions for safety consideration and efficient design of the piping systems.

4.2 Experimental observations

Both uniaxial and multiaxial ratcheting experiments were conducted by Bhabha Atomic Research Centre, Mumbai; on the same specimen geometries used for LCF tests. The evolution of the engineering and true ratcheting strain as a function of number of cycles during engineering and true stress-controlled experiments are shown below. It is observed that significant amounts of ratcheting strain are accumulated before failure with large reduction in the cross-sectional area.

4.2.1 Uniaxial Ratcheting:

The accumulation of ratcheting strain with number of cycles is represented in figure 4.1. This curve resembles a conventional creep curve with three distinct regions designated as primary, secondary and tertiary regions, though the deformation mechanisms are hugely different.

Ratcheting is associated with dislocation movement, their interactions and cell formations (Gaudin and Feaugas, 2004), while creep is related to diffusion controlled glide and climb of dislocations, grain boundary sliding and void formation (Wilshire and Burt, 2008). Cyclic hardening/softening plays a key role in decay of ratcheting rate in the primary region (Jiang and Zhang, 2008). Damage induced softening dominates in the tertiary region and beyond the scope of modelling in this work.

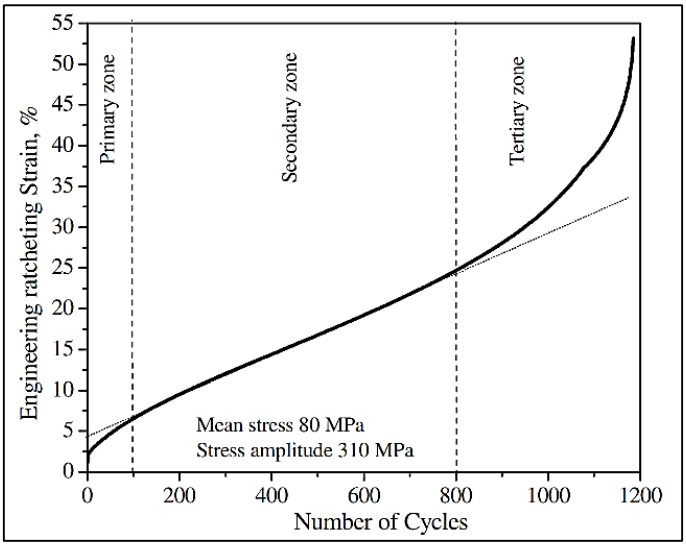

Fig. 4.1: *Ratcheting curve with three distinct zones: at stress amplitude 310 MPa and mean stress 80 MPa.*

From figure 4.2a and figure 4.2b, it is evident that, ratcheting strain increases and hence ratcheting life decreases with increase in mean stress or stress amplitude. During tests, it is also noted that most of the specimens failed by necking rather than by fatigue crack propagation, which is not a common observation during LCF testing. This type of failure behaviour is due to uncontained increase in true strain, which leads to localization of deformation and necking.

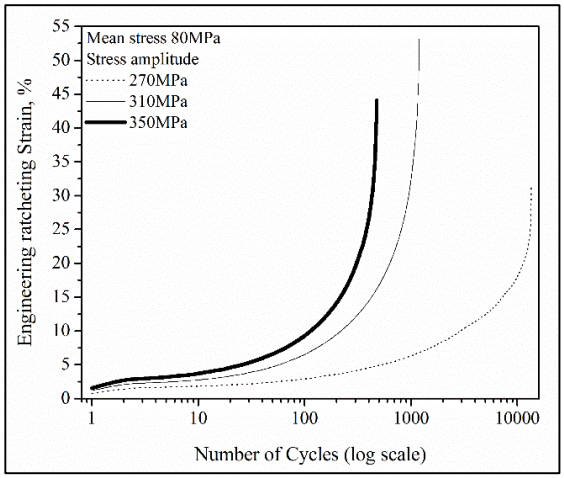

Fig. 4.2a: *Engineering ratcheting strain vs. number of cycles at constant mean stress of 80 MPa and stress amplitude of 270 MPa, 310 MPa and 350MPa.*

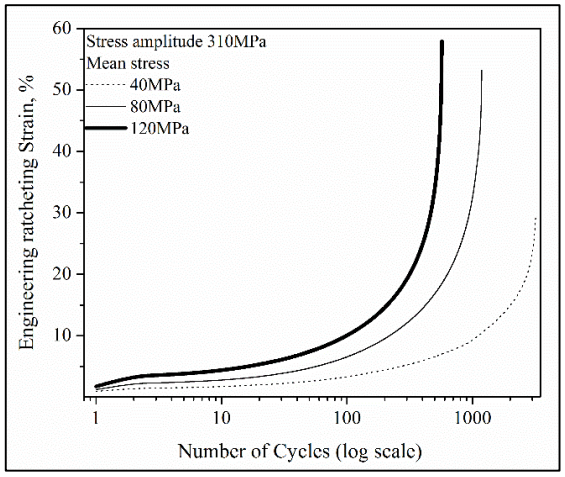

Fig. 4.2b: *Engineering ratcheting strain vs. number of cycles at constant stress amplitude of 310 MPa and mean stresses 40 MPa, 80 MPa and 120 MPa.*

Ratcheting tests carried out in laboratory are generally by controlling engineering stress for the ease to measure. However, due to the associated change in cross-sectional area, the true mean stress and true stress amplitude increases uncontrollably (figure 4.3) with accumulation of ratcheting strain in engineering stress controlled test.

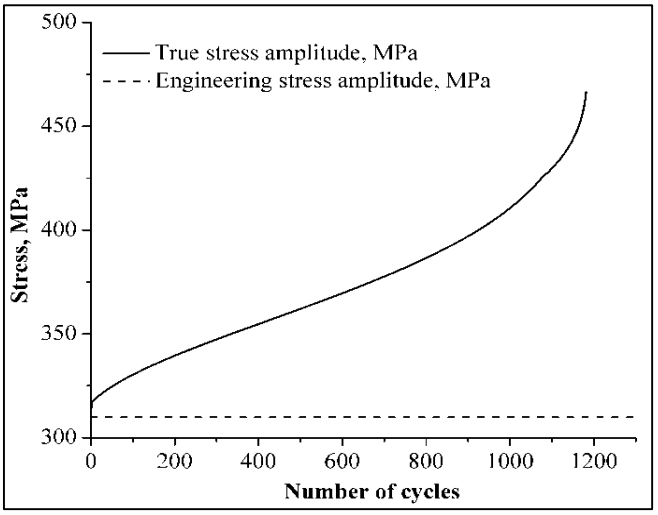

Fig. 4.3: *Alteration of true maximum stress and stress amplitude with number of cycles in engineering stress control test, stress amplitude 310 MPa and mean stress 80 MPa.*

Since true stress and true strain gives the actual deformation response in materials, it is scientifically more appropriate to conduct ratcheting tests under true stress control where substantial cross-sectional area alteration is envisaged (Paul, 2011). A contention may be raised that the true stress control tests become relevant only when significant strain accumulation and consequent change in cross-sectional area are demonstrated. However, it may be argued that conducting ratcheting tests under true stress control may be considered to be a good practice irrespective of ratcheting strain developed so that controversies with regard to the necessity for area correction may be avoided.

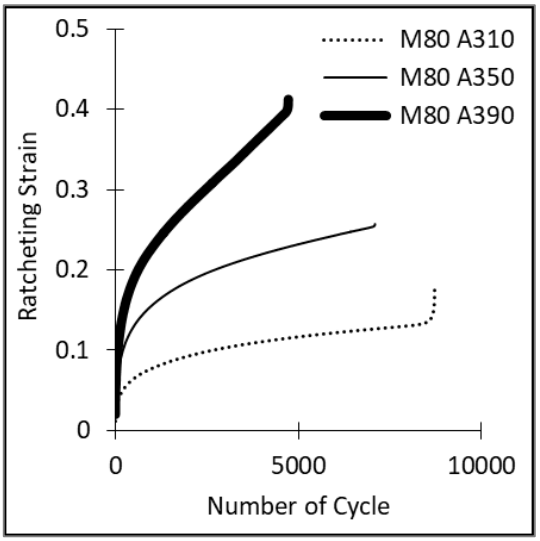

Fig. 4.4a: *True stress controlled ratcheting of SA333, showing a comparison between stress amplitudes of 310 MPa, 350 MPa and 390 MPa, for a constant mean stress of 80 MPa.*

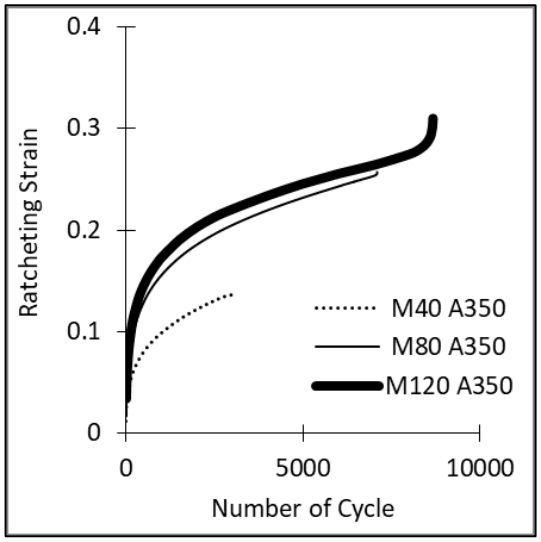

Fig. 4.4b: *Stress controlled ratcheting for SA333, Showing a comparison between mean stresses of 40 MPa, 80 MPa and 120 MPa, for a constant stress amplitude of 350 MPa.*

Ratcheting tests are conducted under engineering/true stress control, specified by the mean stress and the stress amplitude. It is observed for engineering stress control as well as for true stress control that, ratcheting strain increases and life decreases with increase in the

stress amplitude. According to Jiang and Sehitoglu (1994), accumulation of ratcheting strain takes place in the direction of mean stress, similar things are observed during experimentation. It is also observed that both the ratcheting strain and fatigue life increases with increasing mean stress. Increase in ratcheting life with increasing mean stress is thought to be cause by mean stress dependent hardening, which is described as the increment of the size of hysteresis and decrement of the hardening with increasing mean stress for constant stress amplitude.

The improvement in fatigue life due to increasing mean stress can be explained by plastic strain energy during cyclic deformation. The plastic strain energy represented by the area enclosed by stress-strain hysteresis loop signifies the ability of the material to cyclically deform. More the hysteresis loop area, the material is expected to absorb more energy and hence shorter will be the fatigue life (Xia et al., 1996).

The fatigue life of the material was found more for true stress controlled experiments than under the engineering stress control. The reasons are: rapid accumulation of ratcheting strain in case of engineering stress control tests, uncontrollable increase of true stress and eventually followed by instability and neck formation. The true stress controlled failure, on the other hand, occurred by the initiation and growth of fatigue cracks.

It generally observed in the ratcheting tests that, initially, the ratcheting strain accumulation rate is higher (primary stage) followed by a gradual decrease and then stabilizes at a constant rate throughout the major part of the life (secondary stage). The phenomena is termed as 'ratcheting rate decay' and is clearly noted in the above ratcheting tests. The ratcheting rate decay is associated with plastic slip, dislocation movement and cell formations (Gaudin and Feaugas, 2004). A few interesting facts about the ratcheting rate can be found in the literature, such as:

i) Depending on the level of asymmetry in loading, the ratcheting strain and ratcheting rate decay are characterised. Ratcheting is most likely to occur under wavy slip condition.

ii) Initially, due to the asymmetry in the stress controlled loading, plastic strain gets accumulated at higher rate and dislocation gets generated profusely. It is mainly observable in the stage – I of the ratcheting or cyclic creep.

iii) With time, the abundant dislocation entangle and produce hardening. The hardening results in a gradual decay in the ratcheting rate. The decay eventually stabilized when dislocation sub-cell formation starts. This is generally occur in stage – II. In this stage, dipolar dislocation structures are observed to be formed.

iv) The transition from ratcheting rate retardation to acceleration is a critical state in which cross-slips act under cyclic loading and long-range internal stress fluctuation may be observed. In the stage – III, the ratcheting rate rapidly and uncontrollably increases leading to catastrophic failure.

4.2.2 Multiaxial ratcheting

Multiaxial ratcheting tests were conducted on thin tubular specimens subjected to balanced torsion cycles with axially imposed tensile mean stresses. A biaxial extensometer was used to measure the axial and shear strains.

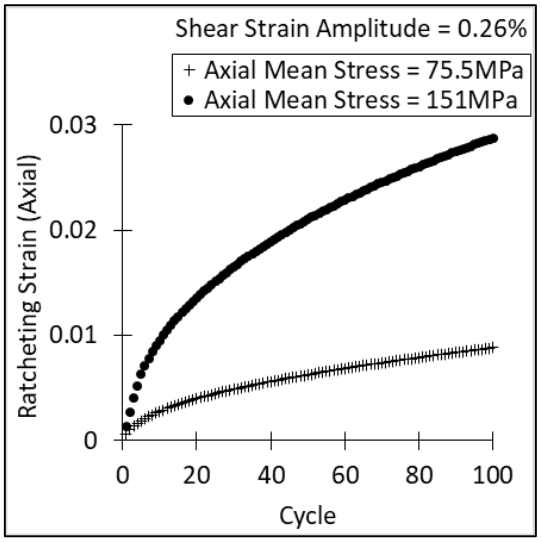

Fig. 4.5a: *Biaxial ratcheting of SA333, comparison shows axial mean stresses 75.5 MPa and 151 MPa, for constant shear strain amplitude 0.26%.*

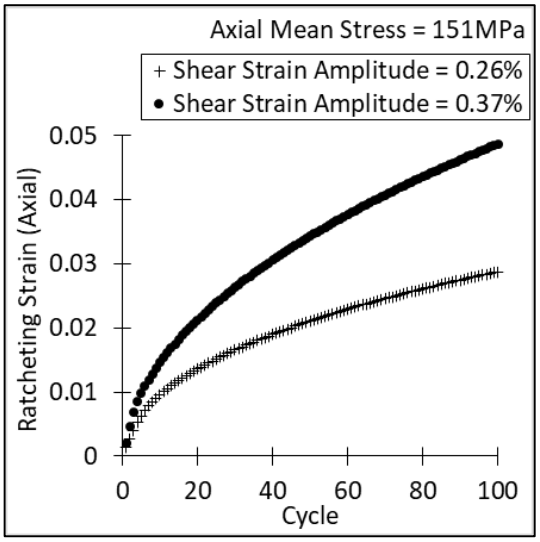

Fig. 4.5b: *Biaxial ratcheting of SA333, comparison shows shear strain amplitudes 0.26% and 0.37%, for constant axial mean stress 151 MPa.*

The axial strains demonstrated ratcheting response as shown below in figure 4.5a-b. Two different mean stresses and two different shear strain amplitudes are shown.

It is observed in the experimental results that the ratcheting strain significantly increases for increasing either mean stress or strain amplitude. The primary and secondary stages of multiaxial (tension-torsion) ratcheting strains are shown in both the figures (4.5a-b), because the damage induced tertiary stage is beyond the scope of the present study.

4.3 Phenomenological modelling

It is observed in the experimental results that, in the primary phase, ratcheting rate is high because the material is softer. Then, gradually it hardens and ratcheting rate decays. Finally, the ratcheting gets saturated in the secondary stage. These phenomena can be apprehended by controlling the dynamic recovery contribution of KH rule. The Ohno-Wang (1993a) KH rule has a provision of pragmatic adjustment of the parameter χ^k (chapter 2, Eq. 2.6) to control the dynamic recovery contribution. FE simulations have been carried out with different values of χ^k by trial and error to comply with uniaxial cases (figure 4.6). The χ^k is kept constant during the simulation.

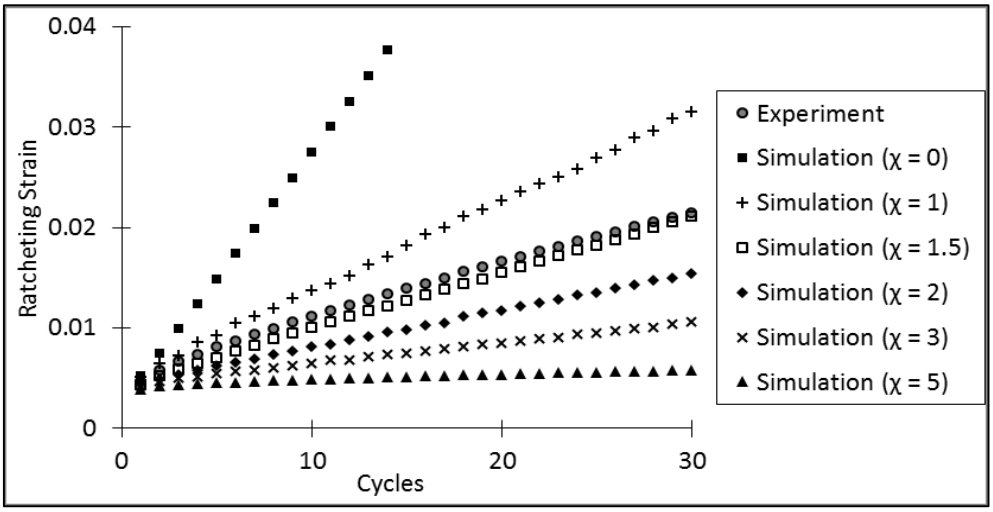

Fig. 4.6: *Comparison of simulations with different χ^k from 0 to 5 and with the experimental result for true stress controlled ratcheting (mean stress 80 MPa amplitude 310 MPa).*

It is reported in the literature (Ohno and Wang, 1993a) that though χ^k can be increased infinitely but beyond the value $\chi^k = 5$, it has least significant effects on the material response. In addition, the adjustments made to the parameter χ^k have influence on the stress response in case of symmetric loading conditions (figure 4.7). There are about 3% (for 0.75% strain amplitude) or less over-prediction is observed.

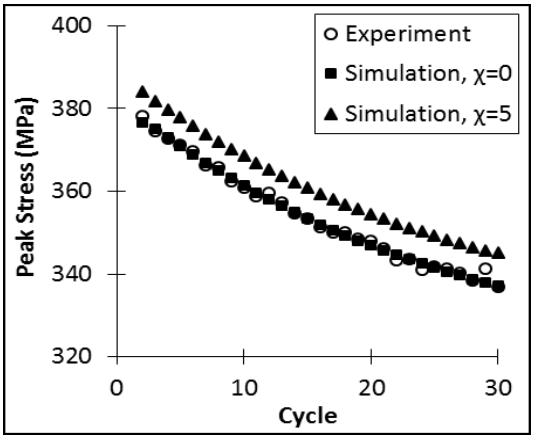

Fig. 4.7a: *Variation of χ^k for uniaxial symmetric loading (strain amplitude 0.35%).*

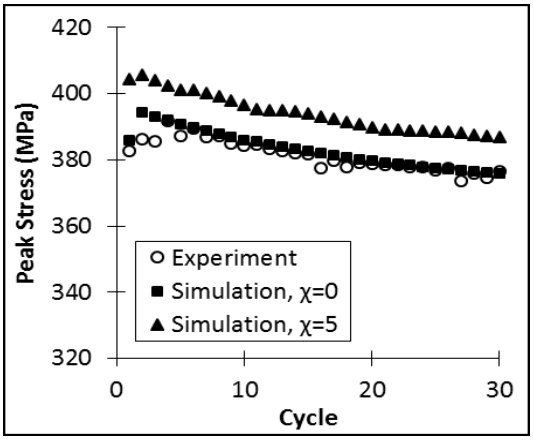

Fig. 4.7b: *Variation of χ^k for uniaxial symmetric loading (strain amplitude 0.75%).*

Furthermore, a significant efforts were devoted for the development of constitutive models to simulate ratcheting along with extensive experimental studies (Chaboche and Nouailhas, 1989, 1991; Hassan and Kyriakides, 1994; Ohno and Wang, 1993b; Delobelle et al., 1995; McDowell, 1995; Bari and Hassan, 2000). Most of the constitutive models were based on the size of the yield surface and translation of this yield surface (Jiang and Zhang, 2008). The multiaxial ratcheting is over-predicted by these models and not so utterly successful even in uniaxial cases. These models are able to predict ratcheting strain if hysteresis loops open up i.e. stress amplitude crosses double of the cyclic yield stress.

From the literature it is hypothesized that, in the initial cycles the softer material allows higher ratcheting strains and but gradually the material need to harden to confer a better

agreement with the transitions to the secondary stage. At the secondary stage, the hardening remains constant with fixed ratcheting rate. The study reported in the literature proves that the phenomenological modelling could not sufficiently describe even the uniaxial ratcheting phenomena and therewithal, lacks the physical explanations. Therefore, an attempt is made in this work to explain the phenomena based on dislocation dynamics and model the material behaviour accordingly.

4.4 Tunnelling Electron Microscopy

To understand the dislocation dynamics, TEM imaging is done in Philips CM200 operated at 200 kV. The TEM micrographs of the material in the as received condition (figure 4.8a) show no definitive dislocation structures. There are, nevertheless, weak traces of dislocation structures formed during previous plastic deformation.

SA333 C-Mn steel subjected to asymmetric loading (mean stress 80 MPa; stress amplitude 310 MPa) shows delayed formation of dislocation substructures as compared to symmetric LCF loading shown in the TEM micrographs (figure 4.8b-d). In this unbalanced loading condition, even at half of the lifetime to failure (5000 cycles) no distinct substructure is formed (figure 4.8b).

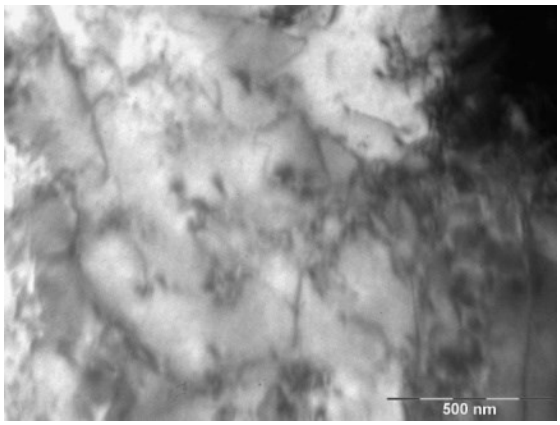

Fig. 4.8a: *TEM micrograph of SA333 'as received'.*

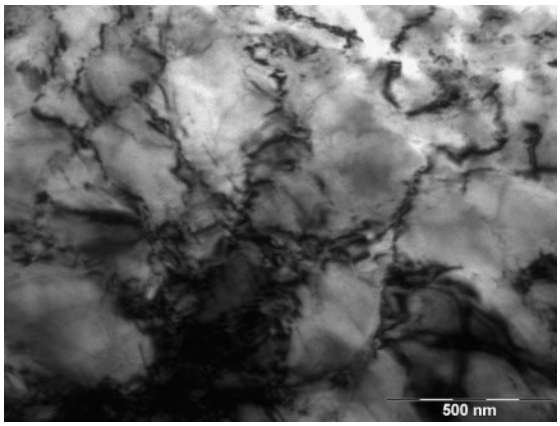

Fig. 4.8b: *TEM micrograph of SA333 after half-life.*

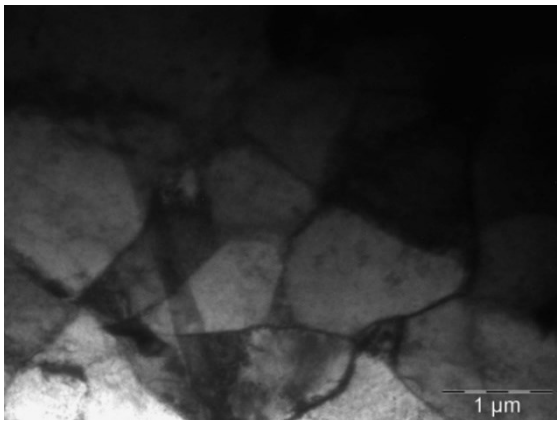

Fig. 4.8c: *TEM micrograph of SA333 after failure (longitudinal section of the specimen).*

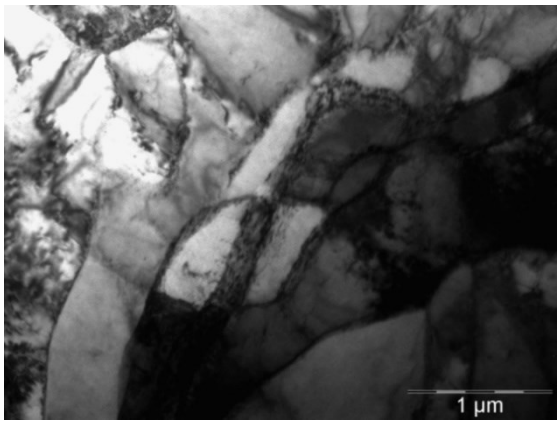

Fig. 4.8d. *TEM micrograph of SA333 after failure (cross section of the specimen).*

Continuous generation of new dislocations, due to the ratcheting strain, adds in the dislocation interactions and entangling behaviour is observed. Eventually, however, the generation rate of new dislocations gradually decreases and a sub-cellular dislocation structure is formed (figure 4.8c,d). There are reasons to believe that, in the latter half of the secondary stage of ratcheting, the dislocation substructures are began to form leading to a stable ratcheting rate.

4.5 Dislocation based modelling

The ratcheting phenomenon is observed as the accumulation of plastic strain when subjected to unbalanced cyclic loading. This work is solely focused on the modelling of the ratcheting behaviour of the material within its primary and secondary stages.

Micro-mechanism based modelling of primary and secondary ratcheting is a meticulous task. The nature of a ratcheting curve in the stages considered above closely resembles with a hardening curve of a stress controlled analysis, likely showing a gradual decrement of ratcheting strain with cycle. The standard practice for simulating this behaviour is to increase the hardening gradually.

Metallurgical evidence can explain the theory of ratcheting as, the increase of accumulated plastic strain in a gradually decreasing rate and thus the increase in strain memory surface is due to generation of new dislocations. They interact with other dislocations in the vicinity ending up with only entanglement initially, and then pilling up as well as annihilation. Therefore, they influence hardening and recovery at the same time but hardening is dominated with a decreasing rate as experimental evidences show for primary and secondary stages.

It is evident from TEM micrographs that, no specific dislocation structures develop during early stages of deformation. Rather, it can be observed after scrutinizing TEM micrographs of ratcheting and LCF samples that, dislocation sub-cell formation usually delayed in case of ratcheting. The delay occurs due to continuously dominated dislocation generation due to ratcheting strain. By the time, randomly distributed dislocations are susceptible to pile-up and also have a considerable probability to get annihilate within a compatible pair.

Mecking and Kocks (1981) shows that the dislocation density has exponential type growth. To quantify the change in dislocation density due to ratcheting only, the same evolution of dislocation density, as described in the previous chapter (chapter-3, Eq.3.8), can be employed as a function of the size of the plastic strain memory surface.

$$d\rho = \frac{1}{bL}\frac{M\,dq}{S_n} - \frac{2y}{b}\rho M\,dq \qquad (4.1)$$

Here, dq is the increase of the size of the strain memory surface. Memory surface, ideally, do not increase or shift for balanced/symmetric loading conditions but withthe ratcheting (asymmetric) strain accumulation, the size of the memory surface increases. Therefore, in this analysis, dq is considered as the measure of the ratcheting strain. Another important

aspect of choosing the memory surface is that, changes made in loading condition i.e. in amplitude or mean of loading spectrum, has direct reflection in the size of the memory surface. Chaboche, Dang Van and Cordier (1979) have introduced the plastic strain memory surface in plastic strain space as described in the previous chapter (chapter 3, in article 3.6.2).

A function, defined by the dislocation density, is employed to control the intensity of hardening by modifying the r^k values of the Ohno-Wang KH law (discussed previously in chapter-1, article 2.4), motivated by the fact that with time, randomly distributed newly generated dislocations are susceptible to pile-up. The function is defined as:

$$f = 1 - \exp\left(-\frac{\rho - \rho_c}{\rho_c}\right) \tag{4.3}$$

There is a critical density of dislocations (ρ_c) corresponding to the first quarter cycle of the loading, beyond which the unbalanced loading effect come into play. The critical dislocation density acts like a threshold for entry into the ratcheting domain. The function f acts like a scaling function, which operates between 0 to 1 denoting initial and saturated values of r^k respectively. Accordingly, the r^k values are modified as:

$$r^k = r^k\left\{1+\left(\bar{\chi}\text{-}1\right)f\right\} \tag{4.4}$$

The evolution of r^k values, shown above, is actually controlled by the function f and the parameter $\bar{\chi}$. The rate of hardening is modulated by the function f and the amount of hardening is governed by the parameter $\bar{\chi}$. For each segment of the KH rule, the function and the parameter are kept unchanged for simplicity. The evolution of $\bar{\chi}$ with ratcheting strain is considered exponential:

$$\bar{\chi} = \chi_0 + \chi_{sat}\left[1 - \exp\left(-B\,q\right)\right] \tag{4.5}$$

From the experiment al observations, χ_0 and χ_{sat} are determined. χ_0 is taken as 1 to ensure the LCF phenomena in balanced loading. For balanced LCF loading ratcheting strain (q) is zero. Hence $\chi = \chi_0 = 1$. Therefore, no change in r^k occurs. Within the critical dislocation density no evolution of r^k is allowed. Beyond that point, r^k evolve up to a saturation value of χ_{sat}. The values of χ_{sat} and the rate parameter B is found from the secondary ratcheting curve and calibrated by trial and error.

4.6 Determination of material parameters

The elasticity and plasticity parameters of the material SA333 Grade-6 C-Mn steel are described previously. The evolution of strain memory size considers two parameters η and ξ. Here, $\eta = 1$ and $\xi = 0$ are taken allowing only the expansion of memory surface, not considering any shift of the centre. Therefore, q remains constant ($dq = 0$) and equals to the plastic strain amplitude in case of symmetric LCF loading and goes on increasing for

asymmetric ratcheting loading, measuring the ratcheting strain. The additionally required material parameters are listed below in table 4.1.

Table 4.1: *Material parameter for ratcheting model.*

S_n	M	b (nm)	α	K	$\rho_0\ (m^{-2})$	χ_0	χ_{sat}	B
5	2.99	0.25	0.3	100	10^8	1	0.7	133

S_n represents the number of active slip systems, M is the average Taylor factor and b is the magnitude to the Burger's vector. The value of the initial dislocation density is conventionally chosen.The interaction constant K is defined by Rauch et al. (2007)and α is the average weighted interaction coefficient. The parameters are described in previous chapters. The χ_0, χ_{sat} and B are fitting parameters, and are chosen by trial and error.

Both screw and edge dislocations exist in the mobile dislocations. Their proportion can be used to calibrate the value of 'critical annihilation distance'. For FCC crystal, the values of the critical annihilation distances are about $1.6\ nm$ for pure edge dislocations and about $50\ nm$ for pure screw dislocations (Sauzay, 2005). For BCC crystal, no such value is reported in the literature, and hence FCC values are adopted. In this present study, considering both edge and screw dislocations, an average critical annihilation distance $14\ nm$ is found to be effective in the simulations.

Mean free path is the function of geometric features like grain size and current dislocation density. Since the material has no dislocation substructure formed, the effective mean free path can be taken same as the ferrite grain size $(22\ \mu m)$ as it is assumed. Being softer, ferrite is accommodating the deformations alone.

The critical dislocation density (ρ_c) is taken as the value of dislocation density generated in first quarter cycle (before first reversal of load) and presented in the figure 4.9 with the corresponding size of plastic strain memory surface in semi-log scale.

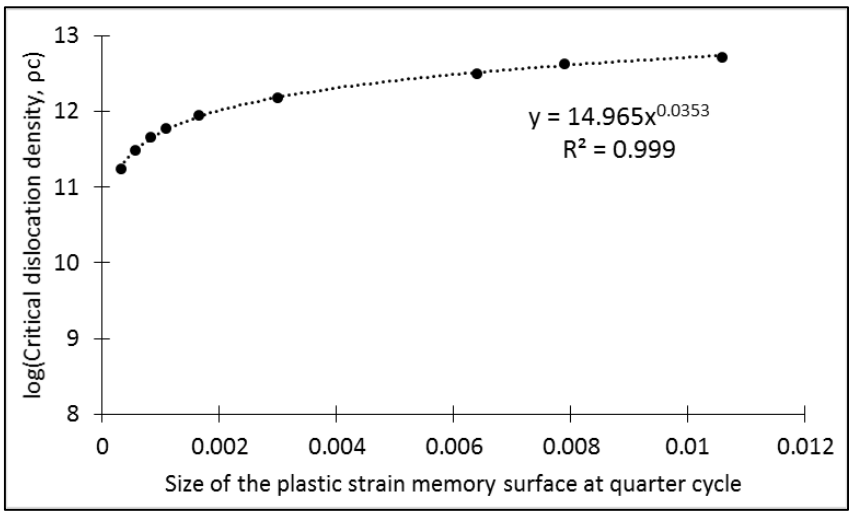

Fig. 4.9: *Critical dislocation density (logarithmic values) vs. size of the plastic strain memory.*

With the required material parameters cited above, the finite element simulation can be launched with the material model described.

4.7 FE Simulations of uniaxial asymmetric loading

The primary microscopic investigations showed that no initial dislocation substructure formed during ratcheting till the latter half of the secondary stage. Therefore no softening model is adopted in the present material model. The material model, in this study, only describes the hardening due to the pile-up of the newly generated dislocations due to ratcheting strain. The ratcheting strain is quantified from the increase in the plastic strain memory surface. The size increment of the memory surface therefore, gives the newly generated dislocation density due to ratcheting strain which are susceptible mainly to pile-up and increase the hardening characteristic of the material. The hardening rate gradually decreases to a saturation and the ratcheting shows a transition from primary to secondary stage.

The hardening characteristic is exhibited through KH parameters of the material. The model considers an exponential function of newly generated dislocation density to map the changes in the hardening characteristic. The material model is plugged into commercial finite element software ABAQUS as user subroutine. The experiments are simulated and one of the simulated stress-strain curve is represented below in figure 4.10 showing uniaxial ratcheting behaviour of SA333 Grade-6 C-Mn steel.

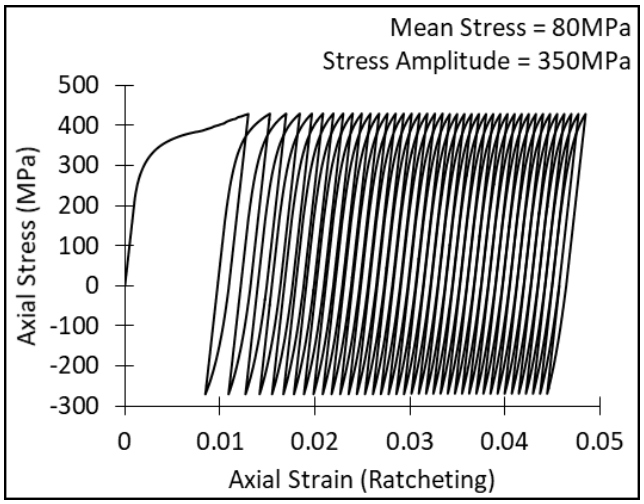

Fig. 4.10: *Uniaxial ratcheting behaviour SA333.*

The ratcheting strains are calculated and are compared with the respective experimental results as shown below in the figure 4.11 and 4.12. Ratcheting rate can be observed in the plots below.

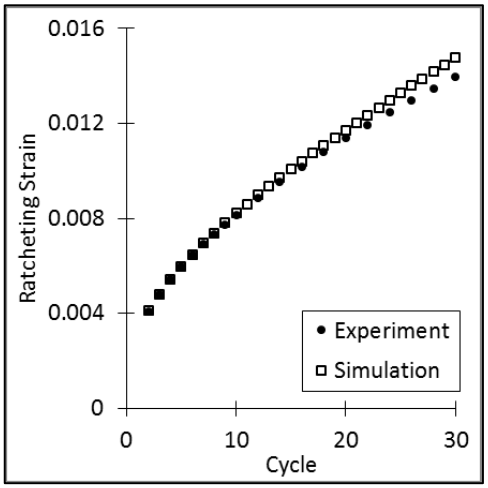

Fig. 4.11a: *Comparison of uniaxial ratcheting experiment with simulation for mean stress 80 MPa and stress amplitude 310 MPa.*

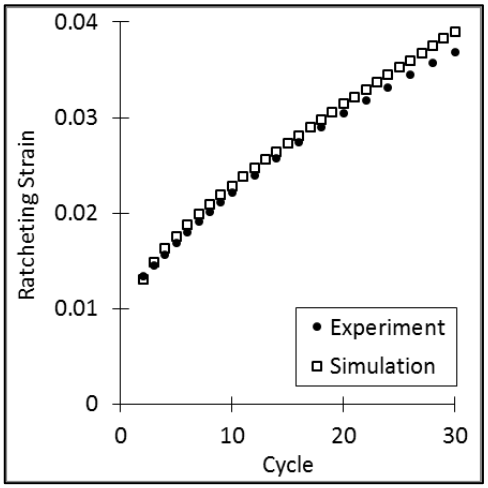

Fig. 4.11b: *Comparison of uniaxial ratcheting experiment with simulation for mean stress 80 MPa and stress amplitude 350 MPa.*

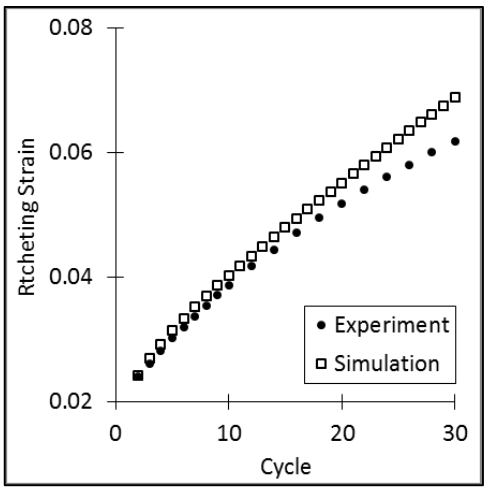

Fig. 4.11c: *Comparison of uniaxial ratcheting experiment with simulation for mean stress 80 MPa and stress amplitude 390 MPa.*

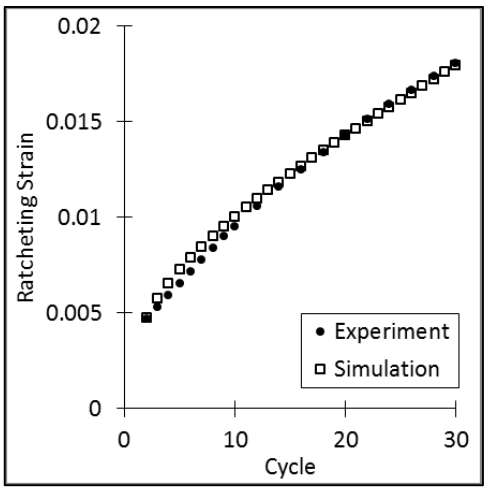

Fig. 4.12a: *Comparison of uniaxial ratcheting experiment with simulation for mean stress 40 MPa and stress amplitude 350 MPa.*

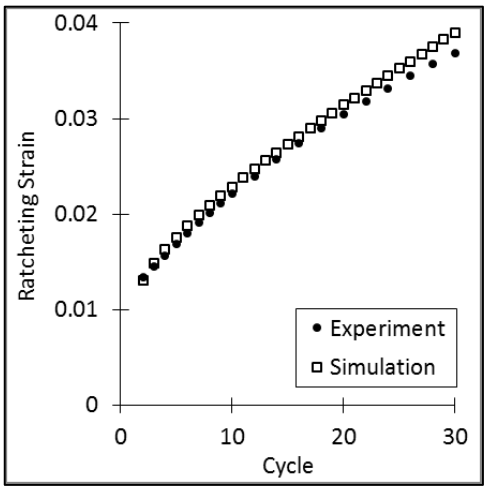

Fig. 4.12b: *Comparison of uniaxial ratcheting experiment with simulation for mean stress 80 MPa and stress amplitude 350 MPa.*

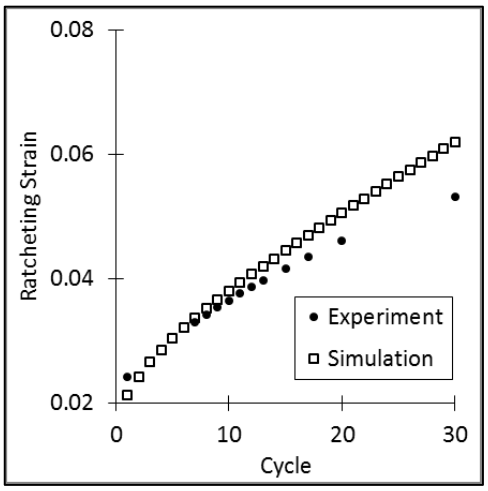

Fig. 4.12c: *Comparison of uniaxial ratcheting experiment with simulation for mean stress 120 MPa and stress amplitude 350 MPa.*

4.8 FE Simulations of multiaxial asymmetric loading

The multiaxial loading arrangements do not trigger any sudden strain path change and therefore no latent hardening effects are influencing the material behaviour. Therefore, the transferability of the material model, developed for the uniaxial behaviour of the material, can be checked in case of multiaxial (tension-torsion) ratcheting.

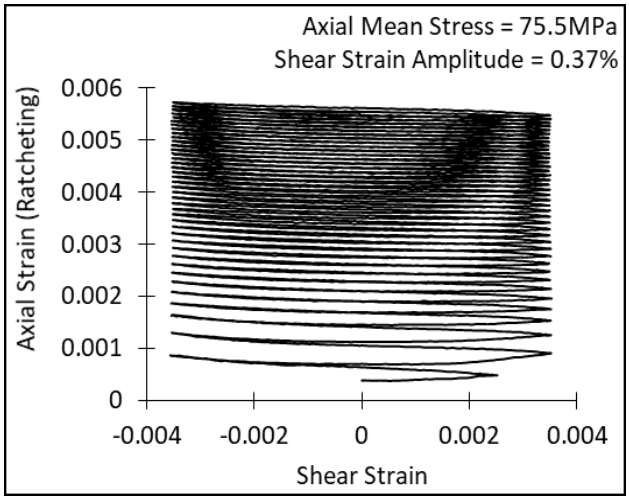

Fig. 4.13: *Multiaxial (tensile mean stress, symmetric torsion cycling) ratcheting behaviour SA333.*

The axial direction of a thin tubular specimen is loaded with constant tensile mean stress, whereas a constant amplitude torsion cycle is applied. The experiments were carried out for different mean stress and stress amplitude combinations and simulated the same. The typical multiaxial ratcheting response of SA333 Grade-6 C-Mn steel are shown in figure 4.13 above subject to tensile mean stress with symmetric torsional cycling. The ratcheting strains are calculated and are shown below in a comparative manner with the experimental results in figure 4.14 and 4.15.

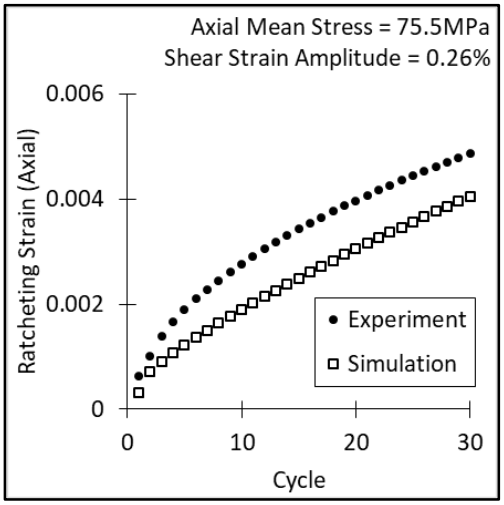

Fig. 4.14a: *Comparison of biaxial (tension-torsion) ratcheting experiment with simulation for axial mean stress 75.5 MPa and shear strain amplitude 0.26%.*

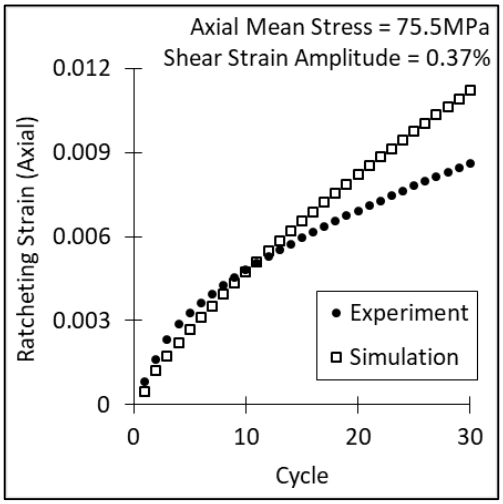

Fig. 4.14b: *Comparison of biaxial (tension-torsion) ratcheting experiment with simulation for axial mean stress 75.5 MPa and shear strain amplitude 0.37%.*

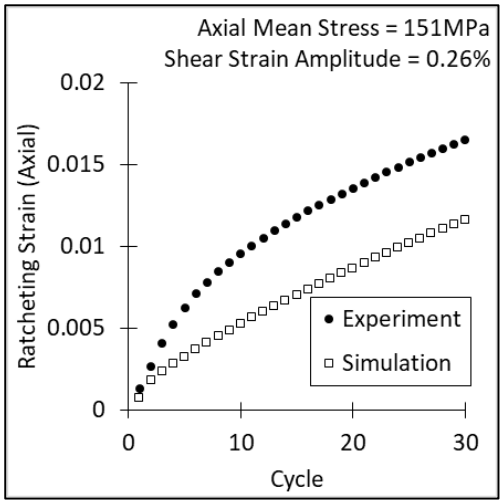

Fig. 4.15a: *Comparison of biaxial (tension-torsion) ratcheting experiment with simulation for axial mean stress 151 MPa and shear strain amplitude 0.26%.*

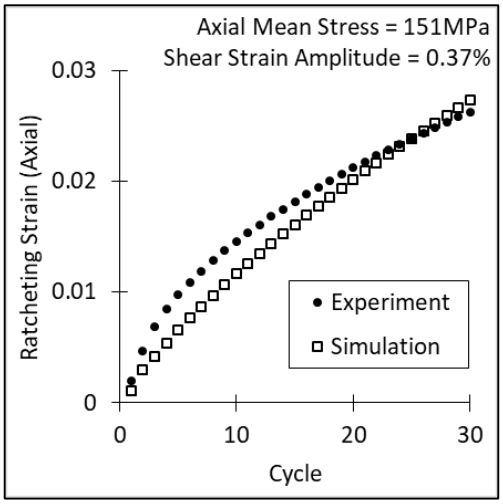

Fig. 4.15b: *Comparison of biaxial (tension-torsion) ratcheting experiment with simulation for axial mean stress 151 MPa and shear strain amplitude 0.37%.*

4.9 Discussion

The non-closure of the hysteresis loops administrate the generation of new dislocations in every cycle. These newly generated dislocations hinder the formation of stable substructure and therefore, no definitive dislocation structure observed in the TEM micrographs till the latter half of the secondary stage. Accordingly, the condition required to felicitate the cyclic softening based on the annihilations of the sub-cell boundary dislocations is not prevailed. Therefore, no cyclic softening mechanism is incorporated in the material model.

The ratcheting tests were done for different combinations of mean stress and stress amplitudes for both uniaxial and multiaxial loading conditions. In the experimental results, the effects of mean stress and stress amplitudes are observed differently. A single parameter (dislocation density) approach is attempted in this study to capture different macroscopic influences. The ratcheting responses of the material are simulated closely with the material model.

It is observed that the uniaxial ratcheting strain and the ratcheting rate are simulated well by the single parameter approach. The influences of mean stress and stress amplitude are also well described by the material model. For biaxial ratcheting, the simulations at low strain amplitudes show good estimations of the ratcheting rates with tolerably over-estimated ratcheting strains. However, for higher strain amplitudes, noticeable departures of the ratcheting rate is observed. A plausible comprehension for the observation can be, at higher strain amplitudes, the required hardening cannot be achieved due to the saturation of KH parameter (r^k). The Further calibration of the material parameter χ_{sat} at higher strain may improve the predictions.

4.10 Conclusion

The material model designed for simulating the asymmetric loading constitutes of Ohno-Wang KH rule (1993a) and a single parameter (dislocation density) based hardening modifier function. The main set of KH parameters were extracted from symmetric uniaxial cyclic plastic experiment and further modified by the exponential modifier function, accordingly evolved by the loading controls during asymmetric loading simulations. The modifier function is exponential, chosen depending on the nature of the ratcheting responses of the material. The function variable is the dislocation density solely evolved from the ratcheting strain and only indulge in raising the hardening response of the KH rule. The model seem to be phenomenological but has a strong foundation of micro-mechanism. The good agreements of simulation results with the experimental responses show effectiveness of the material model.

4.11 Acknowledgements

The authors acknowledge Bhabha Atomic Research Centre, Mumbai for financial assistance through collaborative project and National Metallurgical Laboratory, Jamshedpur for experimental support. The authors also acknowledge Dr. Surajit Kumar Paul, National Metallurgical Laboratory, Jamshedpur for TEM micrographs.

4.12 References

3DS Simulia Abaqus v6.8, Users' Manual

1979, Chaboche, J.L., Dang Van, K., Cordier, G., Modelization of the strain memory effect on the cyclic hardening of 316 stainless steel, SMiRT-5, Berlin.

1981, Meckings, H., Kocks, U. F., kinetics of flow and strain-hardening, Acta Metallurgica, Volume 29, pp1865-1875.

1985, McDowell, D. L., A two surface model for transient nonproportional cyclic plasticity, Part I: Development of Appropriate Equations, Journal of Applied Mechanics, Volume 52, Issue 2, pp 298-302.

1989, Chaboche, J. L., Nouailhas, N., Constitutive modeling of ratchetting effects – Part 2: possibilities of some additional kinematic rules, Journal of Engineering Materials and Technology, Volume 111, Issue 4, pp 409-416.

1989, Thomas, K., Creep ratchetting tests and analysis of a pressurized elbow at 593°C subjected to cyclic bending, Nuclear Engineering and Design, Volume 116, Issue 3, pp 199-213.

1991, Chaboche, J. L., On some modifications of kinematic hardening to improve the description of ratcheting effects, International Journal of Plasticity, Volume 7, Issue 7, pp 661-678.,

1992, Hassan, T., Kyriakides, S., Ratcheting in cyclic plasticity, Part I: uniaxial behaviour, International Journal of Plasticity, Volume 8, Issue 1, pp 91-116.

1993, Li, G., Berton, M. N., Cyclic behavior of a pipe section subjected to bending, ovalization or torsion loads in the case of a perfectly plastic material, International Journal of Pressure Vessels and Piping, Volume 54, Issue 3, pp 363-386.

1993a, Ohno, N., Wang, J. D., Kinematic hardening rules with critical state of dynamic recovery, part I: Formulation, International Journal of Plasticity, Volume 9, Issue 3, pp 375-390.

1993b, Ohno, N., Wang, J. D., Kinematic hardening rules with critical state of dynamic recovery, part II: Application, International Journal of Plasticity, Volume 9, Issue 3, pp 391-403.

1994, Hassan, Tasnim, Kyriakides, Stelios, Ratcheting of cyclically hardening and softening materials, I: uniaxial behaviour, International Journal of Plasticity, Volume 10, Issue 2, pp 149-184.

1994, Jiang, Y., Sehitoglu, H., Cyclic ratchetting of 1070 steel under multiaxial stress states, International Journal of Plasticity, Volume 10, Issue 5, pp 579-608.

1995, Delobelle, P., Robinet, P., Bocher, L., Experimental study and phenomenological modelization of ratchet under uniaxial and biaxial loading on an austenitic stainless steel, International Journal of Plasticity, Volume 11, Issue 4, pp 295-330.

1995, McDowell, D. L., Stress state dependence of cyclic ratchetting behavior of two rail steels, International Journal of Plasticity, Volume 11, pp 397-421.

1996, Xia, Z., Kujawski, D., Ellyin, F., Effect of mean stress and ratcheting strain on fatigue life of steel, International Journal of Fatigue, Volume 18, Issue 5, pp 335-341.

2000, Bari, Shafiqul, Hassan, Tasnim, Anatomy of coupled constitutive models for ratcheting simulation, International Journal of Plasticity, Volume 16, Issues 3-4, pp 381-409.

2004, Gaudin, C., Feaugas, X., Cyclic creep process in AISI 316L stainless steel in terms of dislocation patterns and internal stresses, Acta Materialia, Volume 52, pp 3097-3110.

2007, Rauch, E. F., Gracio, J. J., Barlat, F., Work-hardening model for polycrystalline metals under strain reversal at large strains, Acta Materialia, Volume 55, pp 2939-2948.

2008, Wilshire, B., Burt, H., Damage evolution during creep of steels, International Journal of Pressure Vessels and Piping, Volume 85, Issue 1-2, pp 47-54.

2008, Jiang, Y., Zhang, J., Constitutive modeling of cyclic plasticity deformation of a pure polycrystalline copper, International Journal of Plasticity, Volume 24, pp 1890-1915.

2009, Arcari, A., Vita, D. R., Dowling, E. N., Mean stress relaxation during cyclic straining of high strength aluminum alloys, International Journal of Fatigue, Volume 31, pp 1742-1750.

2011, Paul, Surajit Kumar, Experimentation and material modelling for cyclic plastic deformation behaviour in primary heat transport piping (PHT) materials, Ph.D. Thesis, Jadavpur University, India.

Blank Page

Chapter 5

SUMMARY AND CONCLUSION

In this chapter, the overall achievements and drawbacks of the present work are discussed and further modifications and possible extension of the present work are suggested.

Content **Page**

Blank Page

5.1 Closing remarks:

It is reported in the literature that the material, SA333 Grade-6 C-Mn steel, is sensitive to cyclic plastic loading and it has a safety-critical field of application where cyclic plastic loading is likely to occur. Therefore, in the first chapter, the aim of the present work is set to model the material behaviour for SA333 steel subjected to symmetric and asymmetric uniaxial and multiaxial cyclic plastic loading. To obtain the goal, a systematic approach is proposed and some benchmarks are set. The approach gradually approaches towards the complex loading conditions starting from symmetric uniaxial cyclic plastic loading to complex multiaxial loading. In every benchmark, as described in the previous respective chapters, mechanical tests are performed to get the macroscopic material responses. Some existing phenomenological approach is opted for the modelling of the material behaviour but due to the lack of sufficient physical explanation in the approach, further metallurgical investigations are carried out. Realizing the micro-mechanism, modelling of the material behaviour is attempted mainly based on the evolution and interactions of dislocations and represented by a single parameter – the dislocations density. After considerable literature survey it is realised that the cyclic plastic behaviour of metals can be modelled by incorporating appropriate hardening rules where, the rules are governed by instantaneous dislocation density which is controlled by the interaction of dislocations.

The micro-mechanism behind the material behaviour are needed to be evaluated thoroughly for accurate description of the material in the model. The kinematic hardening rule is the essential feature that can simulate closed loop stress-strain hysteresis curve with Bauschinger effect. Isotropic hardening rule is required for modelling of cyclic hardening/softening and non-proportional hardening behaviour. The respective hardening rules are governed by the dislocation density that evolve from the appropriate micro-interactions.

In the first benchmark as discussed in the second chapter where, the material behaviour subjected to symmetric uniaxial tension-compression loading condition is considered. The material shows Bauschinger effect, which is captured by using the Ohno-Wang kinematic hardening rule; and initial non-Masing behaviour which is recognised as the variation in the cyclic yield stresses and modelled by cyclic softening mechanism. The material predominantly shows cyclic softening in the initial transient cycles. After metallurgical (TEM) investigations it is comprehended that the micro-mechanism behind the cyclic softening is annihilation of dislocations forming low angle sub-grain boundaries. The observation is modelled and implemented as user material subroutine in ABAQUS FE platform to simulate the uniaxial cyclic plastic behaviour of SA333. The results show optimistic simulation and validate the model.

The second benchmark deals with the symmetric and biaxial tension-torsion loading conditions. The material (thin tubular specimen) is subjected to two types of biaxial loading conditions namely, proportional (in-phase) and non-proportional (out-of-phase) conditions. For proportional loading, the material response is identical to symmetric uniaxial case and therefore, the model has not been modified. The transferability of the model is checked by

comparing FE simulated results to the experiments and a comparable agreement is observed.

The non-proportional loading condition evolve additional hardening as observed in the experimental results. It is realised that the additional hardening is evolved from the activation of new slip systems and dislocation pile-ups in them due to the in-process strain-path changes. The phenomena is described as latent hardening and accordingly modelled. The forest pile-ups in the newly active slip systems offers isotropic hardening though, may induce anisotropy in the long run. The previously described material model has been modified with the philosophy of latent hardening and simulated in commercially available FE platform. The results show considerable match with the actual material behaviour and validated the model.

In the next benchmark, the material is subjected to asymmetric (ratcheting) loading for both uniaxial and biaxial case. The material shows extra hardening due to the ratcheting strain and consequently, ratcheting rate decay progressively in secondary stage. Observing the material behaviour, the ratcheting strain is quantified by the increment of the size of the plastic strain memory surface. The estimated ratcheting strain in every cycle generates new dislocations which contribute in the hardening. The increment in the forward dislocation density should directly be reflected in the hardening part of the kinematic hardening rule and therefore, a function of dislocation density due to ratcheting strain is designed to modify the kinematic hardening parameters accordingly. The modified model is simulated in FE platform and compared with experimental results. A good estimation of the ratcheting strain and ratcheting rate is observed by the material model.

The final version of the material model holds some important features, as discussed below:

1) The contributions from the forward and reverse dislocation families are considered in the kinematic hardening rule. The isotropic softening and non-proportional hardening mechanisms are modelled on the dislocation densities evolved and engaged in different interactions. The softening mechanism is developed from the annihilation of low angle sub-grain boundary dislocations and non-proportional hardening is contributed by latent family of dislocations. The increase in the dislocation density due to ratcheting strain can be considered as forward dislocations and therefore, the kinematic hardening parameter is modified to conserve the contribution of dislocation families.

2) It is attempted to construct a material model in such a way that, it can produce appropriate material response in respective loading conditions by sensing and activating suitable hardening functions when required. It is done by converging the reasons of all the macroscopic behaviour onto a single parameter (dislocation density) and including triggering mechanism based on material responses.

   For example: the non-proportionality parameter only triggers the non-proportional hardening if non-parallel strain-path change occurs. Similarly, the size of plastic strain memory surface increases considerably if there is asymmetry in the loading.

For symmetric strain controlled LCF loading no change in plastic strain memory surface occurs.

3) The material parameters are mostly extracted from physical observation and a few others are calibrated by trial and error during numerical simulations.

The uniqueness of the model architecture noted above made it compatible with uniaxial, multiaxial (proportional and non-proportional) loading in symmetry or asymmetry when subjected to static loading conditions.

5.2 Future scope:

At the end of the present work, the research indicates a few possible extensions to be explored in future. During the course of the work, many assumptions were made to simplify the problem definition and small variations are left unanswered and with that, there remains a scope of modification for the betterment of the existing model.

1) Non-proportional loadings induces anisotropy as observed in the experimental results (stress-path) which is not considered in this work. A thorough investigation on active slip systems in in-situ electron microscopy may reveal the actual phenomena. Ratcheting, on the other hand, induces plastic strain in the loading directions which produce a directional hardening in stress space. Hence, the applicability of von-Mises isotropic yield function with associative flow rule may be reconsidered. A pear-shaped yield function that incorporates the directional hardening could be a better choice for the purpose.

2) The complete multiaxial loading with tension, torsion and internal pressure in the tubular specimen is not examined. This experimentation especially on thick (plane strain) specimen may reveal different material responses. The effect of the triaxiality on cyclic plastic responses and the fatigue life of the material can be an area worth exploring.

3) The non-proportional hardenings are quite sensitive to strain paths. It is worth studying if the material shows any strain path dependent hardening responses and the present model works efficiently under different strain paths (for example, diamond, bow-tie etc.).

4) The effect of strain-rate and temperature are not considered in this study. The temperature and rate sensitive micromechanical evolution can change the micro-mechanism as comprehended in the present study. The influences of the microstructure and the contributions of the alloying elements can be a controlling aspect to the macroscopic behaviour of the material.

Blank Page

– End –